Advanced Architectures and Control Concepts for

MORE MICROGRIDS

Contract No: SES6-019864

WORK PACKAGE A

TASK TA 2: Implications of line parameters on Microsource controller algorithms

Deliverable DA5: “Microsource local controllers capable to deal with resistive and inductive coupling of interconnecting lines”

Final Version

November 2009

Document Information

Title: Microsource Local controllers capable to deal with resistive and inductive coupling of interconnecting lines

Date: 09-11-2009

Task(s): TA 2. Implications of line parameters on Microsource controller algorithms

Coordination:	Dominik Geibel	dgeibel@iset.uni-kassel.de
Authors:	Dominik Geibel	dgeibel@iset.uni-kassel.de
	Christian Hardt	christian.hardt@sma.de
	Jörg Jahn	
	Thorsten Reimann	treimann@iset.uni-kassel.de
	Boris Valov	bvalov@iset.uni-kassel.de
	David Tinarwo	

Access:

__ Project Consortium
_ European Commission
X PUBLIC

Status:

_ For Information
_ Draft Version
_ Final Version (internal document)
_ Submission for Approval (deliverable)
X Final Version (deliverable, approved on_)

CONTENTS

1. Executive summary

Microgrids comprise low voltage distribution networks with distributed energy sources, storage devices and controllable loads operating as a coordinated, controlled entity.
In contrary to high and medium voltage networks having an inductive character, low voltage distribution networks are mostly resistive. This results in a coupling between active power and voltage. On the low voltage level voltage control through reactive power is very limited. Advanced voltage control approaches in Microgrids for low voltage networks are investigated in this report.

Voltage controlled battery inverters using droop control functionality come into operation for establishing the power equilibrium of generation and consumption in Microgrids consisting of an appreciable share of renewable generation. For providing additional functionalities used by the developed advanced voltage control strategies the control and the load flow management system have been extended.

- Modules for the load flow management system "DroopControl" based on ISET SELFSYNC control method are developed for the Sunny Island 5048 battery inverter by the SMA Solar Technology AG.

Nonetheless direct voltage control using "DroopControl" functionality is not always possible. However advanced voltage control strategies are needful to maintain the voltage profile within certain limits. Two different strategies are discussed within this report by means of simulations and measurements:

- The approach of voltage control within meshed low voltage networks is successfully proofed by simulations and measurements.
    - The voltage profile at designated points of a meshed low voltage network with a pure resistive character consisting of inverters with droop functionality Q(V) is influenced systematically by reactive power injection.
    - The amount of reactive power depends on the slope of the Q(V)-droop of the battery inverter with droop control. The higher the slope the less reactive power for the same voltage change is needed.
    - The amount of reactive power required for a fixed voltage change using investigated approach is notable smaller than the amount of reactive power using conventional methods without droop mode inverters.
    - The voltage at a user-defined point of the network can be hold at a defined set-point achieved through a superordinated control responsible for the injection of the required amount of reactive power.
- The approach of inductive decoupling of long low voltage lines is successfully proofed by simulations and measurements.
    - The development of selection criteria for the essential size of the decoupling inductor is done by means of calculation results.

- Quasi-stationary voltage deviations within 230V ± 10 % are controlled to a given set-point (e.g. 230 V) for loads in the inductive decoupled sub-network at the end of the long low voltage line.
- Dynamic voltage deviations are damped significantly for loads in the inductive decoupled sub-network at the end of the long low voltage line.
- The voltage profile is considerably enhanced for loads in the sub-network at the end of the long low voltage line.

Both approaches of advanced voltage control strategies for low voltage Microgrids have been investigated by simulations, successfully implemented in prototype systems and tested on laboratory experimental level.

2. Network Configuration and Energy Transmission in Electrical Networks

Configuration of electrical networks complies with several requirements. These requirements are for example costs, security of supply or protection effort. For choosing the right form of network configuration afterwards the three most common types of networks are described. Second part of this chapter handles with energy transmission of electrical networks where several kinds of transmission mechanisms come into consideration. Especially for developing additional voltage control strategies knowledge of energy transmission mechanisms is essential.

2.1. Network configuration of transmission and distribution networks

2.1.1. Radial networks

Radial networks are in fact one-side fed branch lines which can be found on utilities low and medium voltage level for supply of small loads. Normally several radial networks are not meshed among each other. Radial networks also are used at medium voltage level for weak load conditions implemented as overhead lines and for heavy load conditions in case of short transmission distances. Figure 1 shows a typical appearance of a radial network.

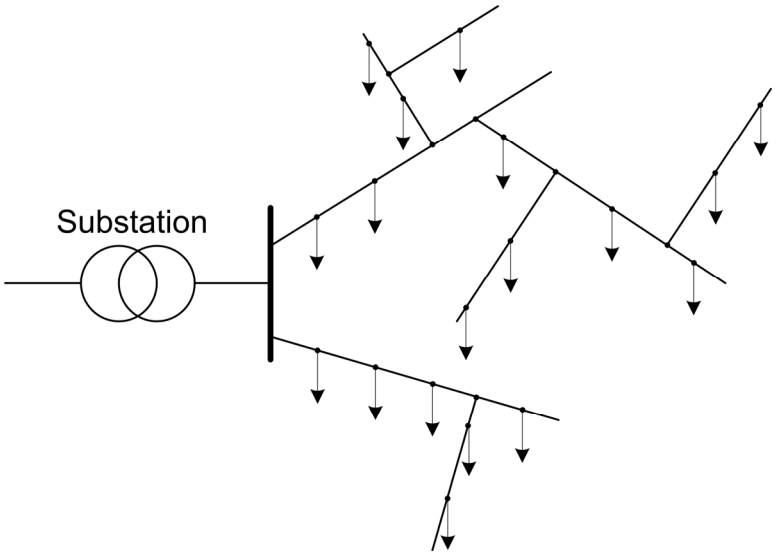

Figure 1: Radial network; one-side fed branch lines with loads

Disadvantage of radial networks is the voltage drop due to switching of big loads [Han05].

2.1.2. Loop networks

In general loop networks are special cases of double fed branch lines because of an existing common point of supply. Using double-side feeding a higher security of supply can be

assured for loads. Within the medium voltage level loop networks are used to supply substations with laminar building density and multiple small load centres or substations which are distant from transmission stations.

Often low voltage networks are built as loop networks. During normal operation the loop is opened, so that in fact a radial network exists. But if a grid fault occurs within the loop network, it is possible to clear the faulted part of the line by opening the bordering disconnecting points and closing the disconnecting point in the middle of the loop in order to supply the connected loads further.

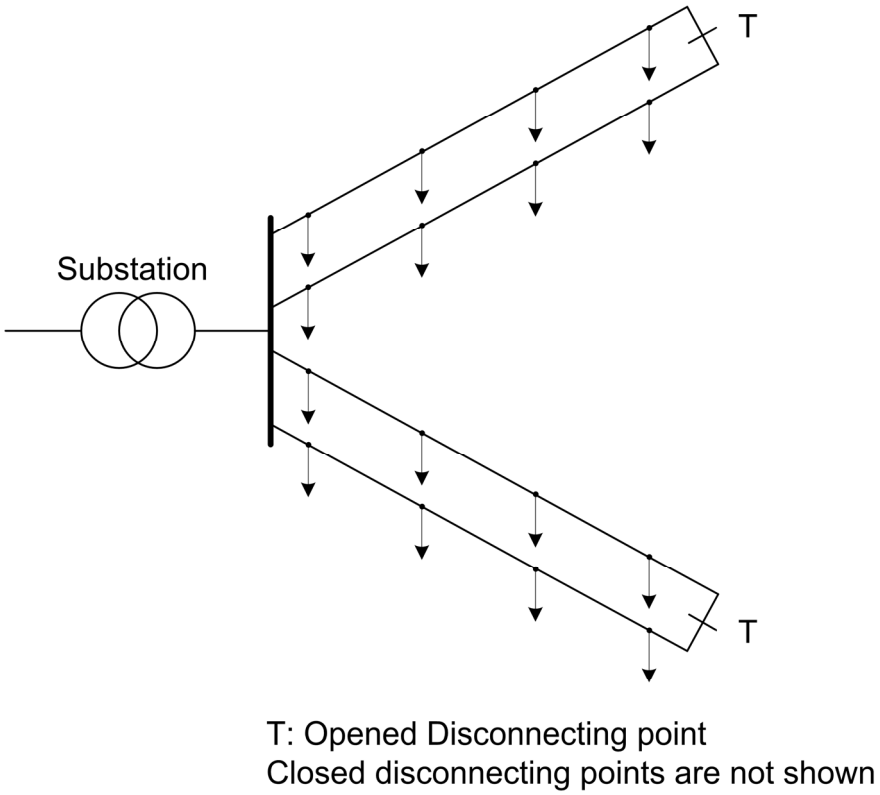

Figure 2: Network operated as open-loop

2.1.3. Meshed networks

Meshed networks assure security of supply for single load consumers through connection of feeders among each other and through several in-feeds in an optimum way. As shown in Figure 3 every branch can drop out without influence on security of supply. Enough parallel supply branches can compensate the loss of a line within the meshed network. Particular transmission grids used for transmission of high power amounts across long distances (380 kV, 220 kV and 110 kV networks) are built in a meshed style. For dispersion of electrical energy in smaller geographic regions, as for example in a city, meshed grids are not used that often due to several factors. Main factor is protection complexity. Also different line

lengths between two points of supply could lead to a load flow problem and overload of particular network lines.

Important characteristics of meshed networks are intrinsic safety, high voltage stability and low network losses. But after blackouts it is quite difficult to perform a black start in meshed networks.

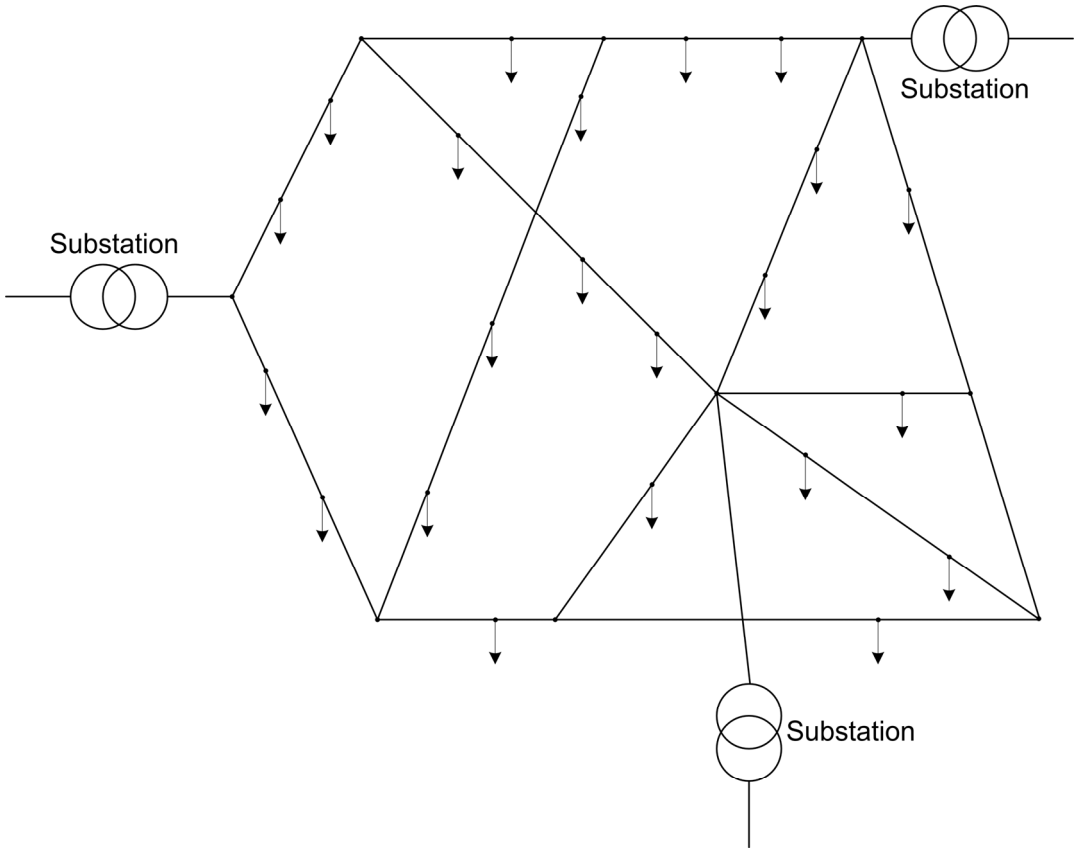

Figure 3: Example of a meshed network

A specialty is a meshed network on the low voltage level. Security of supply of such kind of networks is very high because due to reserves by other lines in parallel. They are used for load densities higher than 5 MVA/km^2. Loading of the line is according to the line impedance and load sharing within the network. According to the type of in-feed from medium voltage level into meshed low voltage grids different kinds of terms are used [Sch05].

- station wise fed-in networks
- single-stranded fed-in networks
- multiple-stranded fed-in networks

2.2. Energy transmission mechanism in transmission and distribution networks [Jah07]

2.2.1. Differences of electric networks on transmission and distribution level

Electrical networks on transmission and distribution level do not only differ regarding their voltage level but also in respect of their coupling between the connected voltage sources. Whereas resistance load per unit length clearly outbalance the inductance load per unit length at the low voltage level, the arrangement reverse at the high voltage level (cp. Table 1). The ratio between the resistive and inductive share of the line parameters is often adducted in literature for evaluation of network behaviour and labelled as R/X-ratio:

$$\frac{R}{X} = \frac{R_{Grid}}{X_{Grid}} = \arctan\left(\varphi_{Grid}\right) = \frac{\Re\left\{\underline{Z}_{Grid}\right\}}{\Im\left\{\underline{Z}_{Grid}\right\}} \tag{2.1}$$

According to this R/X-ratio coupling of voltage sources with R/X-ratio > 1 is indicated as a coupling with a predominantly resistive character, whereas couplings between voltage sources with R/X-ratio < 1 show a predominantly inductive character. On the basis of extreme values of the pure inductive and pure resistive coupling respectively difference of energy transmission mechanism can be illustrated clearly.

Table 1: Typical parameter of transmission and distribution lines [Heu05]

Voltage Level	R $[\Omega/km]$	X $[\Omega/km]$	I_n $[\Omega/km]$	$\frac{R}{X}$
Low Voltage	0.642	0.083	142	7.7
Medium Voltage	0.161	0.190	396	0.85
High Voltage	0.06	0.191	580	0.31

In the following sections energy transmission in ideal inductive and ideal resistive coupled networks is firstly described in detail. Afterwards the common case of a mixed resistive-inductive coupling is assumed.

2.2.2. Electric networks with inductive coupling

In Figure 4 inductive coupling of two voltage sources is presented. The active and reactive power flow depends on the amplitude and the phase difference between both voltage sources.

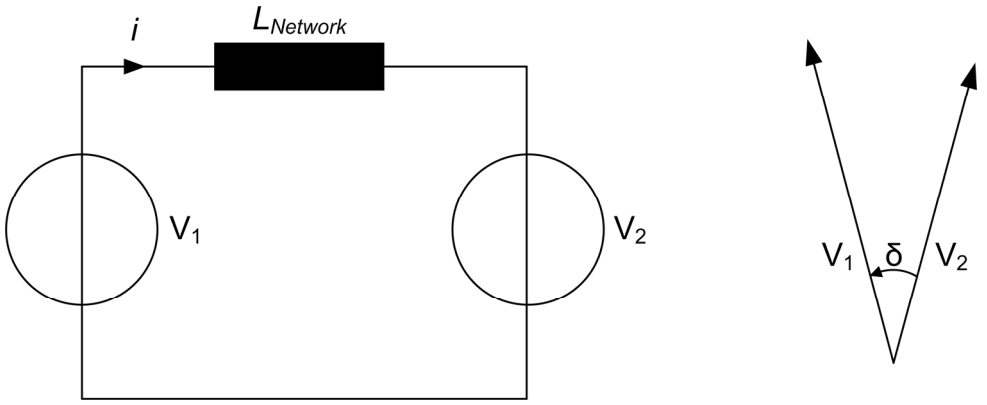

Figure 4: Inductively coupled voltage sources on the left, pointer diagram of the voltages on the right [Eng01]

With the voltages

$$v_1 = \hat{v}_1 \cdot e^{j\omega_N t} \tag{2.2}$$

and

$$v_2 = \hat{v}_2 \cdot e^{j\omega_N t} \cdot e^{-j\delta} \tag{2.3}$$

as well as the network impedance $L_{Network}$ the complex current can be calculated which arise due to the difference of the amplitudes and the phases angles of the two voltage sources.

$$\begin{aligned} \underline{i} &= \frac{\underline{v}_1 - \underline{v}_2 \cdot e^{-j\delta}}{j\omega_N \cdot L_{Network}} \cdot e^{j\omega_N t} \\ &= -j\left(\frac{\hat{v}_1}{\omega_N \cdot L_{Network}} - \frac{\hat{v}_2}{\omega_N \cdot L_{Network}} \left(\cos\delta - j\sin\delta\right) \right) \cdot e^{j\omega_N t} \\ &= \left(\frac{\hat{v}_2}{\omega_N \cdot L_{Network}} \cdot \sin\delta - j\left(\frac{\hat{v}_1}{\omega_N \cdot L_{Network}} - \frac{\hat{v}_2}{\omega_N \cdot L_{Network}} \cdot \cos\delta \right) \right) \cdot e^{j\omega_N t} \end{aligned} \tag{2.4}$$

With the voltage from equation (2.2) and the current from equation (2.4) the complex apparent power can be determined:

$$S = P_1 + jQ_1 = \frac{1}{2}\underline{v}_1\underline{i}^*$$

$$S = \frac{1}{2}\cdot\hat{v}_1\cdot\left(\frac{\hat{v}_2}{\omega_N\cdot L_{Network}}\cdot\sin\delta + j\left(\frac{\hat{v}_1}{\omega_N\cdot L_{Network}} - \frac{\hat{v}_2}{\omega_N\cdot L_{Network}}\cdot\cos\delta\right)\right)\cdot e^{j\omega_N t}\cdot e^{-j\omega_N t} \quad (2.5)$$

$$= \frac{1}{2}\cdot\left(\frac{\hat{v}_2\cdot\hat{v}_1}{\omega_N\cdot L_{Network}}\cdot\sin\delta + j\left(\frac{\hat{v}_1^{\,2}}{\omega_N\cdot L_{Network}} - \frac{\hat{v}_1\cdot\hat{v}_2}{\omega_N\cdot L_{Network}}\cdot\cos\delta\right)\right)$$

Therefore the active and reactive power results in:

$$P = \Re\{S\} = \frac{V_{1,RMS}\cdot V_{2,RMS}}{\omega_N L_{Network}}\sin\delta \quad (2.6)$$

$$Q = \Im\{S\} = \frac{V_{1,RMS}^2}{\omega_N L_{Network}} - \frac{V_{1,RMS}\cdot V_{2,RMS}}{\omega_N L_{Network}}\cos\delta \quad (2.7)$$

With the equations (2.6) and (2.7) it is obvious that for inductive coupled voltage sources and a small angle δ the active power flow is dependent from angle δ by itself. The reactive power flow depends from the difference of the voltage amplitudes. This is corresponding to the energy transmission mechanism of networks within the transmission system, wherein voltage control can be achieved with reactive power.

2.2.3. Electric networks with resistive coupling

In Figure 5 reverse network conditions in comparison with section 2.2.2 by means of a pure resistive coupling are shown.

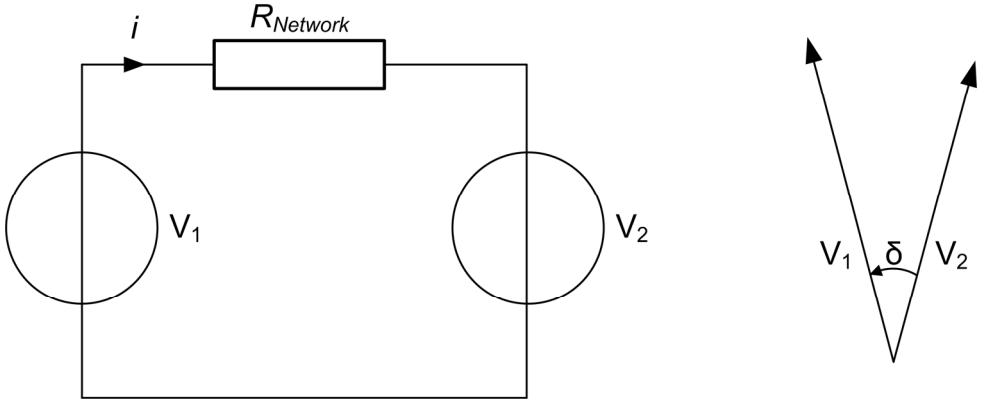

Figure 5: Resistive coupled voltage sources on the left, pointer diagram of the voltages on the right [Jah07]

For further calculations of active and reactive power flows the equations (2.2) and (2.3) are starting points again.

In this case the complex current results in:

$$\begin{aligned}\underline{i} &= \frac{\underline{v}_1 - \underline{v}_2 \cdot e^{-j\delta}}{R_{Network}} \cdot e^{j\omega_N t} \\ &= \left(\frac{\hat{v}_1}{R_{Network}} - \frac{\hat{v}_2}{R_{Network}} \left(\cos\delta - j \sin\delta \right) \right) \cdot e^{j\omega_N t} \\ &= \left(\frac{\hat{v}_1 - \hat{v}_2 \cdot \cos\delta}{R_{Network}} + j \frac{\hat{v}_2}{R_{Network}} \cdot \sin\delta \right) \cdot e^{j\omega_N t}\end{aligned} \tag{2.8}$$

The complex apparent power is given through:

$$\begin{aligned}S &= \frac{1}{2} \cdot \hat{v}_1 \cdot \left(\frac{\hat{v}_1 - \hat{v}_2 \cdot \cos\ \delta}{R_{Network}} - j \frac{\hat{v}_2}{R_{Network}} \cdot \sin\ \delta \right) \cdot e^{j\omega_N t} \cdot e^{-j\omega_N t} \\ &= \frac{1}{2} \cdot \left(\frac{\hat{v}_1^{\ 2} - \hat{v}_2 \cdot \hat{v}_1 \cdot \cos\ \delta}{R_{Network}} + j \frac{\hat{v}_2 \hat{v}_1}{R_{Network}} \cdot \sin\ \delta \right)\end{aligned} \tag{2.9}$$

and the active and reactive power is:

$$P = \Re\{S\} = \frac{v_{1,RMS}^{\ 2}}{R_{Network}} - \frac{v_{2,RMS} \cdot v_{1,RMS}}{R_{Network}} \cdot \cos\delta \tag{2.10}$$

$$Q = \Im\{S\} = \frac{v_{1,RMS} \cdot v_{2,RMS}}{R_{Network}} \cdot \sin\delta \tag{2.11}$$

Contrary to the inductive coupling, active power flow now depends of the voltage amplitude difference, whereas the reactive power flow is dependent from the angle δ. This kind of energy transmission mechanism predominately occurs in low voltage networks.

2.2.4. Electric networks with resistive-inductive coupling

Figure 6 shows the equivalent circuit diagram of two parallel connected voltage sources with a mixed resistive and inductive coupling.

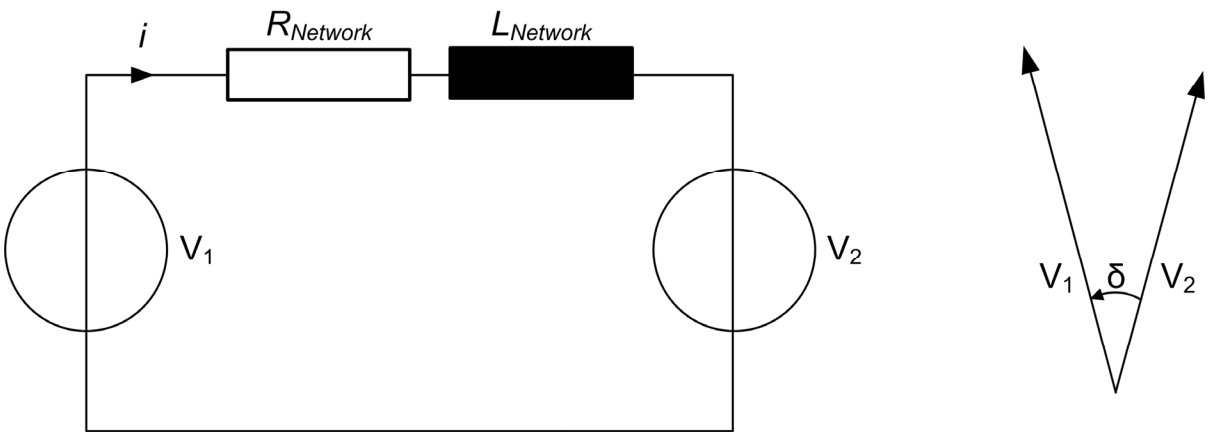

Figure 6: Mixed (resistive and inductive) coupled voltage sources on the left, pointer diagram of the voltages on the right [Jah07]

Unlike the extreme conditions for a pure resistive or a pure inductive coupling, described in the sections before, the denominator of the complex current is not either pure real or pure complex any longer.

$$\underline{i} = \frac{\hat{u}_1 - \hat{u}_2 \cdot e^{-j\delta}}{R_{Network} + j\omega L_{Network}} \cdot e^{j\omega_N t} \tag{2.12}$$

Therefore the equations cannot be merged as before and the result loses clearness.
Based on the network impedance according to DIN EN 61000-3-3 of

$$\underline{Z} = 0.4\Omega + j\omega 0.8mH = \left|Z\right| \cdot e^{j\omega_N t} \tag{2.13}$$

for low voltage networks, it appears that the network angle

$$\varphi_{Network} = \arg\left(\underline{Z}\right) = 0.561 \mathrel{\hat{=}} 32^\circ \tag{2.14}$$

can not be considered as pure resistive, what is also expressed by the R/X-ratio which is significant nearer to 1 than stated in Table 1.

$$\frac{R}{X} = \frac{0.4\Omega}{j\omega 0.8mH} = 1.59 \tag{2.15}$$

This deviation can be constituted because the network impedance of the DIN EN 61000-3-3 also considers loads connected to the network and Table 1 only shows values for lines the corresponding networks are built of. The difficulty of having a clear view on the energy transmission mechanism is originated by the increasing number of parameters. In the following the energy transmission mechanism is explained by varying the network impedance angle.

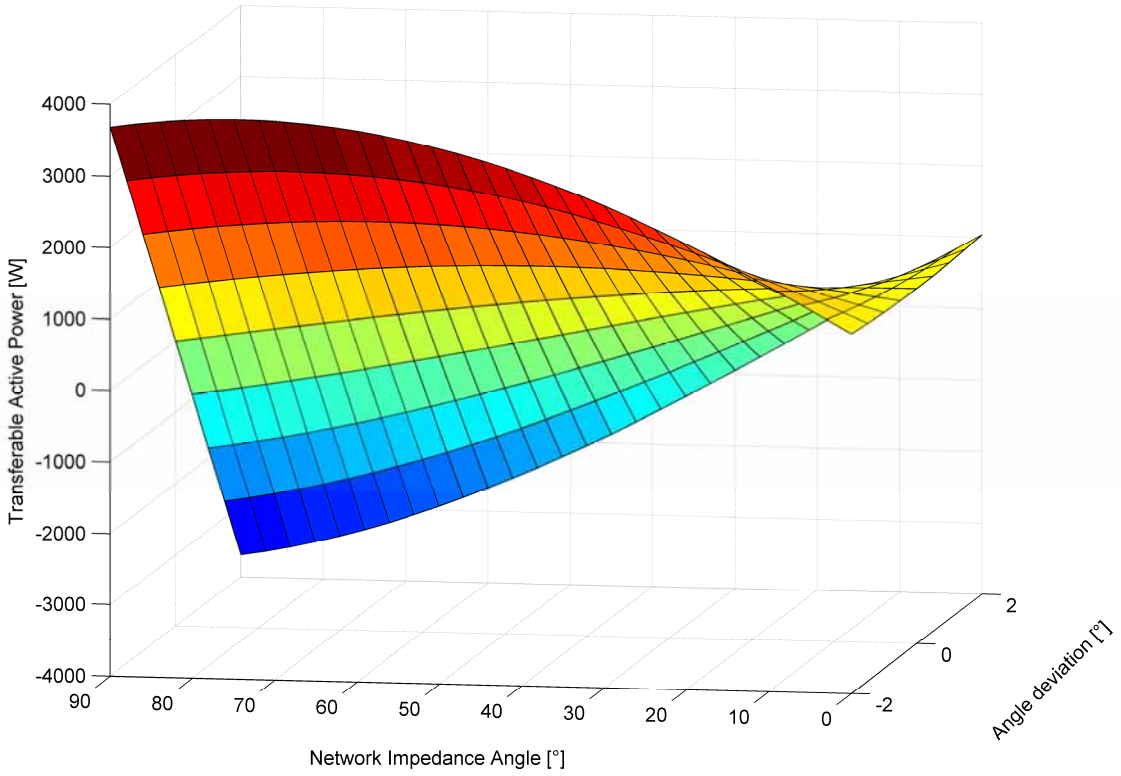

Figure 7: Illustration of transferable active power dependent of the network impedance angle and the angle deviation of the voltage sources. MATLAB calculation result.

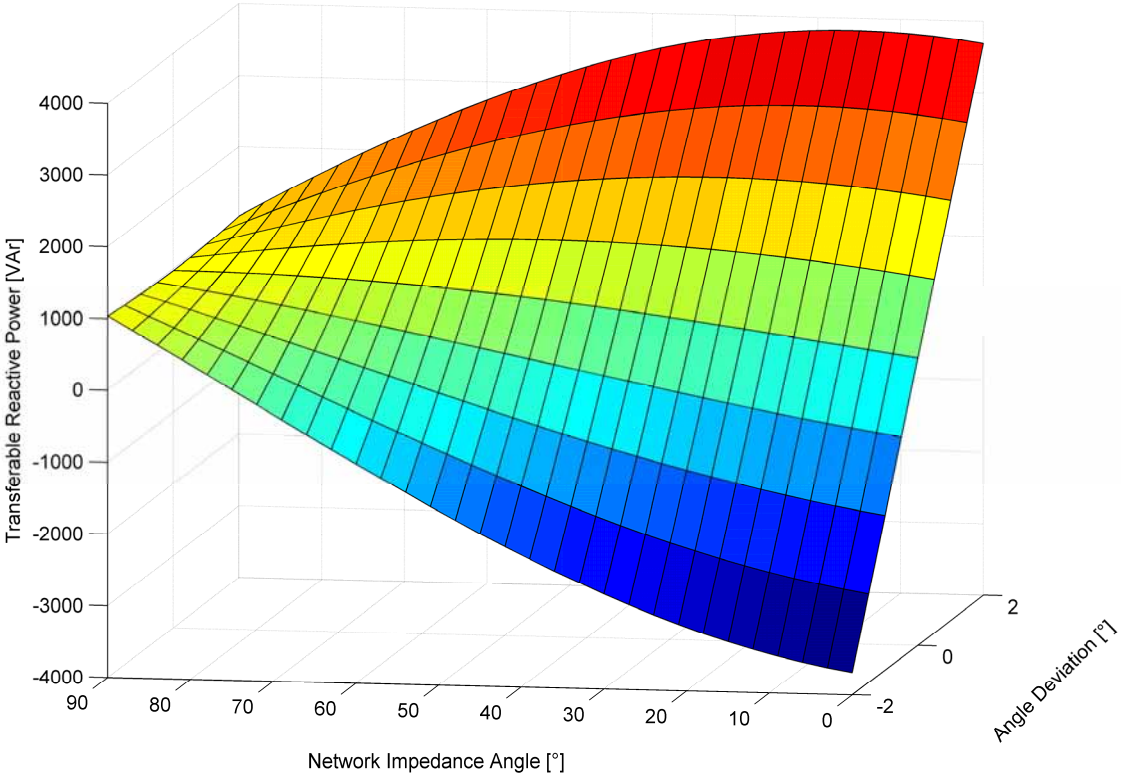

Figure 8: Illustration of transferable reactive power dependent of the network impedance angle and the angle deviation of the voltage sources. MATLAB calculation result.

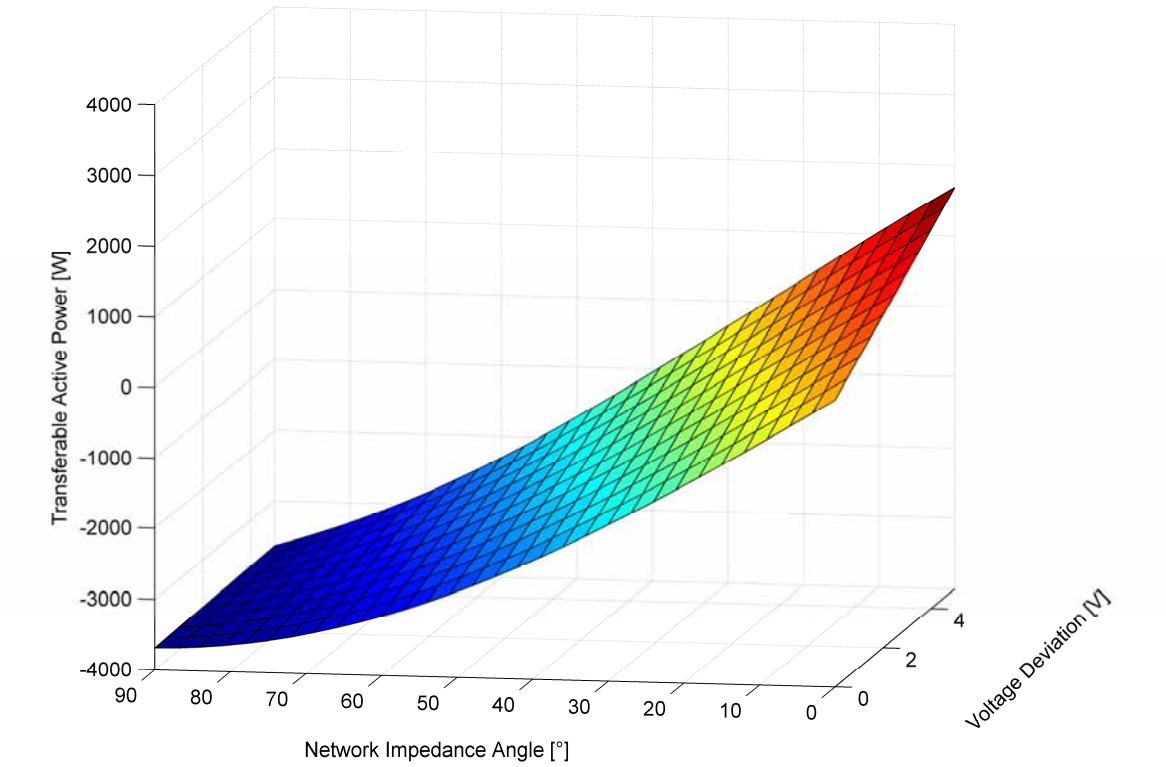

Figure 9: Illustration of transferable active power dependent of the network impedance angle and the voltage deviation of the voltage sources. MATLAB calculation result.

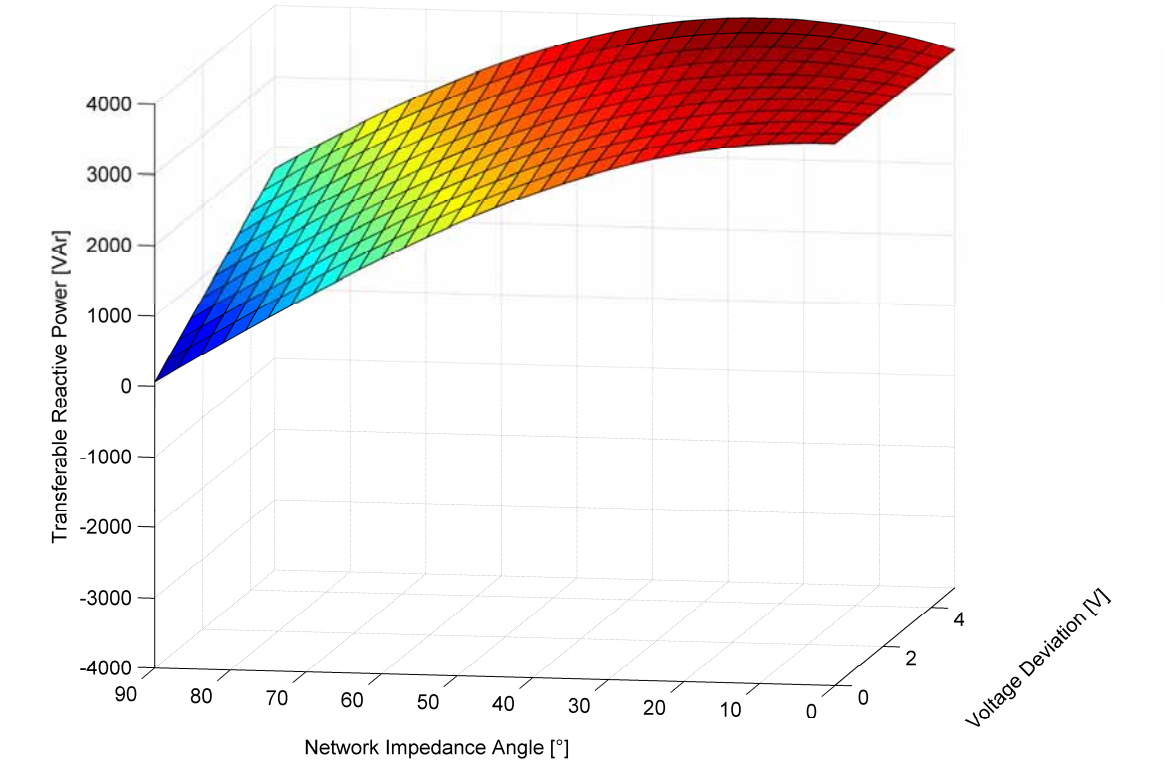

Figure 10: Illustration of transferable reactive power dependent of the network impedance angle and the voltage deviation of the voltage sources. MATLAB calculation result.

Figure 7 and Figure 8 show the transferable active and reactive power in dependence of the network impedance angle and the angle deviation of the voltage sources. Therefore the absolute value of the network impedance is kept constant at 0.5 Ω**.** The voltage difference between the two voltage sources is 3 V. At the extreme values of 0° and 90° for the network impedance angle the behaviour described in the equations (2.6) and (2.7) rather (2.10) and (2.11) can be seen.

In Figure 9 and Figure 10 instead of the angle deviation, the voltage deviation is used as parameter. The absolute value of the network impedance is kept constant at 0.5 Ω again. Now the angle deviation between the voltage sources is 2°. Once again the changes of the energy transmission behaviour due to the kind of coupling can be seen. It is obvious that for small network impedance angles the transferable reactive power is getting more and more independent from the voltage difference.

2.2.5. Specific characteristics of weak low voltage networks

As described in section 2.2.1 low voltage networks are characterised by a R/X-ratio > 1. The problem of energy transmission is getting worse for network branches with a particular high absolute value of the network impedance. A network can be supposed as weak if the network impedance is higher than 10% of the ratio between rated voltage to rated current [Org02].

$$\left|\underline{Z}\right| > 0.1 \cdot \frac{\left|\underline{U}_N\right|}{\left|\underline{I}_N\right|} \tag{2.16}$$

Generally complex power fluctuations produce fluctuating voltage drops at the active and reactive parts of the network impedance [Klo97].

$$\Delta\underline{V} = \frac{\Delta P \cdot R_{Network} + \Delta Q \cdot jX_{Network}}{V_{Network\,RMS}} = \underline{Z}_{Network} \cdot \Delta\underline{I} \tag{2.17}$$

The voltage ratio is

$$\frac{\Delta\underline{U}}{\underline{U}_{Network,RMS}} = \frac{\Delta\underline{S}}{S_{kV}} \tag{2.18}$$

whereas S_{kV} is the apparent power at the Point of Common Coupling (PCC).

With equation (2.18) it is obvious that the sign of the voltage fluctuation depends on the direction of the apparent power fluctuation. Hence voltage fluctuations increase in network

areas where power generation represent an essentially part of consumption. Furthermore the voltage change is proportional to the value of the network impedance (cp. equation (2.17)).
In general it can be stated that system perturbation caused by distributed generation increases with the rated apparent power of the generation unit and decreases with the short circuit power at the PCC [Wie01], as shown schematically in Figure 11.

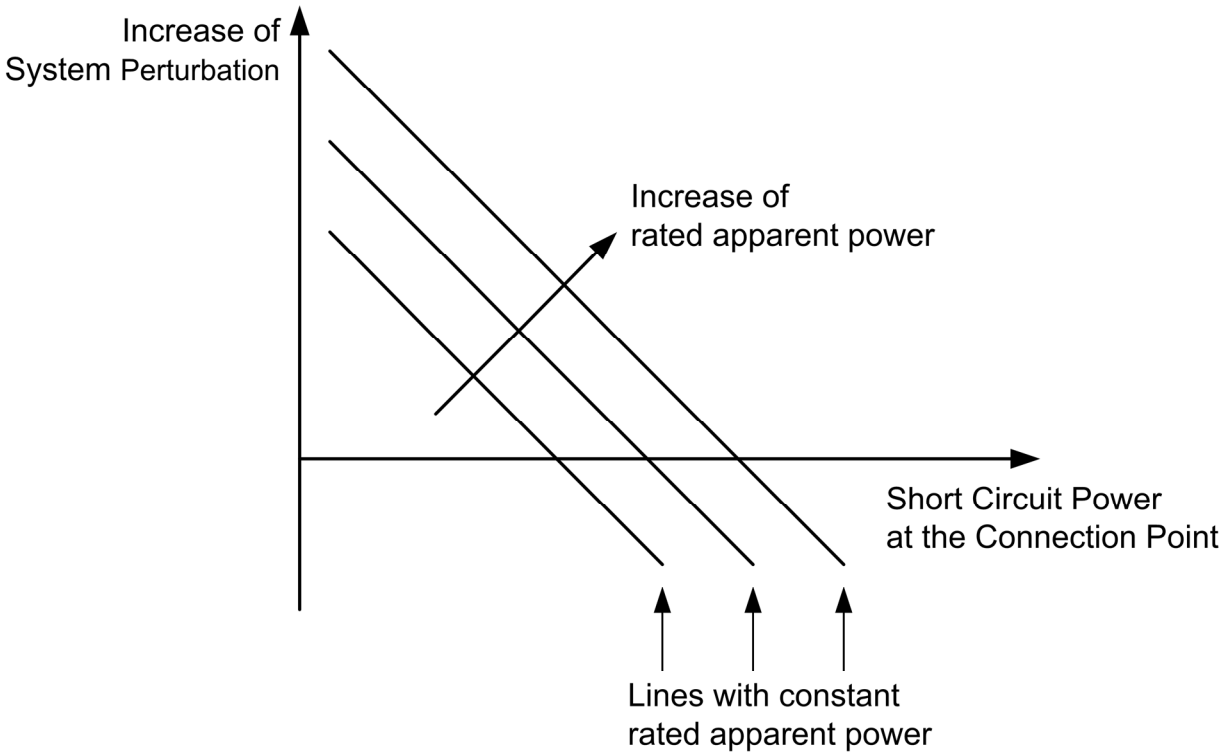

Figure 11: Schematically, qualitative relation of system perturbation intensity [Wie01]

In order to clarify in what degree a voltage rise through a decentralised or renewable feed-in at several network configurations will occur, a simulation computation according to the equivalent circuit diagram of Figure 12 is performed.

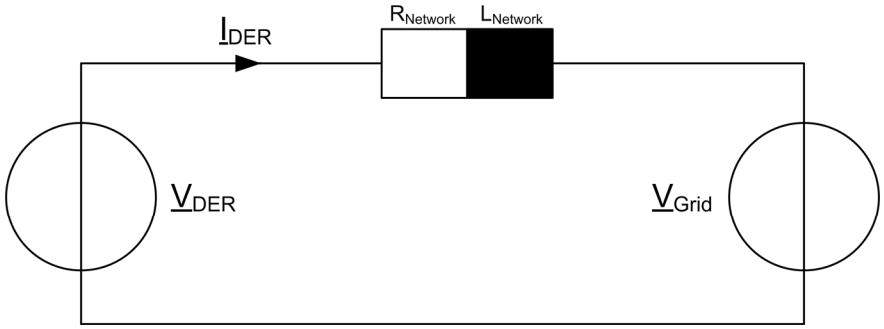

Figure 12: Equivalent circuit diagram of a distributed energy resource connected to an stiff grid

Therefore a Distributed Energy Resource (DER) with constant current injection over concentrated network impedance having a constant absolute value is coupled to a stiff voltage source $\underline{V}_{Grid}$. This assembly correspond to the connection to a superior, strong grid over the secondary windings of a transformer.

The network angle from 0° (pure resistive) to 90° (pure inductive) as well as the phase angle of the injected current

$$\underline{V}_{DER} \angle \underline{I}_{DER} \tag{2.19}$$

are varied as parameters from -90° to +90°. The exemplary pointer diagram, shown in Figure 13, reflects the means of the equivalent circuit diagram in Figure 12. The adjustable ranges of the phase angle and the network angle are drawn dashed. Because of simplifying the system by injecting only a constant current, the pointer length of the voltage drop at the network impedance is also constant.

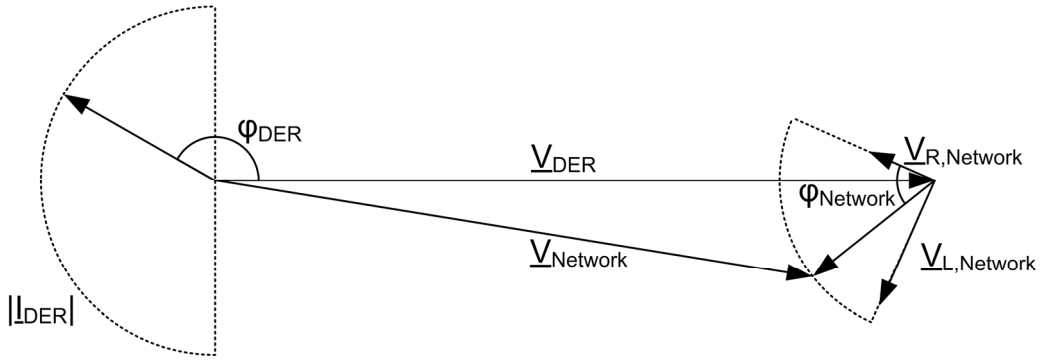

Figure 13: Exemplary pointer diagram of the equivalent circuit diagram in Figure 12

It is obvious that the output voltage of the DER unit for the case above has to be higher than the constant network voltage in order to drive a current through the network impedance.

In Figure 14 the voltage difference in dependence of the network angle and the phase angle is presented. In the special case of a pure resistive coupling (network angle 0°), it is evident that any injection increases the voltage at the point of supply. In case of a pure injection of reactive power the voltage rise is lowered by the orthographic position of the current pointer. A decrease of the voltage is only possible if the injected power is reduced.

For an increasing network angle the phase angle with the maximal voltage rise is reduced respectively. For the special case of a pure inductive coupling (network angle of 90°) the injection of an active current has no influence of the voltage level whereas the voltage can be both increase and decreased by an injection of a reactive current.

Regarding low voltage networks with predominantly resistive coupling the voltage rise can be decrease only very limited by injection of reactive power. Moreover a very high amount of

reactive current would be needed which would load the network lines and network equipment additionally. This implies that additional voltage control strategies for low voltage networks with a predominantly resistive coupling are required. Two approaches are introduced in the following chapter.

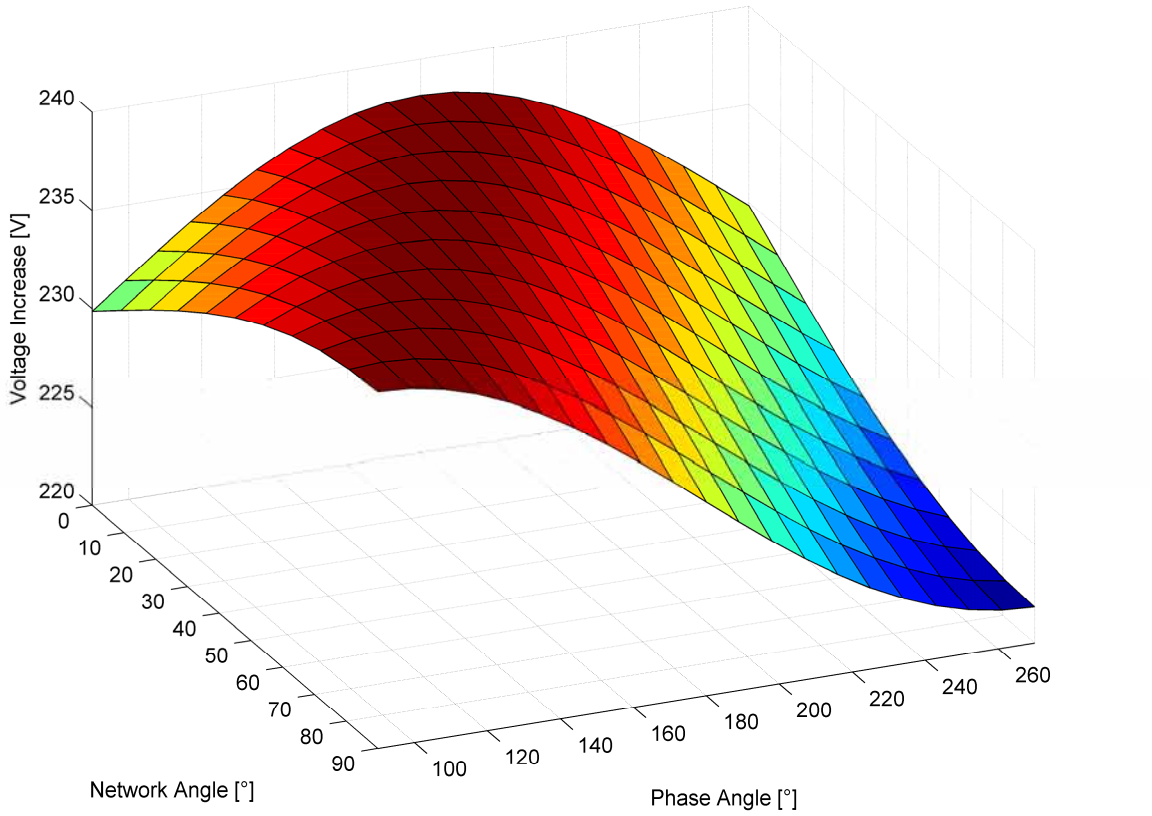

Figure 14: Voltage deviations due to injection of 16 A dependent of network angle and phase angle. MATLAB calculation result.

3. Approaches of voltage control capabilities

Voltage control capabilities become more important within the low and medium network due to an increasing number of distributed generating units. At the moment there is a paradigm change for DER units connected to the interconnected grid. Now these units have to support the network in transient and steady-state case, what includes the possibility of providing voltage control capabilities. Mainly voltage control is done through injection of reactive power. But as described in chapter 2, the effectiveness of voltage control through reactive power depends on the network characteristic.

3.1. Voltage control capabilities in interconnected operation

Figure 15 describe the influence of a DER unit with voltage control capabilities on the network voltage. The voltage difference between the superior network and a point of connection (PoC) is mainly distinguished by the connection impedance $Z_{Q,PoC}$ and the load impedance Z_{Load}. If the DER unit is not only injecting active power, but also a reactive power component, it is possible to change the voltage at the PoC. The in- or decrease of the voltage at the PoC depends whether the DER units works over- or underexcited.

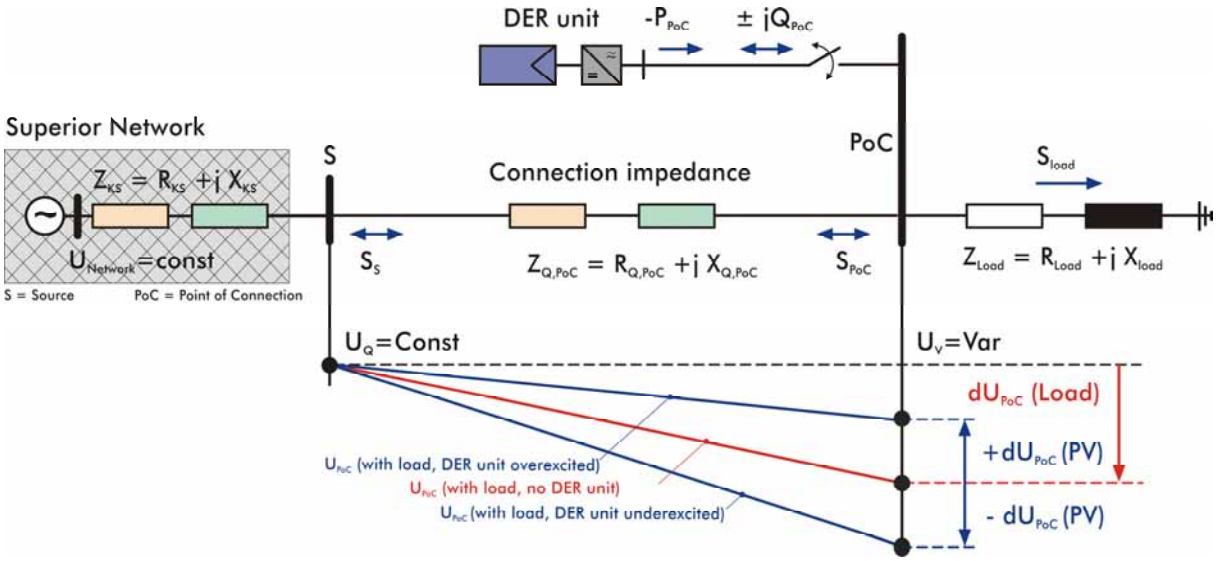

Figure 15: Voltage scheme according to [Val09].

In Figure 15 the influence of the injection of reactive power on the network voltage for several network characteristics is shown. The network behaviour is characterised by the network angle Ψ. The lower the network angle the more resistive is the network. Within this deliverable long low voltage lines and meshed low voltage networks with a considerable resistive part are studied. Therefore network impedance angles lower than 40° could be assumed.

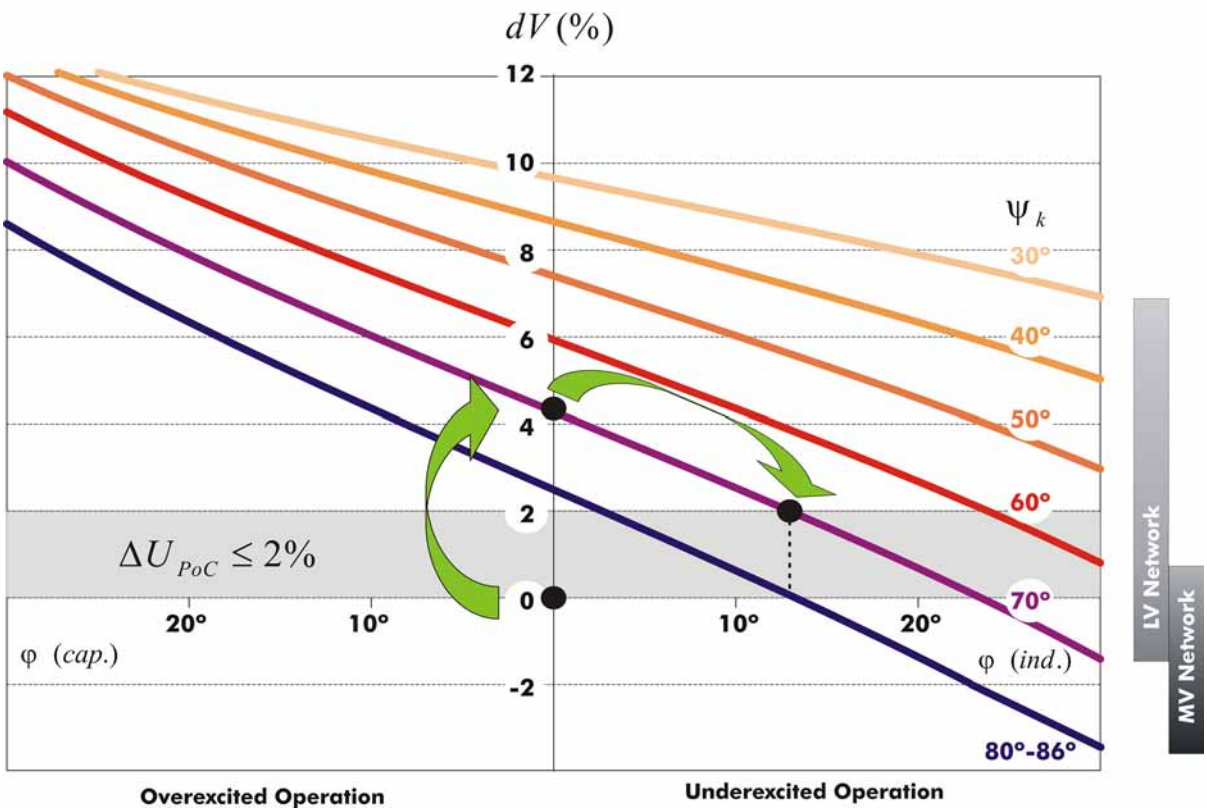

Figure 16: Voltage control through reactive power for several network impedances [Val09]

As shown in Figure 16 especially for weak low voltage grids with low network impedance angles the DER units have a major influence on the network behaviour. If these units inject active power a high voltage rise occur. For compensating this voltage rise, a high amount of reactive power would be needed. This implies that for weak low voltage networks a voltage control though reactive power is not efficient. A possibility of controlling the voltage effectively for this kind of network behaviour would only be a reduction in active power.

This is especially for a Microgrid no desirable solution. Since Microgrid components must have extended control capabilities in comparison to devices only designed for an operation in parallel to the interconnected network, alternative control methods can be used for providing a more effective voltage control. After a description of the extended control capabilities of generation units in Microgrids with a detailed view on the "DroopControl" of the SMA Sunny Island 5048 battery inverter in section 3.2, advanced voltage control strategies in resistive low voltage grids are presented in section 3.2.3. The proof of these approaches is given in chapter 4 and 5 by means of simulations and measurements.

3.2. Extended control capabilities of generation units in Microgrids

Generation units in Microgrids must not only be able to operate in current control mode, but also units with the possibility of a voltage control mode must be available. Challenges for inverters in island operation and an approach of parallel working voltage controlled battery inverters are presented afterwards. Also new developments in case of "DroopControl" operation mode for the new SMA Sunny Island 5048 are given.

3.2.1. Voltage control in island operation [Jah07]

This section describes the problems and changes of voltage controlled inverters operating in interconnected or island mode

3.2.1.1. Voltage control

In opposite to a current controlled inverter the output current of a voltage controlled inverter arise freely if it is operated in interconnected mode with other voltage sources and no additional subordinate controller exists. The output current is driven by the voltage and phase difference of the voltage sources and is limited by the network impedance alone. For these reasons particular requirements for inverters in parallel mains operation have to be pointed out concerning accuracy and dynamics.

In [Eng01] and [Hau02] methods are presented which allow voltage controlled inverters to operate in parallel mains operation. Although the measured output current is not necessary required it is nonetheless reasonable to assign it due to usage for subordinate controllers or for monitoring purposes.

3.2.1.2. Special Case: Island operation

Within an electrical network at least one voltage source has to work as a network former, which the current controlled inverters need as reference for their own power injection. The simplest assembly of an island network is the operation of merely one generator and of the loads that have to be supplied. This is realised in many conventional island networks by having a diesel generator as the network former. If such a network is extended by a renewable source, the diesel generator is relieved by the amount of the renewable source which can lead to an operation at an inappropriate, because noneconomic, operating point. At the borderline case the generated renewable power rises above the load within the island network. Within this case the produced renewable power have to be reduced or additional loads, so called dump loads, have to be switched on, in order to ensure the equilibrium between generation and consumption.

For these reasons it could be reasonable to arrange an additional network former in island networks with an appreciable share of renewable generation, which is able to establish the power equilibrium through intermediate storage of the electrical energy. Battery inverters are well suited for such applications. The disadvantage of battery storage is the high investment cost and the intensive maintenance in order to guarantee a long life cycle. With an appropriate dimensioning of the inverter and the battery storage it is feasible to supply the complete island network for a certain period.

An innovative approach of a parallel connection of voltage controlled inverters has been introduced in [Eng01] for single-phase systems. There the behaviour of inductive coupled voltage sources and synchronous machines, which can be described in form of

$$f_{grid} = f(P) \text{ and } U_{grid} = f(Q) \tag{3.1}$$

was implemented in a voltage controlled inverter. A more detailed description of the droop functionality is given in Figure 17.

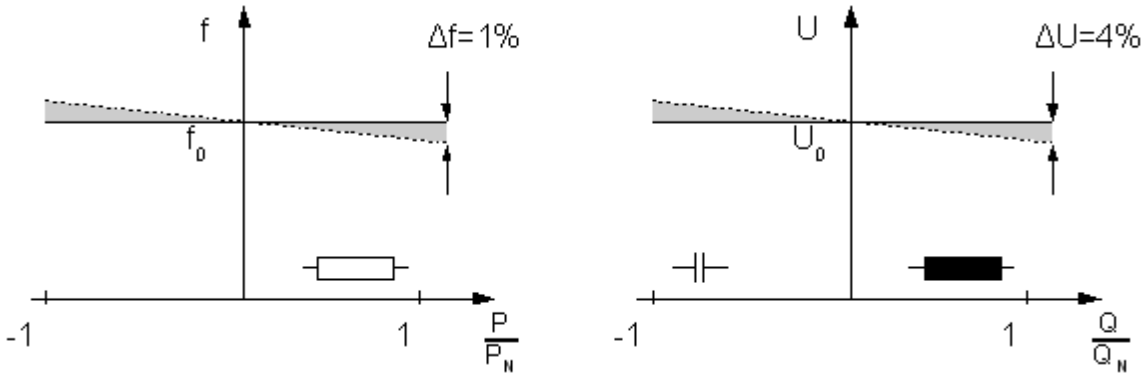

Figure 17: Conventional droops in the interconnected grid [Eng05]

The advantage of this approach lies in the power-output distribution among the sources without using additional communication, because exclusively available quantities as network frequency and network voltage are used. With an appropriate design of the droops a power-output distribution according to the capability of the particular systems is reached. Through an adjustment of the parameters the systems can realise special functions as for example battery charge operation. Supply systems with droop functionality can be extended easily and the reliability of the network increases through the so-called Multi-Master concept where every network participator containing a droop.

As described in section 2.2 the energy transmission in the low voltage network does not base on inductive coupling, but the resistive coupling dominates what in fact demands an adaptation of the droops in form of

$$f_{grid} = f(Q) \text{ and } V_{grid} = f(P) \quad (3.2)$$

In [Eng05] consequences of the coupling of different types and direction of droops are analysed. It was assessed that due to the indirect effectiveness also the conventional droops can be used within the low voltage network in order to maintain the compatibility with generators of superior networks with conventional droops. Alone a direct voltage control with these droops is not possible.

3.2.2. Droop Control

In the following section the developed droop control functionality for the SMA Sunny Island 5048 battery inverter is described in detail.

3.2.2.1. Overview on the system

"DroopControl" is a load flow management system based on the ISET "SELFSYNC" control method [Eng01] for parallel operation of grid forming inverters. This method allows the influence on active/reactive power flows by changing setpoints for frequency/voltage in analogy to a synchronous generator.

The "DroopControl" module covers the following parts of the operational system management of the Sunny Island 5048 battery inverter (Remark: during the devopment phase it was named "SI4248 Series II"):

- Battery charge control
- Voltage / frequency control (in terms of "Secondary and tertiary control")
- Synchronisation to external voltage sources (genset/grid)
- Active and reactive power management
- Steady state overload derating
- Thermal derating

Figure 18 gives an overview on the overall structure. The specific functionality of each part will be described separately below. Table 2 shows abbreviations and terms of Figure 18. In general the structure consists of a set of parallel operating PI or I – controllers. The selection of suitable limitations at the outputs of the controllers decouples the different functions.

Table 2: Abbreviations and terms of Figure 18.

V_loop	Isochronous voltage controlled mode

I_loop	Current controlled mode
V_slfsnc	SELFSYNC-voltage controlled mode (formerly known as "Droop-Mode")
V_ext	SELFSYNC-voltage controlled mode synchronised to external voltage source
Cluster	Set of "Sunny Islands" linked to ONE battery (up to 4 in single phase configuration, 2 or 4 in Split phase config. 3 in three phase configuration)
HOLD MAX / HOLD MIN	Special functions for I-controllers. In case of activation, upper (MAX) or lower (MIN) limit of I controller is dynamically adjusted to the present output value of the integrator

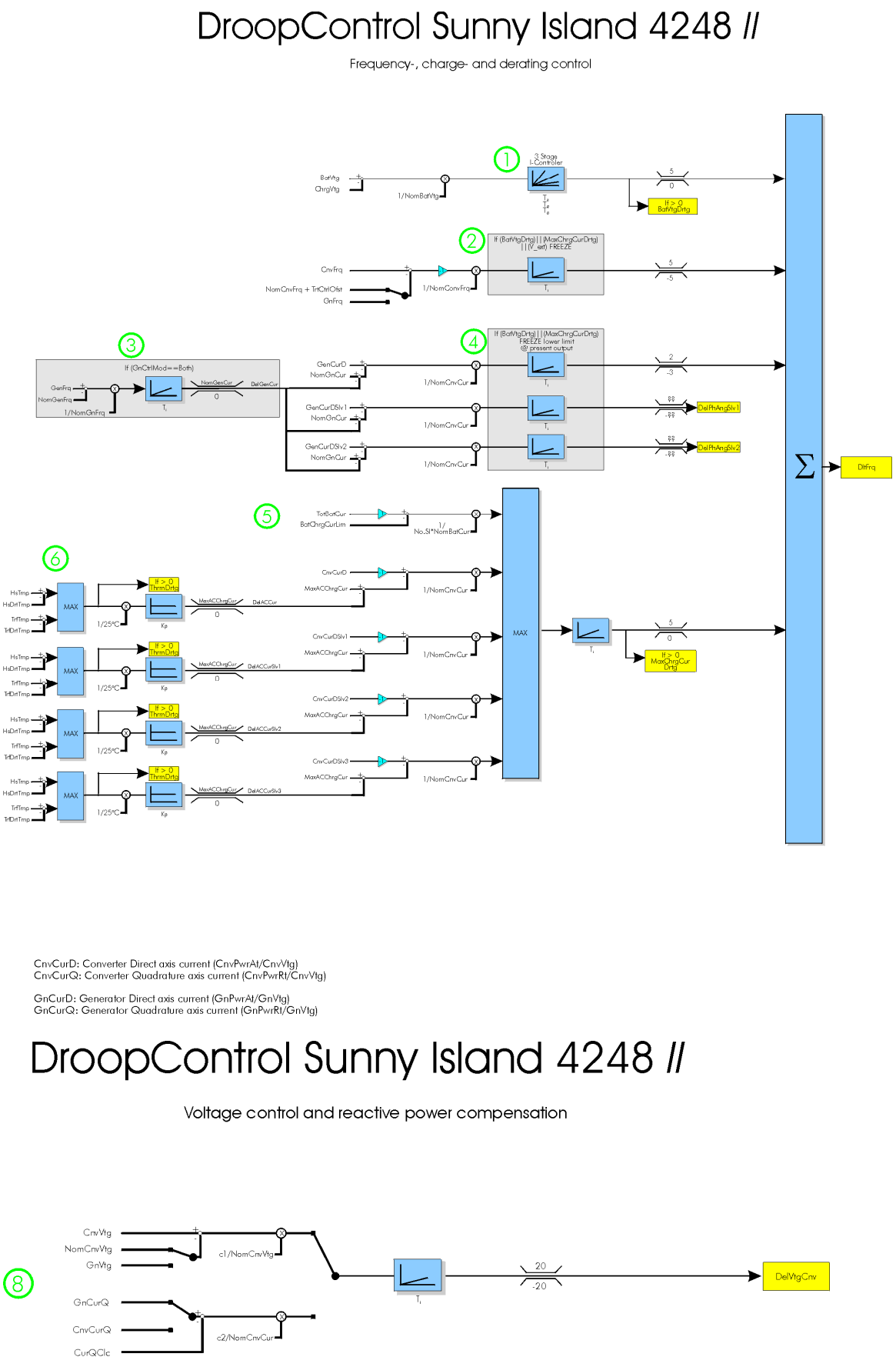

Figure 18: Droop Control of Sunny island 4248

3.2.2.2. ISET-SELFSYNC

Figure 19 shows the usage of the ISET Selfsync algorithm in a three phase configuration. The master inverter (phase L1) generates a synchronisation pulse each wrap around of the sine argument. This signal is transmitted to the slaves. The phase argument of the slaves is then reseted to the specified phase shift (+- 120deg).

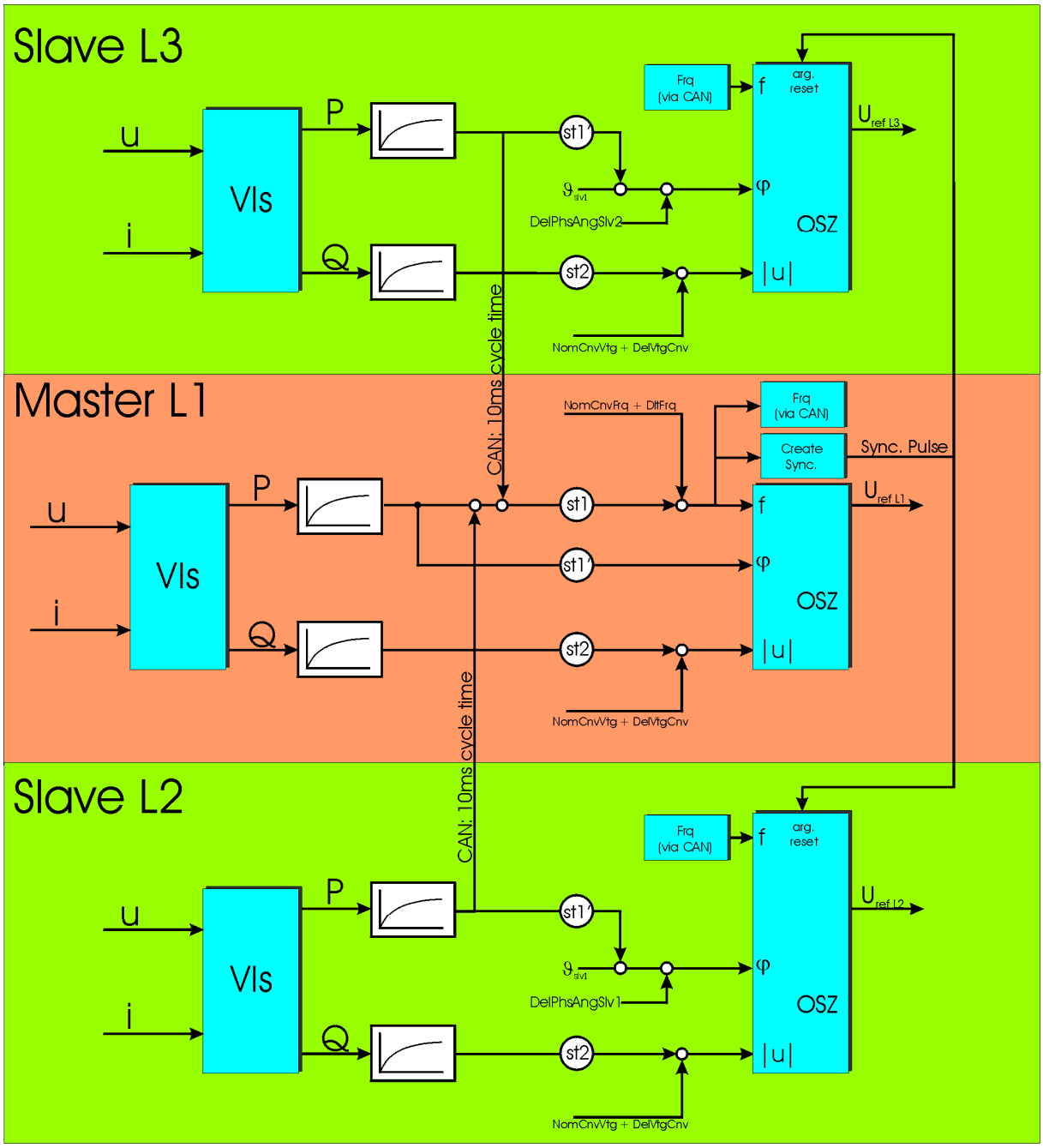

Figure 19: ISET Selfsync in a three phase system

3.2.2.3. Description of the modules

In this section the modules shown in Figure 18 are described in detail.

3.2.2.3.1. Battery voltage control

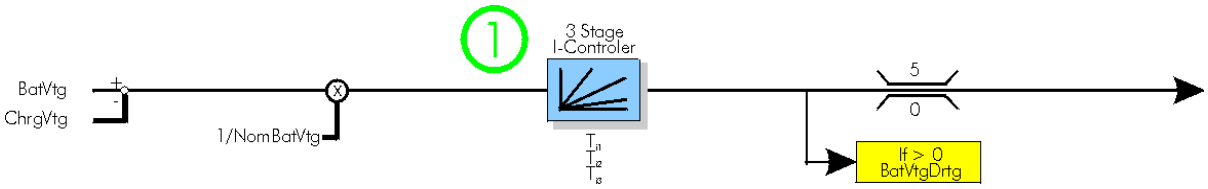

Figure 20: Battery voltage control

Table 3: Description of the battery voltage control

Function	Protects battery from overcharging	
Technology	limited 3 Stage I controller (same as SI4500/SI4248) with dynamic limit adjustment (HOLD-MAX Function) → see Figure 21 According to the stage, a different set of T_i parameters is being used. This method is suited best to handle the very sensitive steady state stability with fully charged batteries and the very fast derating of Sunny Boy inverters	
Activation	Calculated on Master and always "ON" HOLD-MAX, if no power flow (TotCnvPwrAt) from AC -> DC (threshold according to accuracy of measurement and No. SI; Function should be disabled in systems where DC chargers are used as "grid tie system")	
Cycle time	20ms	
Input	BatVtg ChrgVtg	battery voltage charge voltage setpoint
Normalisation	NomBatVtg	nominal battery voltage
Output	deltaFrequency Signal: BatVtgDrt	

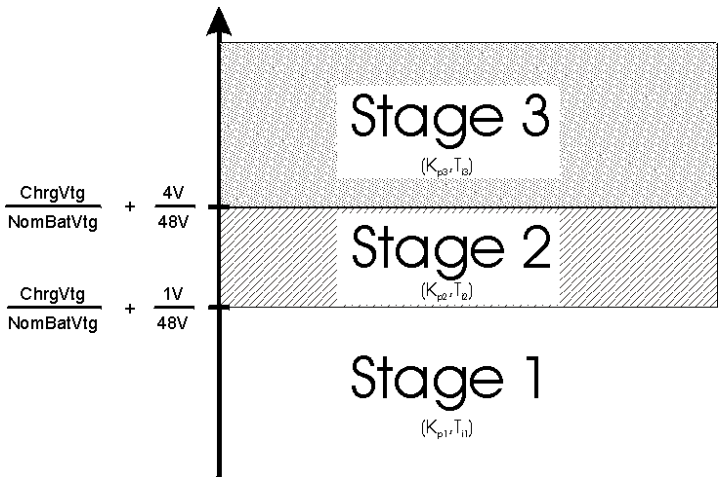

Figure 21: Three stage I-Controller

3.2.2.3.2. Frequency control

During V_slfsnc operation the setpoint "NomCnvFrq + TrtCtrlOfst" is selected. Thus a secondary and tertiary control for the non-isochronous SELFSYNCâ is achieved.

By selecting the measurement value of the external frequency "GnFrq " the system frequency is synchronised to an external source.

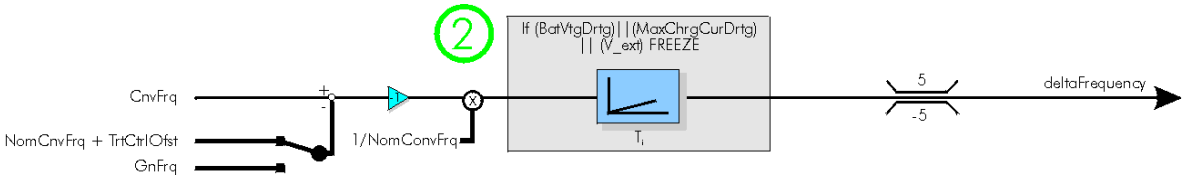

Figure 22: Frequency control

Table 4: Description of the frequency control

Functions	secondary + (part of) tertiary frequency control synchronisation to external frequency (grid, genset
Technology	limited I- controller
Activation	calculated on Master and only in single cluster configuration "On" with setpoint "NomCnvFrq + TrtCtrlOfst": V_slfsnc && FrqCtrl==ENABLED "On" with setpoint "GnFrq": V_slfsnc && Synchronising "Freeze": V_ext || BatVtgDrt || MaxChrgCurDrtg "Off":

	FrqCtrl==DISABLED || with SunnyIsland Control	
Cycle time	100ms	
Input	CnvFrq	converter frequency
	NomCnvFrq	nominal converter frequency
	TrtCtrlOfst	frequency offset due to tertiary control
	GnFrq	frequency of external grid
Normalisation	NomCnvFrq	nominal converter frequency
Output	deltaFrequency	

3.2.2.3.3. External current control (generator, grid)

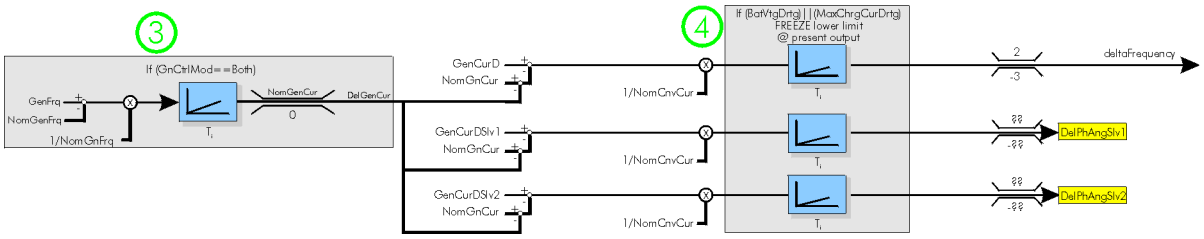

Figure 23: External current control

Functions	(4) Loads generator with its nominal current NomGnCur in order to achieve optimum efficiency. Protects generator from overload. Generator support. Additional function: (3) "generator stall" protection (required for small hydro turbines)
Technology	limited I- controller with output deltaFrequency According to [Eng01] a phase angle deviation determines the active power output of the inverter. An individual active power flow control can be achieved for each phase by controlling the phase angle setpoints. limited I- controller with output deltaPhsAngSlv1 limited I- controller with output deltaPhsAngSlv2 **Remarks:** In Single-Phase configuration all deltaPhsAngSlvX are obsolete. In Dual-Split-Phase configuration deltaPhsAngSlv1= deltaPhsAngSlv3 and deltaPhsAngSlv2 is obsolete. **"Generator stall" protection (3) for hydro turbines:** During "low water" periods the turbine delivers only a fraction of its

	nominal current. The Generator current controller would try to load the turbine up to its nominal current and thus stall it. Frequency drops to the lower boundary of the I-controller. In order to avoid this an additional I-controller is able to lower the setpoint for the nominal generator current NomGnCur.	
Activation	calculated on Master and only in single cluster configuration "On": V_ext "Off": V_slfsnc Freeze lower boundary of (4) @ present output: V_ext && (BatVtgDrt || MaxChrgCurDrtg) On status change V_ext -> V_slfsnc: Ramp integrator of I controllers back to 0	
Cycle time	100ms	
Input	GenFrq	generator frequency
	NomGenFrq	nominal generator frequency
	NomGenCur	nominal generator current
	GenCurD	direct axis generator current
	GenCurDSlv1	direct axis generator current Slv1
	GenCurDSlv2	direct axis generator current Slv2
	GenCurDSlv3	direct axis generator current Slv3
Normalisation	NomCnvCur	nominal converter current (4)
	NomGenFrq	nominal generator frequency (3)
Output	deltaFrequency	
	DelPhsAngSlv1	
	DelPhsAngSlv2	
	DelPhsAngSlv3	

3.2.2.3.4. Thermal derating

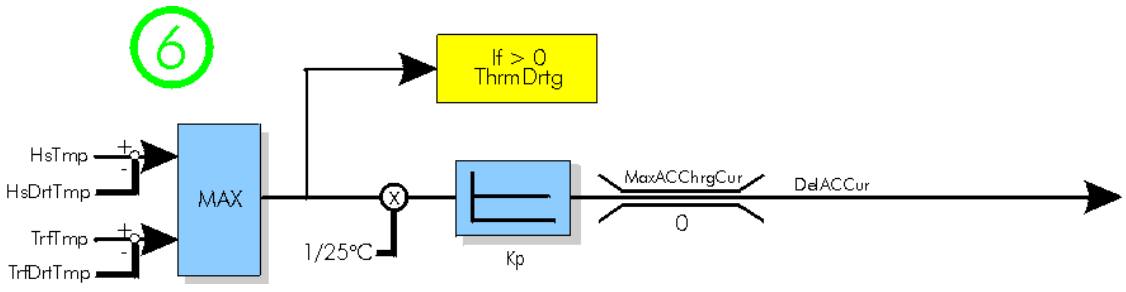

Figure 24: Thermal derating

Functions	Derating of AC current in case of heatsink or transformer overtemperature	
Technology	limited P- controllers with output DelACCur amplification approx. 10A/°K	
Activation	calculated on each SI and always "On"	
Cycle time	>100ms	
Input	HsTmp	heatsink temperature
	HsDrtTmp	heatsink derating temperature
	TrfTmp	transformer temperature
	TrfDrtTmp	transformer derating temperature
Normalisation	25°C	
Output	DelACCur	derating current (input to 0)
	Signal:	ThrmDrtg (for informational purpose only)
Remarks	Thermal derating of one device affects all devices of the cluster	

3.2.2.3.5. Charge current derating

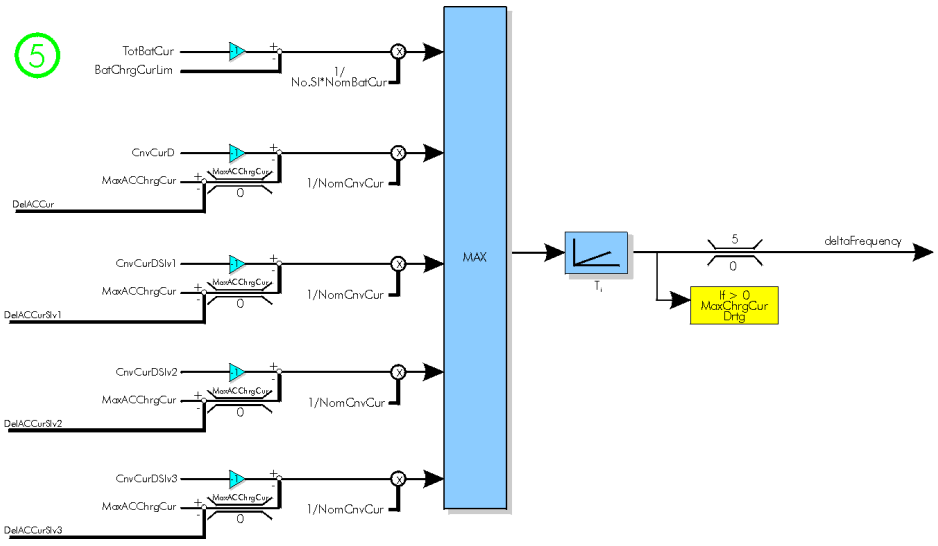

Figure 25: Charge current derating

Functions	Derating of AC charge current in case of steady state overcurrent or thermal derating Derating of DC charge current (TotBatCur).
Technology	limited I- controller
Activation	calculated on Master SI and always "On" TotBatCur derating only if battery current shunt installed

Cycle time	100ms	
Input		
Normalisation	**TotBatCur derating:** (No. Sunny Islands * NomBatCur) **CnvCurD derating:** NomCnvCur	
Output	CnvCurD	Converter current direct axis Master
	CnvCurDSlv1	Converter current direct axis Slave1
	CnvCurD Slv2	Converter current direct axis Slave2
	CnvCurD Slv3	Converter current direct axis Slave3
	DelACCur	derating due to overtemperature
	DelACCurSlv1	derating due to overtemperature
	DelACCurSlv2	derating due to overtemperature
	DelACCurSlv3	derating due to overtemperature
	MaxACChrgCur	max AC charge current
	TotBatCur	battery current
	BatChrgCurLim	max. DC charge current
	No. SI	number of SI in this cluster
Remarks	deltaFrequency Signal: MaxChrgCurDrtg	

3.2.2.3.6. Voltage control / reactive power compensation

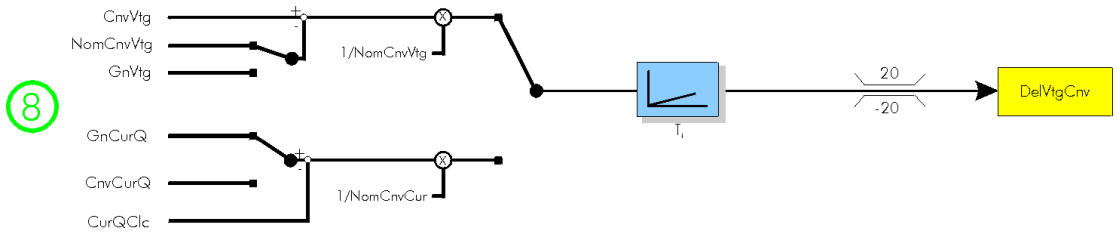

Figure 26: Steady state voltage control

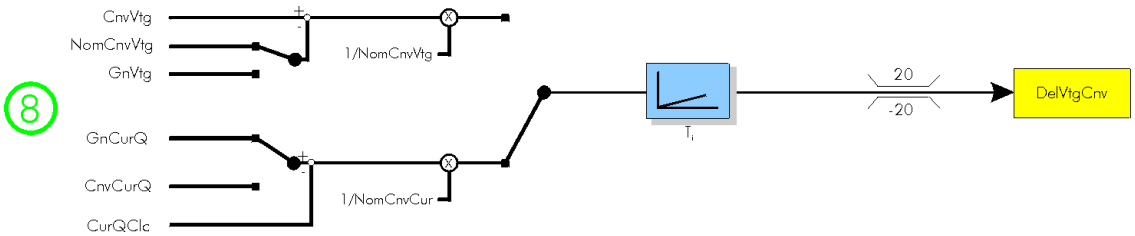

Figure 27: Reactive power control at the generator

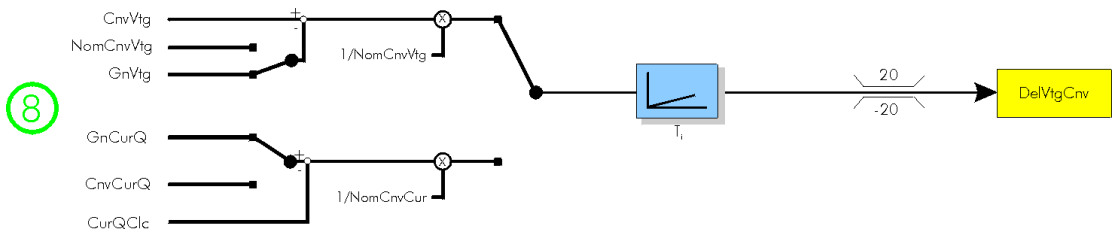

Figure 28: Synchronisation to external voltage

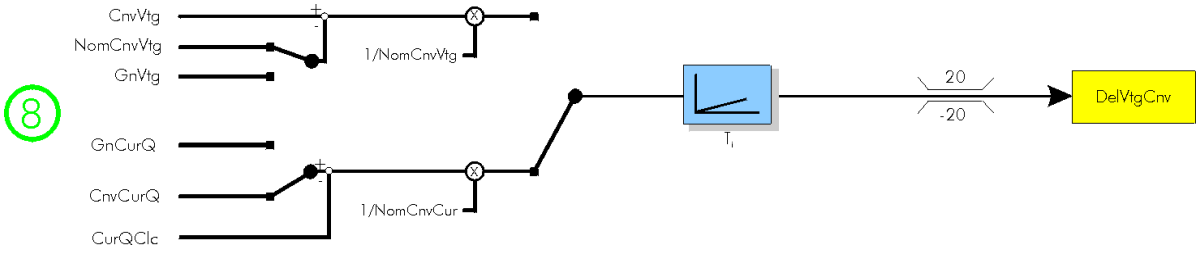

Figure 29: Reactive power control at the Sunny Island

Functions:	- Steady state voltage control (Figure 26) - voltage synchronisation to external voltage source (Figure 28 - reactive power compensation at external voltage source (Figure 27) - reactive power compensation at Sunny Island (Figure 29)	
Technology	limited I- controller	
Activation:	- Once per phase - Only in single cluster systems - OpMode "V_slfsnc" -> voltage control setpoint "NomCnvVtg" during Synchronisation -> voltage control setpoint "GnVtg" - OpMode "V_ext" -> reactive power control setpoint "GnCurQ" or "CnvCurQ"	
Cycle time	100ms	
Input	CnvVtg	Converter voltage
	NomCnvVtg	nominal converter voltage
	GnVtg	generator voltage
	GnCurQ	Generator current quadrature axis
	CnvCurQ	Converter current quadrature axis
	CurQClc	reactive power component (default = 0 A)
Normalisation	NomCnvVtg NomCnvCur	
Output	DelVtgCnv	AC voltage offset for each SI on this phase

3.2.3. Additional control possibilities through developed droop control

Especially through the enhancements of active and reactive power management it is possible to provide additional voltage control functionalities as described in chapter 4. Additionally communication interfaces provide the possibility for defining set-points for the inverter by using a centralised Microgrid-Controller and for coordinate several inverters in a meshed low voltage Microgrid e.g. for voltage control.

3.3. Advanced control capabilities of generation units in Microgrids

In the next chapters advanced voltage control capabilities of generation units are discussed in detail. Therefore simulations and experiments are provided. In chapter 4 an approach of controlling the voltage in meshed low voltage grids with droop inverters is presented. For this approach, simulation calculations and measurement results are given. It should be shown, that using reactive power injection, which can be done through the operational control described in the section before, together with droop concept in resistive networks can control the voltage more effectively than using only reactive power without inverters with the droop mode concept.

The second approach of voltage control strategies is the principle of inductive decoupling. It provides the possibility to control the voltage within a sub-network independently from the superior network within defined borders. Therefore a state of the art inverter with an additional decoupling inductor and advanced control algorithms come into operation. This inverter could be a stand-alone device only responsible for the voltage control in the sub-network, but also a combination of such a device with a PV-inverter is conceivable.

4. Voltage control strategies in meshed low voltage grids

Within this chapter an approach of voltage control within meshed low voltage grids is described. Section 4.1 explains the approach; section 4.2 gives first results from experiments carried out in DeMoTec of ISET, while section 4.3 shows simulation results achieved through simulations in DIgSILENT PowerFactory.

Since in transmission networks the line character is generally inductive and thus the voltage is controlled through reactive power, the reactive power sources and sinks and other reactive power compensation equipments are strategically positioned along the long transmission systems.

Shown in chapter 3 voltage control through injection of reactive power is not very efficient in low voltage networks with a resistive character. But if a network operates as a Microgrid in islanding operation an additional voltage control capability is useful. In chapter 3.2.1.2 it is stated that a direct voltage control with conventional droops is not possible. The following approach provides a possibility of an additional voltage control capability in Microgrids using inverters with droop functionality.

4.1. Approaches of voltage control through injection of reactive power in meshed low voltage grids

Aim of this approach is doing voltage control at the connection point of a load within a meshed low voltage network. In Figure 30 the most simple implementation of a meshed low voltage network is given. It consists of a triangle; an inverter is connected at each edge. In the middle of the network line between the two above inverters a load is connected. The yellow coloured inverters are state of the art battery inverters with droop functionality, e.g. the SMA Sunny Island 4500 or Sunny Island 5048. The lower, magenta coloured inverter has the functionality to inject a preset reactive current. In that case this inverter is able to work in over- and underexcited operation. Since the network has no reactive loads in that case, the injected reactive power has to be compensated by the other inverters. Since they work in droop mode, the compensated reactive power automatically change the output voltage due to the relation Q(V) (cp. Figure 17). The amount of reactive power needed for a voltage change depend on the slope of the Q(V)-curve. The higher the slope the less reactive power is needed for a voltage change. The more inverters running in a system, the more reactive power is needed, because all Q(V)-curve for all inverters have to be influenced through the reactive power.

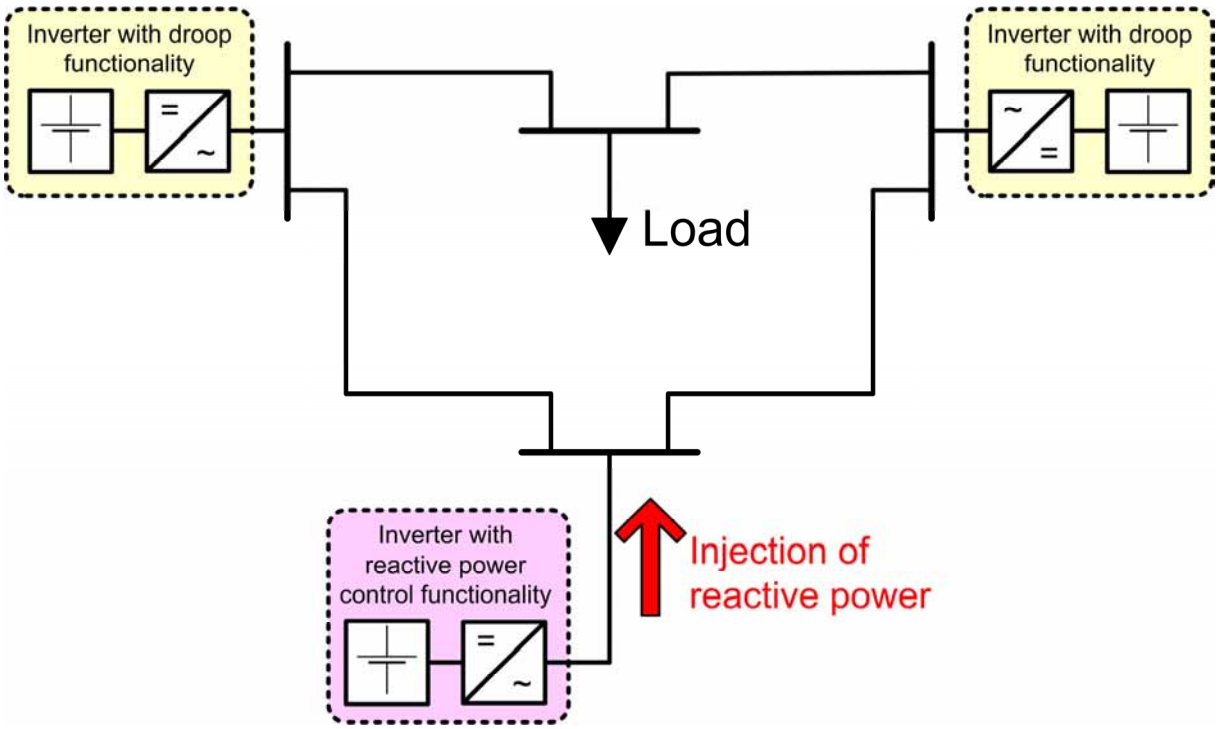

Figure 30: Approach of an additional voltage control capability in meshed low voltage networks through injection of reactive power

4.2. Experimental proof of voltage control capabilities in meshed low voltage grids

The configuration of Figure 30 has been built up in the DeMoTec of ISET. Together with SMA experiments have been done.

4.2.1. Experimental setup

A balanced three phase mesh grid is built up as shown in the diagrams of Figure 31 and Figure 32. Three 3 phase SMA battery inverter Sunny Island clusters are connected through a low voltage grid simulator as seen in Figure 31. The varying resistive load is achieved from a load simulator. Two of the clusters are built up from Sunny Island 4500 and the third from the new SMA Sunny Island 5048. The SI5048 is operated with extended software developed by SMA for this experiment in order to determine the injected reactive current by the inverter. The simulated line lengths are given in the Table 5 as calculated from the typical line parameter information for low voltage lines given in Table 1. Measurements of the required parameters (voltage, current, active and reactive power) are taken at the nodes of each inverter and at the load on phase 1 as shown in Figure 32.

One cluster was switched on to form the grid and the others had to synchronise to this formed grid. A defined load was connected to the grid. Afterwards the reactive power injected

by the SMA Sunny Island 5048 was manually changed. Reactions on the voltage are monitored with the Haag power analyser device. Although the system is build up as a three phase system, measurements were made only for a single phase due to no expected unbalance.

Table 5: Line resistances and lengths of the experiment in the DeMoTec [Tin08]

Line	Line resistance [Ω] of line simulator	Corresponding Line length [m]
R_{12}	0.0575	90
R_{13}	0.045	70
R_{2L}	0.115	179
R_{3L}	0.115	179

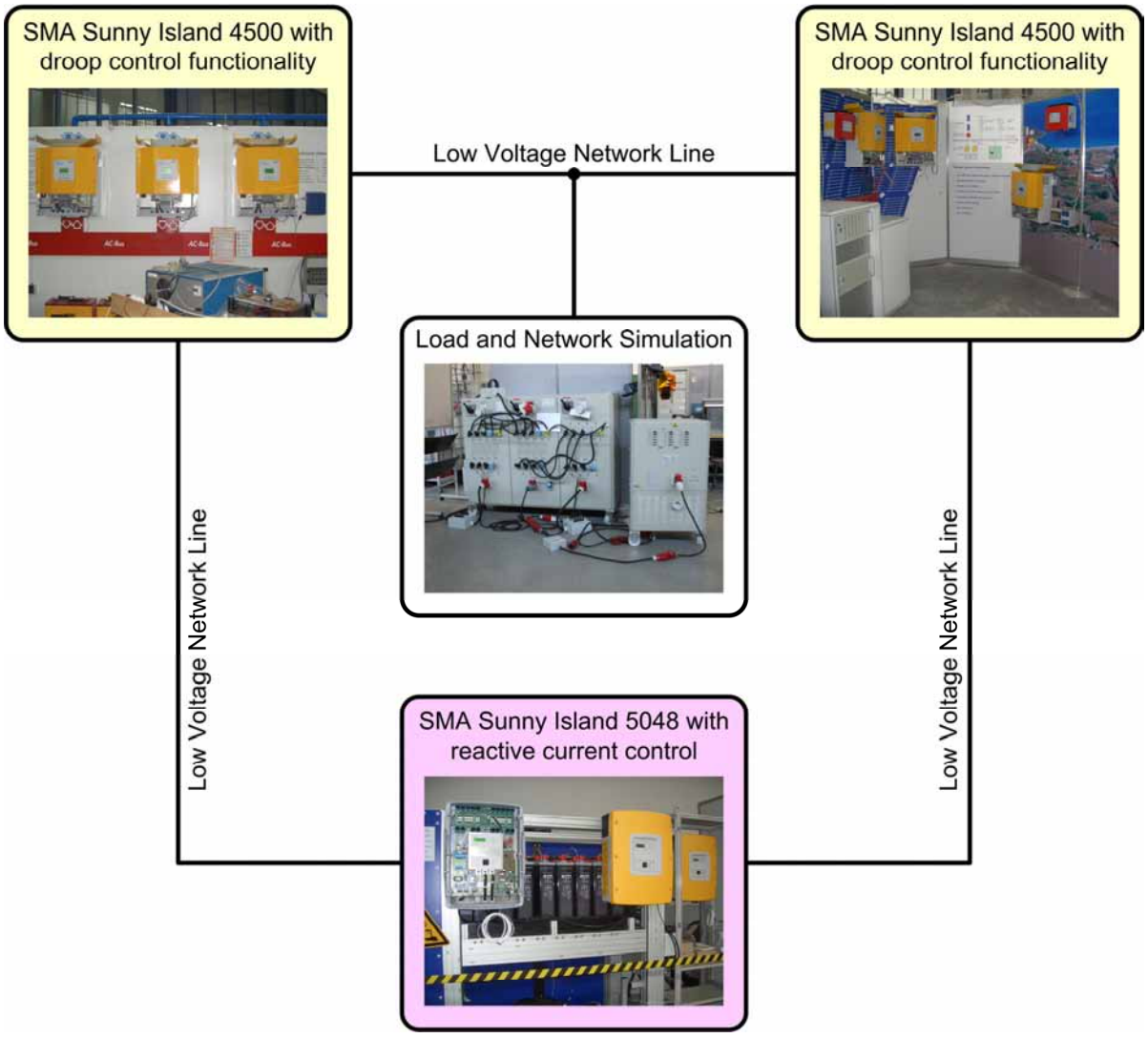

Figure 31: Experiment setup at ISETs DeMoTec hall.

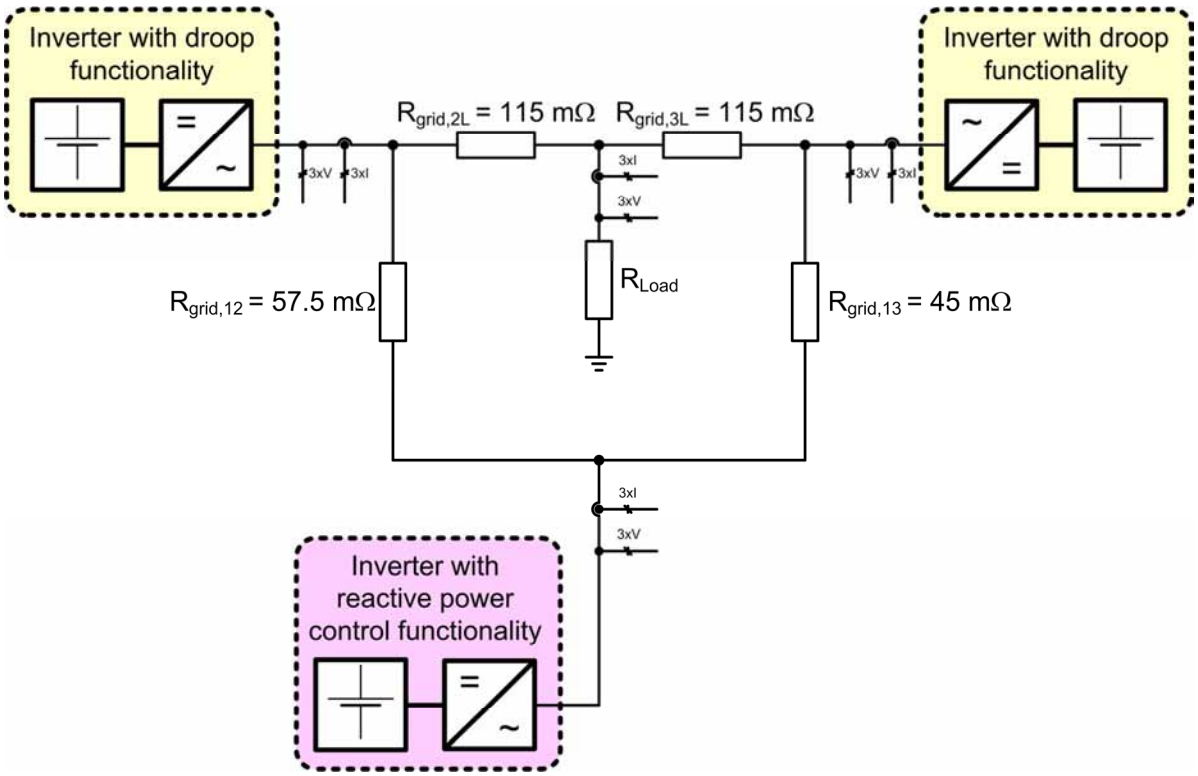

Figure 32: Equivalent circuit diagram of the experimental setup of Figure 31

4.2.2. Experimental results

Figure 33, Figure 34 and Figure 35 show measurement results of the above described experiment. In Figure 33 and Figure 34 a resistive load of 1300 W is used while in Figure 35 a resistive load of 3000 W is connected to the network. The injected reactive current of the SMA Sunny Island 5048 is varied manually. It can clearly be seen that for each change of the reactive current also the voltage at the load changes. The more inductive reactive power is injected by the SMA SI 5048, which has to be compensated by the other Sunny Island inverters with droop mode with capacitive reactive power since there is no reactive load within the network, the higher the voltage at the load becomes (cp. Figure 17). The other way around, if the SMA SI 5048 is injecting capacitive reactive power, the voltage decreases.

Figure 36 describes the relation between voltage at the load and injected reactive power from the SI 5048 for the measurement results. It can be clearly seen that the slope of the curve is independently from the load value, assumed a pure resistive load. The slope of the curve depends of the droop parameters of the inverters working with the droop functionality.

Figure 37 shows a 3D-diagram of the voltage in dependence of the load and the injected reactive current. Out of the measurement points (dots) the shown data is interpolated.

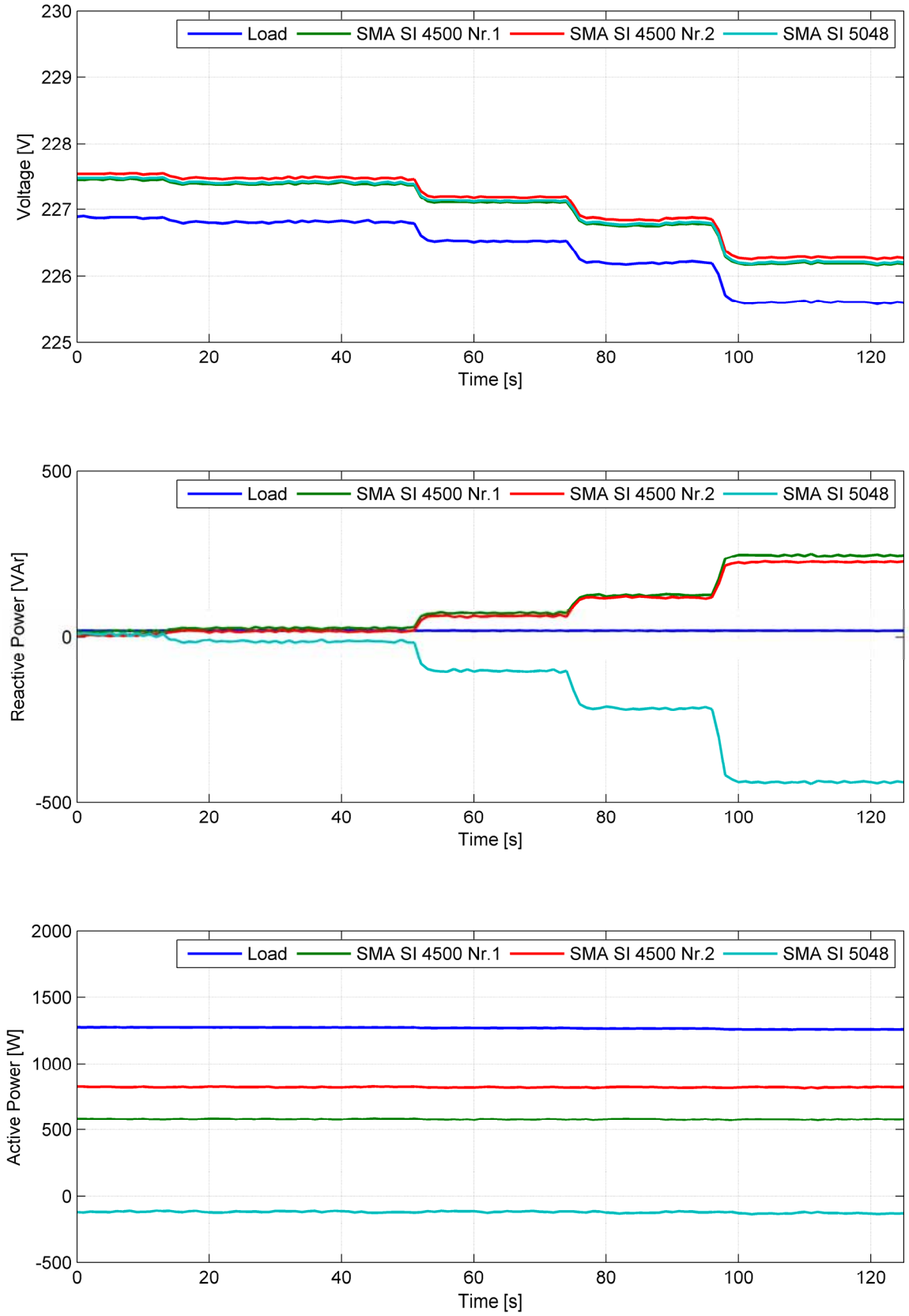

Figure 33: Constant load, Q injection varied in negative direction

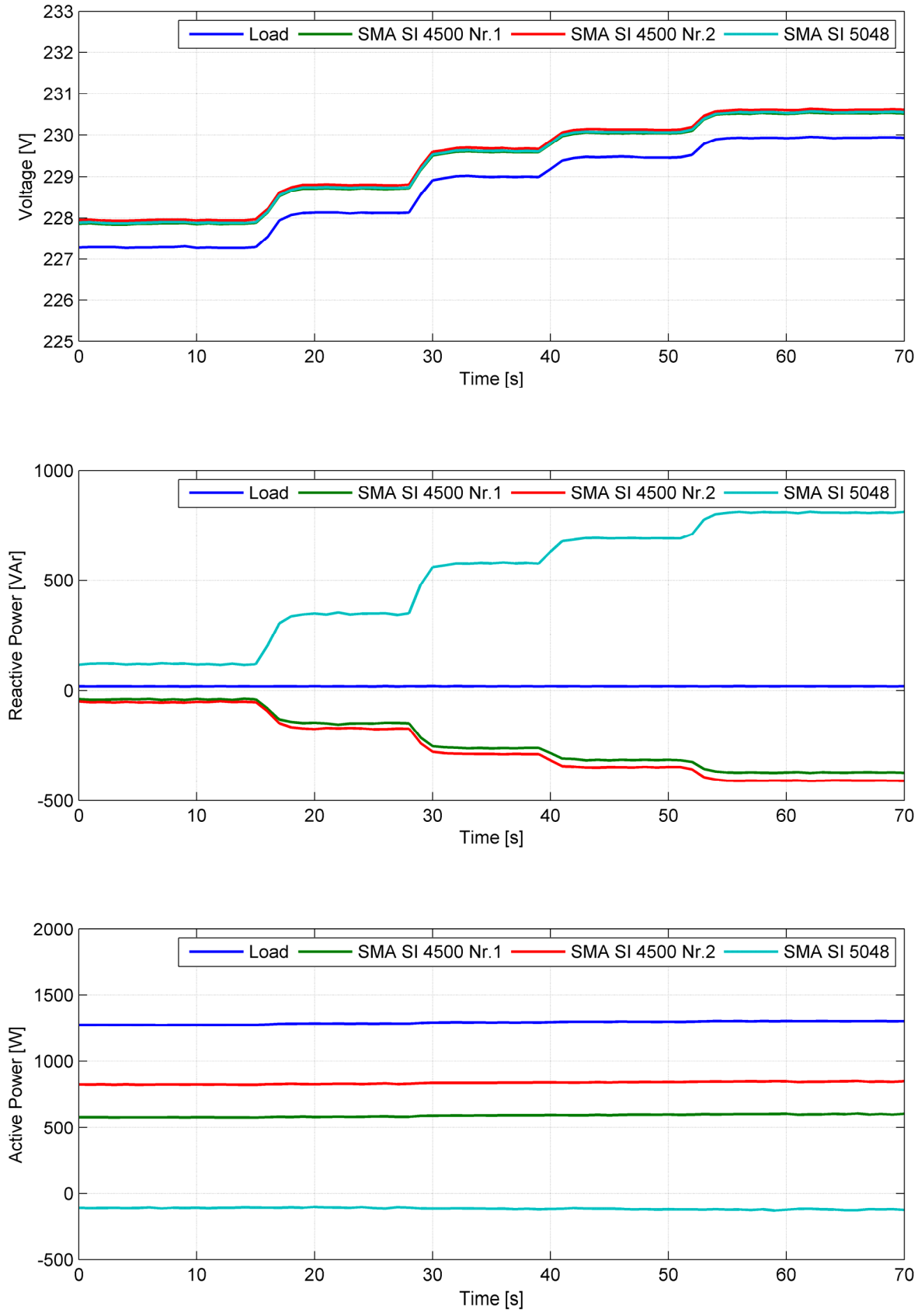

Figure 34: Measurements for a constant load, Q injection varied in positive direction

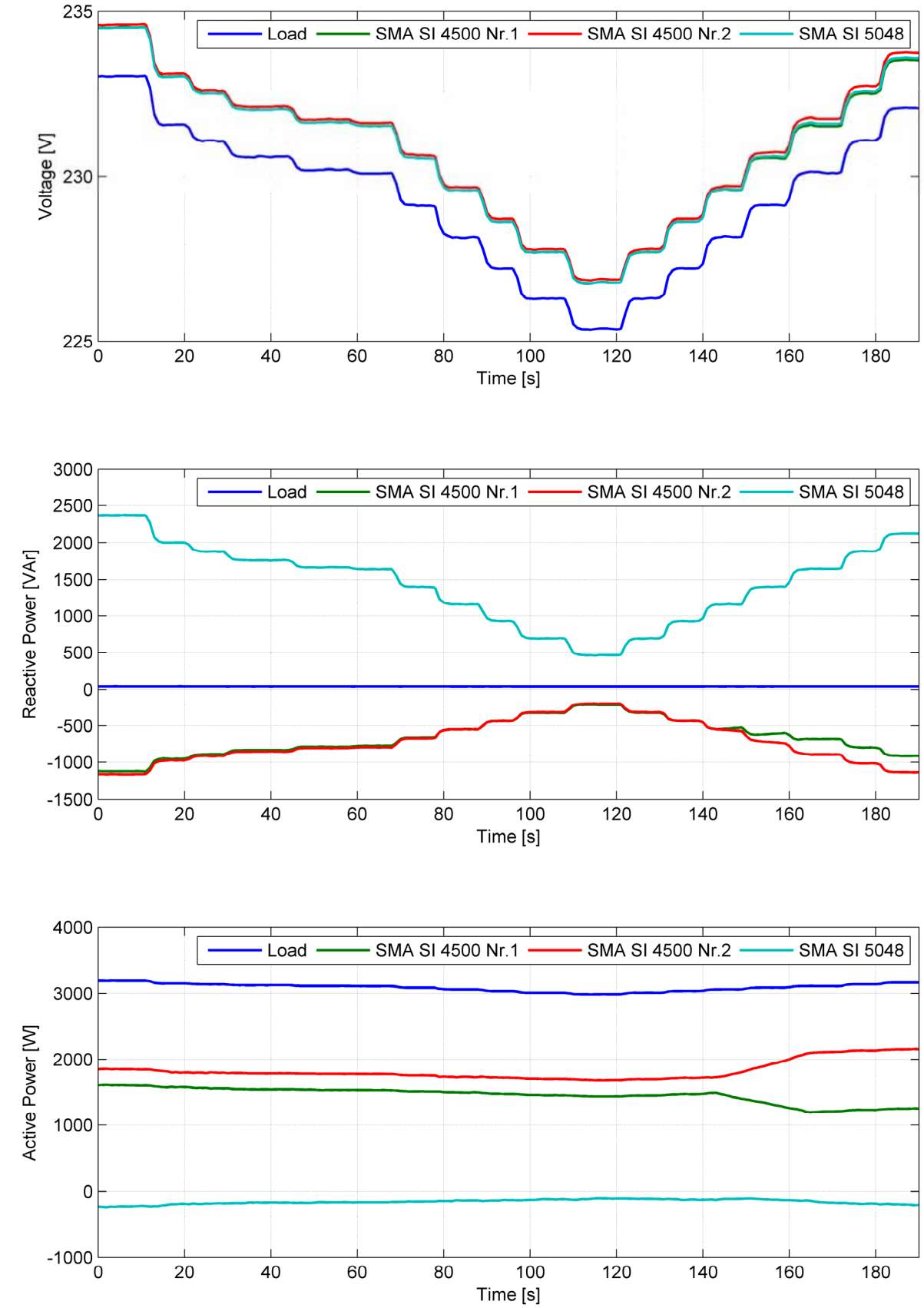

Figure 35: **Measurements for a constant load, Q injection varied.**

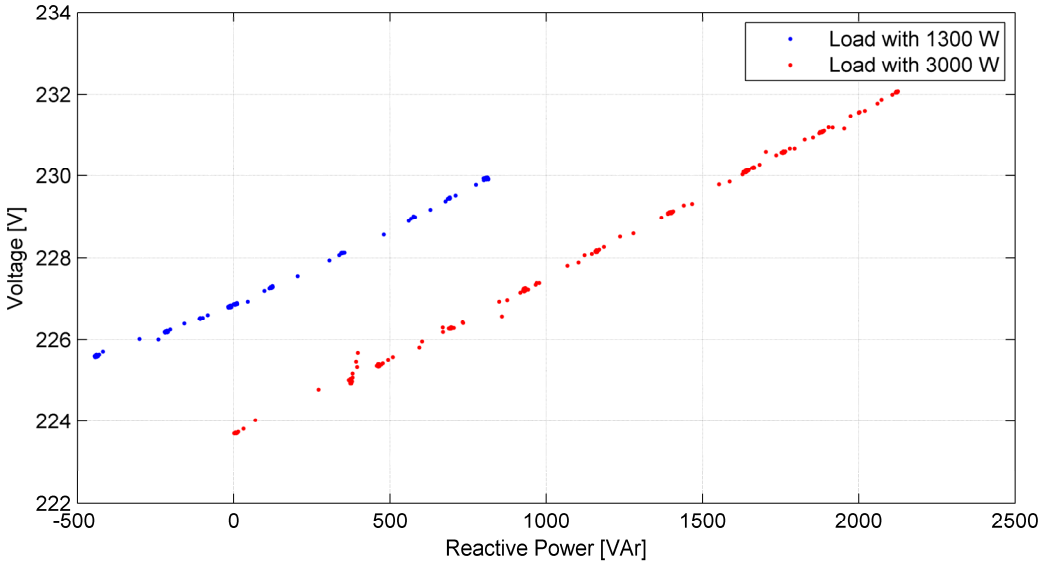

Figure 36: Measured U over Q behaviour for a constant load of 1300 W and for a load of 3000 W.

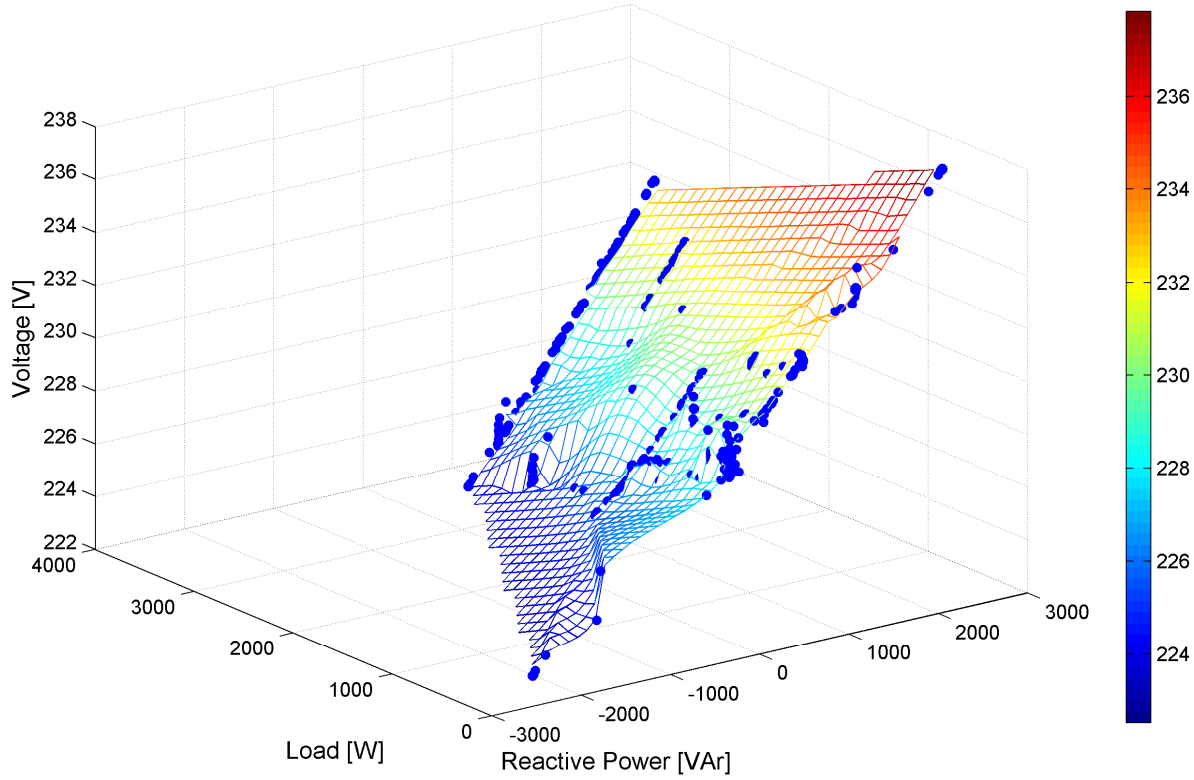

Figure 37: Interpolation of the measurement data. Voltage over reactive power and load.

4.3. Simulations for meshed low voltage grids

Simulations for a detailed proof of the approach are carried out with the program DIgSILENT PowerFactory. The simulation is a three phase, but here given results are only for single phase in order to be comparable with the measured data from the experiment.

4.3.1. Simulation setup

The models used for the simulation of the SMA Sunny Island 4500 with the droop control have already been developed within a diploma thesis [Bra05]. The inverter providing only reactive power for is modelled as "static generator" within PowerFactory. The network lines are combinations of resistive and inductive components in order to set the corresponding network impedance value. The set-points for the active and reactive current output of the inverter are calculated by the control using the active and reactive power of the static generator model. The set-points for the reactive power can be given either by the user or in a second step the reactive power is used for an automatic control of the load voltage.

The simulations are carried out with the so-called instantaneous method for electromagnetic processes with a step size of 0.1 ms. Figure 38 shows the setup of the simulation.

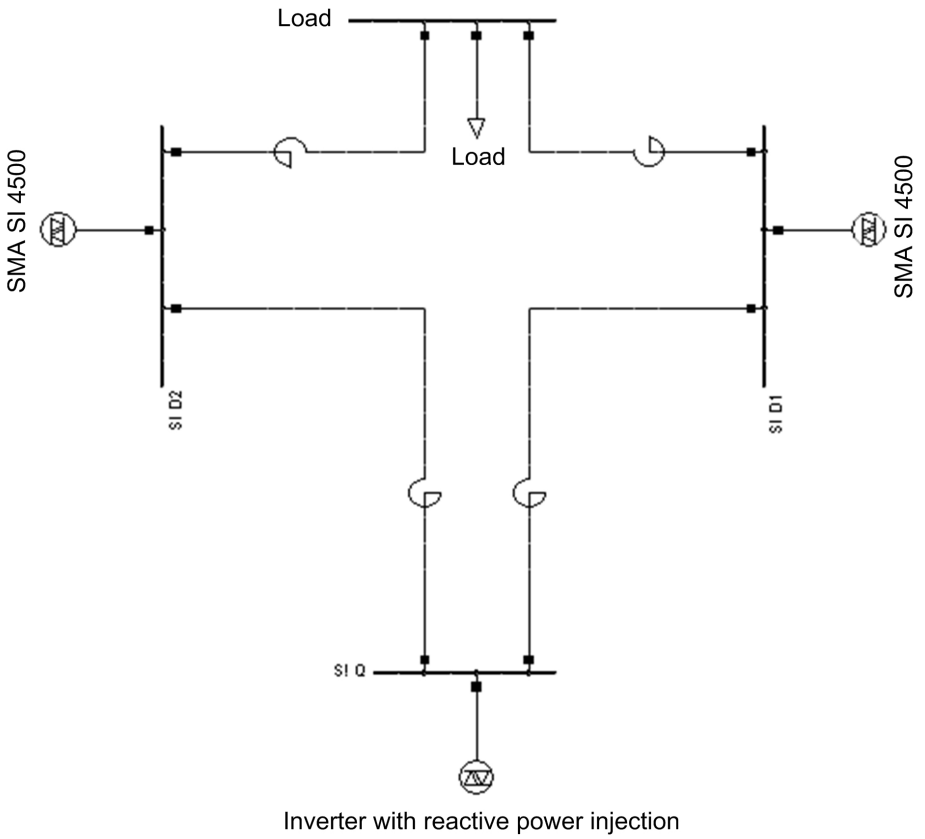

Figure 38: Setup of the simulation within DIgSILENT PowerFactory for comparision with experimental results.

4.3.2. Simulation results

The following subsections present the results of the simulations. After a comparison with conventional methods of voltage control, simulations for this actual approach with varying parameters are performed. In the end a possibility of the direct control of the load voltage is simulated.

4.3.2.1. Comparison with conventional voltage control through reactive power

Figure 39 shows the changes of the voltage at the load for several injections of reactive power. For the simulation the circuit of Figure 38 is used. In order to compare this approach with the conventional method for voltage control through reactive power, two independent simulations with the same boundary conditions are performed. The difference is that for the conventional method the inverters have no droop control. Therefore the voltage change is achieved by the injected reactive power itself.

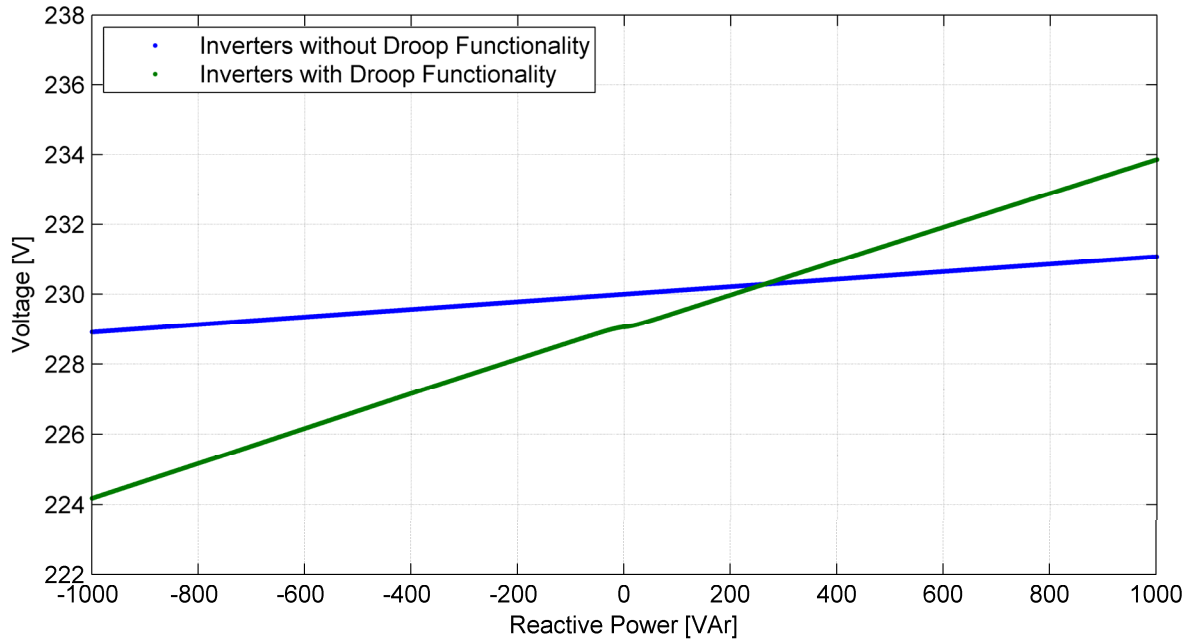

Figure 39: Comparison between conventional voltage control with reactive power and voltage control with inverters having droop functionality. Simulation results.

The simulation results show that the achievable voltage change using the same amount of reactive power for inverters with droop functionality is clearly higher. There is a maximal voltage change of approximately 9.7 V for a reactive power from -1000 VAr to 1000 VAr using this approach. In contrary with the conventional method only a voltage change of 2.2 V for the same range of reactive power can be reached.

For these conditions it can be stated that the approach of injecting reactive power in meshed grids consisting of inverters with droop functionality is five times more efficient than conventional injection of reactive power in regard to voltage control.

4.3.2.2. Influence of the slope of the Q(V)-curve on the voltage change factor

The comparison of the effectiveness of this approach with the conventional method directly depend on the slope of the Q(V)-curve. Figure 40 shows simulation results for two different slopes of the Q(V) droop. The smaller the slope the lower is the voltage change difference for the same amount of reactive power. That means that less reactive power is needed to achieve the same voltage change if a higher slope of the Q(V) droop is used.

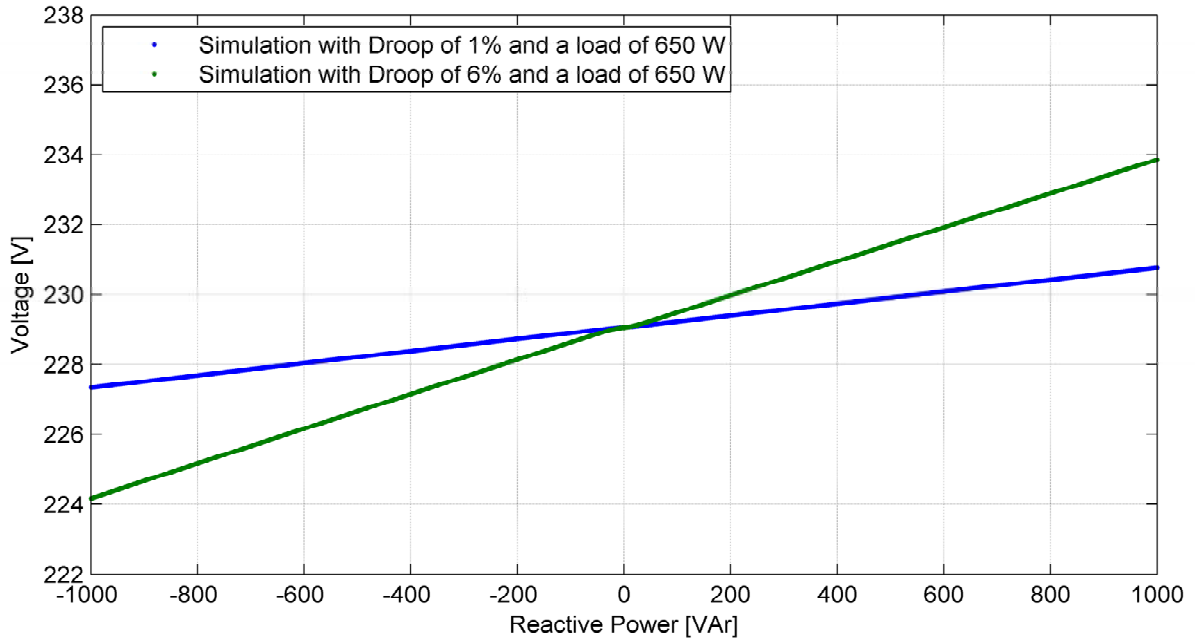

Figure 40: Simulation and measurement result for single phase

4.3.3. Simulation of load and reactive power variations

Figure 41 shows simulation results for variations of the load and the injected reactive power. The load is varied between 0.66 kW and 3.3 kW while the reactive power is varied in steps 0.4 kVAr from 1.2 kVAr capacitive to 1.2 kVAr inductive. The more inductive reactive power is injected, the higher the voltage at the load become. The other way around the more capacitive reactive power is injected; the lower is the voltage at the load. For higher values of the load the voltage decreases for all kind of reactive power injections.

Since in the simulation only selected points are used, in Figure 42 an interpolation of the simulation results is presented. The load is varied from 0 to 4000 W and the reactive power injection is varied from -1.5 kVAr to 1.5 kVAr.

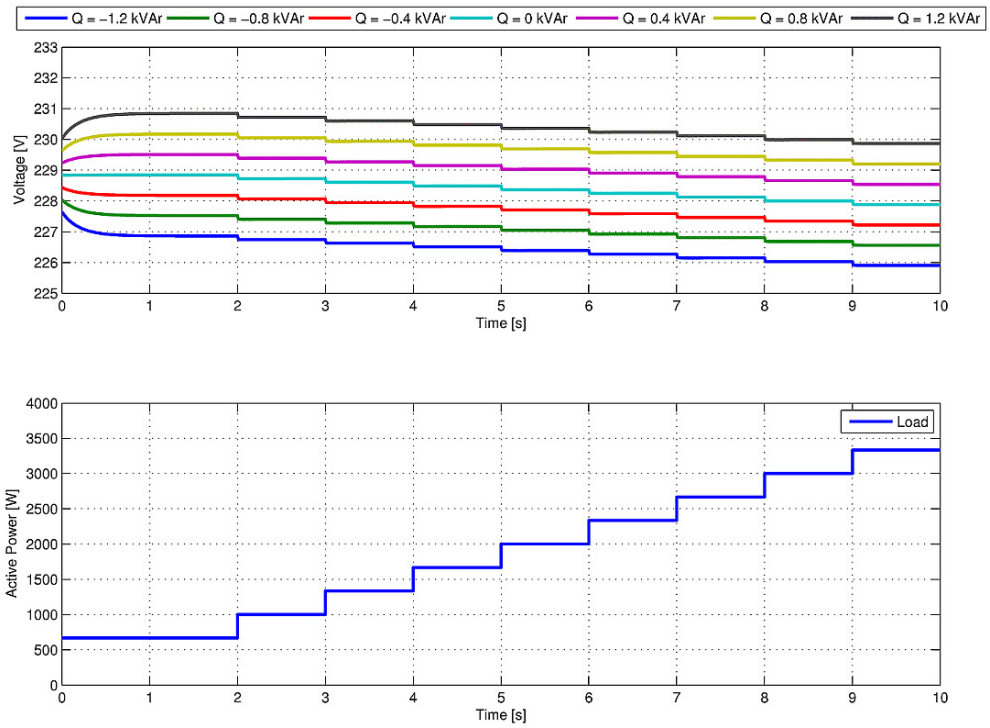

Figure 41: Voltage at the load for several reactive power injections at busbar SI Q of network configuration shown in Figure 38. Simulation results with PowerFactory.

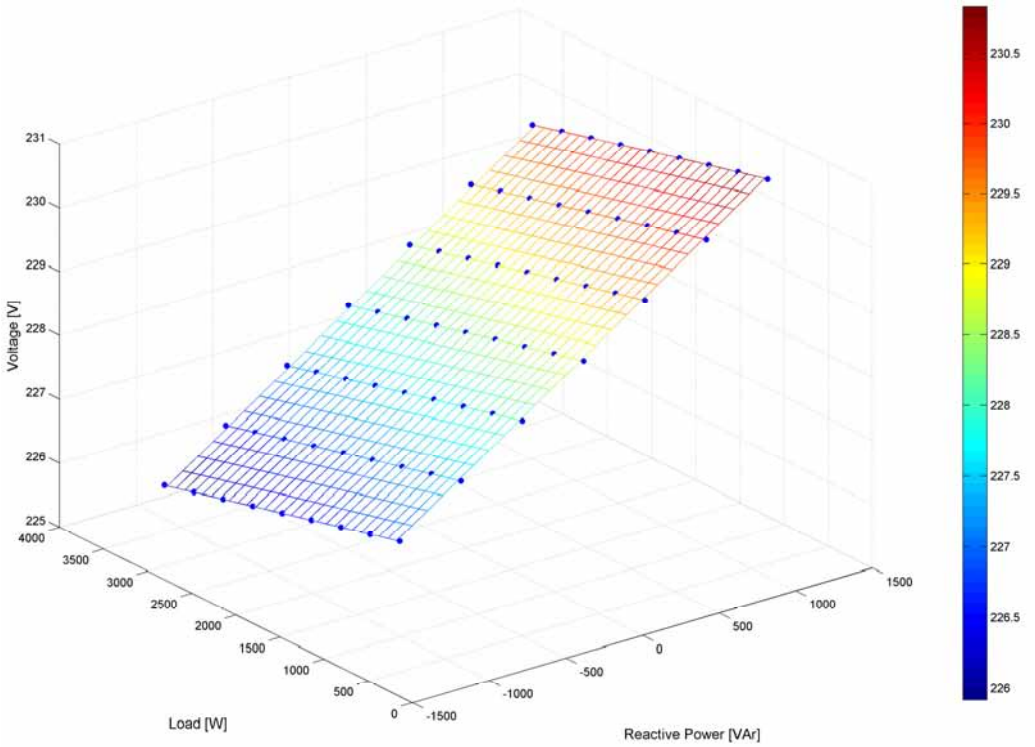

Figure 42: Interpolated data out of simulation results (dots) for following conditions: 0 to 4000 W load, - 1500 to 1500 VAr injection.

4.3.4. Simulation with control of the load voltage

In order to hold the load voltage at a constant predefined set-point, a control algorithm is implemented in the simulation. Figure 43 shows the structure e of the control. The measured load voltage is feed back and subtracted from the given set-point. The control deviation is input for the PI-controller. This controller provides the set-point Q_{set} for the control of the inverter which is injecting the reactive power.

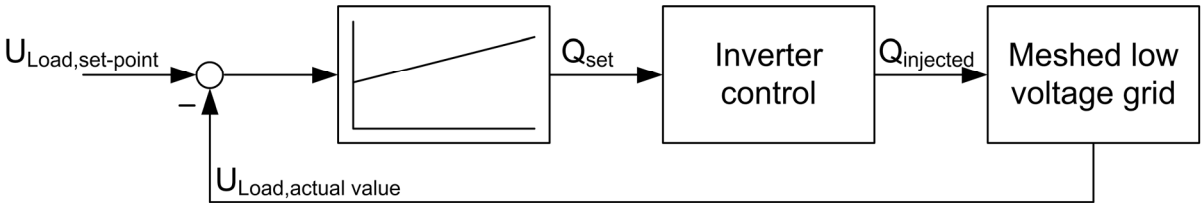

Figure 43: Subordinate control for the load voltage.

Figure 44 shows results of simulations with and without the control scheme of Figure 43. Once again the load is varied in steps from 0.66 kW to 3.3 kW. The load voltage decreases for higher load values if the simulation runs without control (green coloured line). But if the control is used, the load voltage is regulated to the given set-point of 230 V by adjusting the injected reactive power.

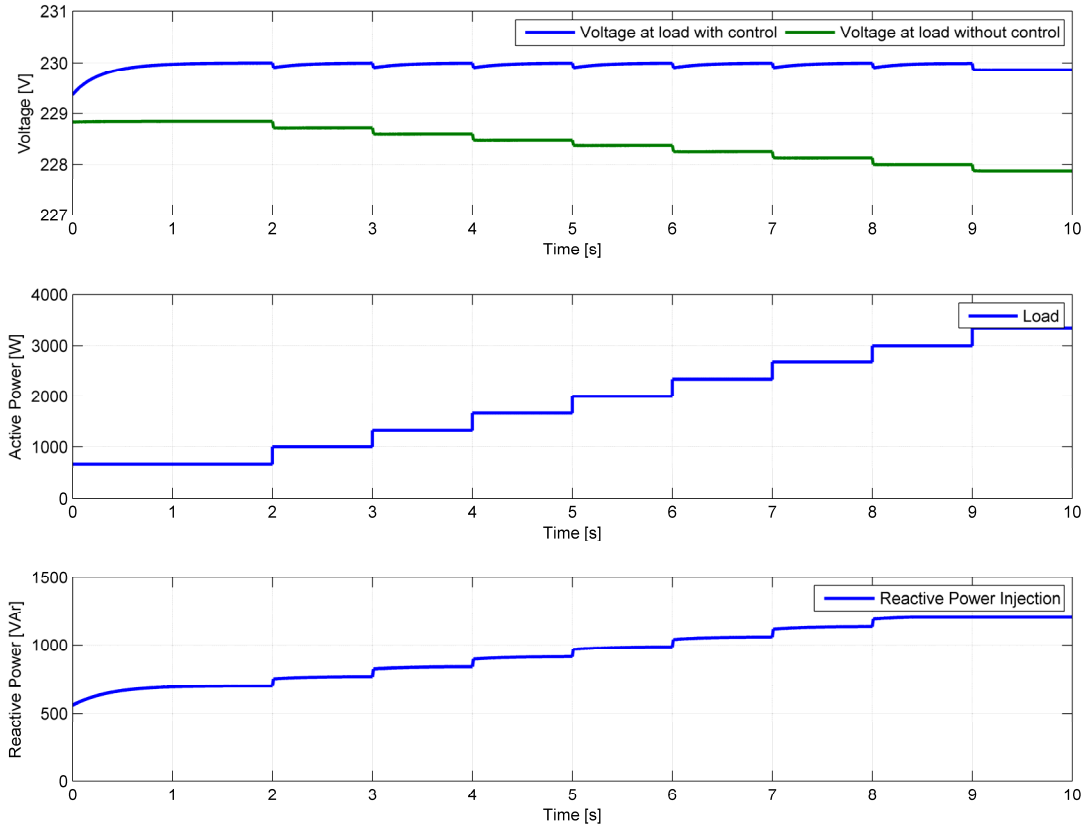

Figure 44: Voltage curve of the load with and without control for several load conditions. Simulation results.

5. Inductive Decoupling of long low voltage lines [Jah07]

As described in Chapter 2.2 current flow of two parallel operating voltage sources is distinguished through amplitude and phase difference of the two voltage sources. Only the network impedance limits the current flow. Regarding the low voltage network, coupling of voltage sources has got a resistive character (R/X > 1). Normally huge amount of reactive power is needed for achieving a voltage change and for compensation respectively.

That leads to the problem that voltage control can't be carried out as in medium or high voltage networks. Using the principal of inductive (de)-coupling of sub-networks these principal restrictions could be solved. In following sections this principal is discussed in detail.

5.1. Assembly of inductive decoupled sub-networks

By including an additional serial inductor (cp. Figure 45) the coupling of an electrical sub-network is shifted from a resistive part to an inductive one. By this, voltage profile of this sub-network can be influenced systematically and widely independently – quasi decoupled – by using reactive power injection. With this kind of control also small-scale in parallel grid-connected power devices with energy storage of small capacity can be used for services normally done by serial coupled devices. But also state of the art PV-inverters can be equipped with this kind of functionality.

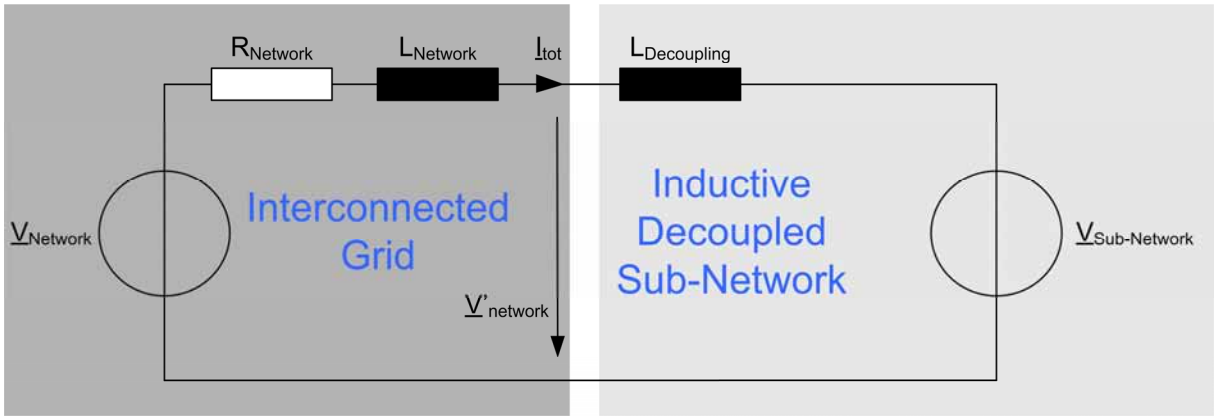

Figure 45: Equivalent circuit diagram of an inductive decoupled sub-network linked to the superior grid

The advantage of the assembly shown in Figure 45 is the combination of different possibilities. The interconnection to a superior grid offers the possibility of a quasi infinite active power dispatch while setting up an inductive decoupled sub-network for supplying sensitive loads with an improved voltage profile.

5.1.1. Control possibilities of the sub-network

State of the art grid converters are able to provide voltage profiles with low THD values. Through integration of a decoupling inductor these inverters with a limited (and with even small) power have got the possibility to improve the voltage quality for sensitive loads.

The needed power of the sub-network power source, in this case of the inverter, is depending from the grade of voltage disturbance in the superior grid, the wished or needed voltage profile in the sub-network and the value of the decoupling inductor.

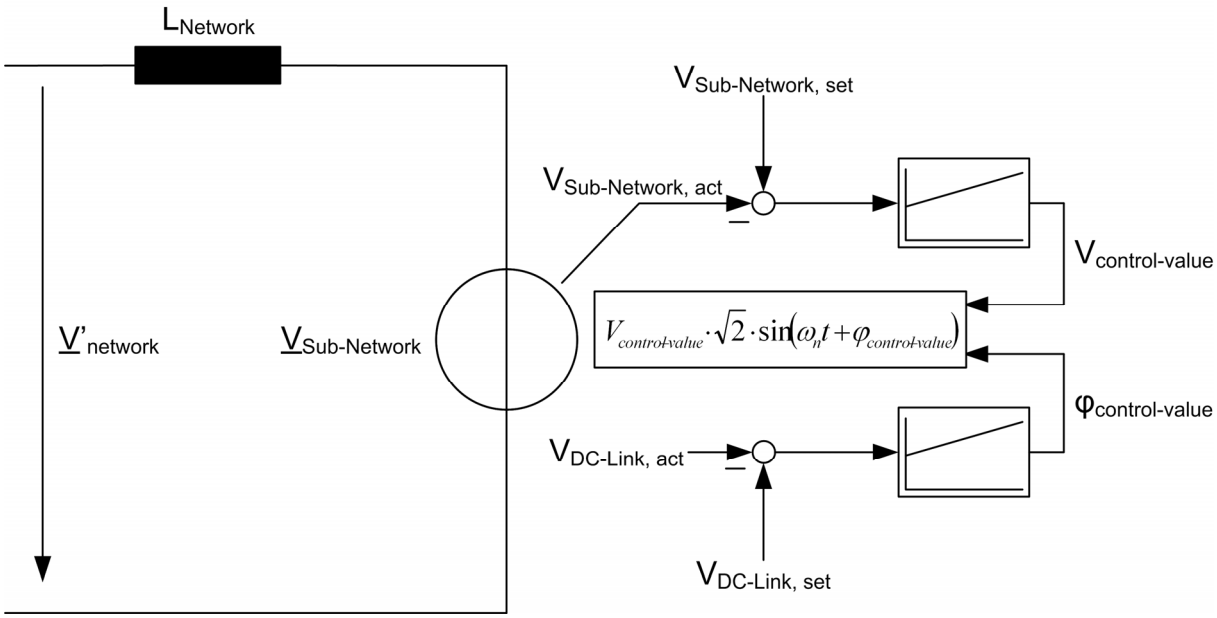

Figure 46: Inductive decoupled sub-network with independent control of active power dispatch to the superior grid and of voltage amplitude in the sub-network

In case of an inverter with short time energy storage as sub-network voltage source, only control algorithms for the root mean square value of the sub-network voltage source and the DC-link voltage are merely needed (cp. Figure 46).

$$V_{sub-network,control-value} = V_{control-value} \cdot \sin\left(\omega_n \cdot t + \varphi_{control-value}\right) \quad (5.1)$$

The control value of the sub-network voltage source consists of the independent controlled values of the voltage amplitude and the phase angle. The voltage amplitude by itself is controlled directly using measurement of the sub-network voltage. The phase angle is adjusted in that way that the DC-link voltage of the inverter is held constant. By using this kind of control concept, it is achieved that the inverter is only taking active power from the superior grid in order to compensate his losses. The voltage amplitude can be set by using only reactive power as it is expected in inductive coupled networks comparing with equation

(2.7). This kind of control can also be used for PV inverters for example. Due to the local generation and consumption of power the long low voltage line could be unload more.

5.1.2. Voltages, currents and power flows in the decoupled sub-network area

As introduced in the beginning of this section, through inserting of an additional inductor, the kind of coupling between network and sub-network is changed.

In order not to overload the superior grid, it has to be evaluated to what extend the decoupling inductor causes an additional reactive power flow. For calculations following simplifications are made:

1. The decoupling inductor is ideal, no resistive losses are regarded.
2. If there are losses in the sub-network voltage source, theses are added to the load.

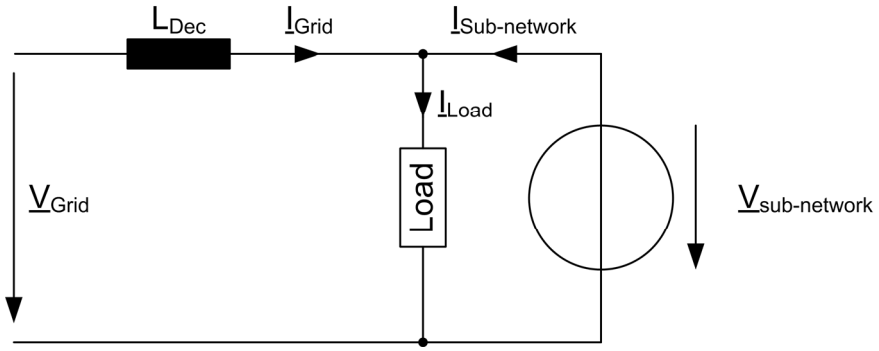

Figure 47: Currents and voltages in the inductive decoupled sub-network

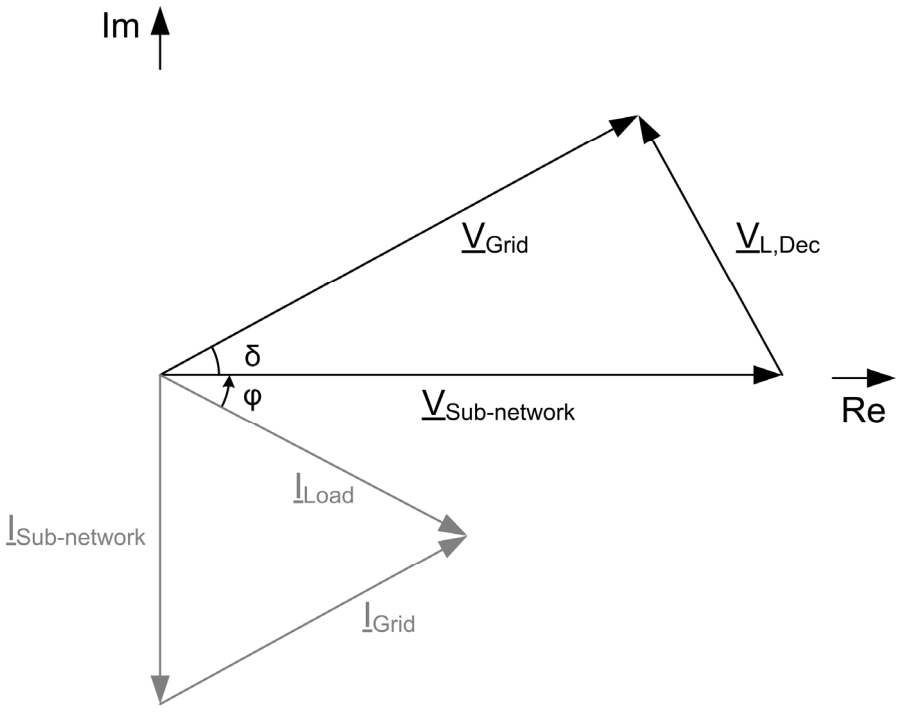

Figure 48: Pointer diagram of assembly in Figure 47

A pointer diagram of an inductive decoupled sub-network (cp. Figure 48) is prepared for calculation of power flows according to currents and voltage of Figure 47.

The sub-network voltage is used as reference value which is placed at the real axis. The load is supplied by the constant sub-network voltage with a constant power, whereas the share of the active power amount of the load is received from the superior grid. Thereby equation (2.6) of section 2.2.2 describing active power flow within inductive decoupled networks can be applied. For this reason the angle δ between the voltage sources can be determined. Thus both absolute value and direction of voltage drop across the inductance are defined.
If the power factor is known the absolute value and the direction of current supplied by the superior grid can be calculated according to:

$$\underline{I}_{Network} = \frac{\underline{V}_{L,Dec}}{\underline{V}_{L,Dec}} \tag{5.2}$$

Using equation (5.3) current of the sub-network voltage source is calculated and therefore also injected reactive power is known.

$$\underline{I}_{Sub-Network} = \underline{I}_{Load} - \underline{I}_{Network} \tag{5.3}$$

Now, influences of voltage difference between superior grid and sub-network as well as the value of the decoupling inductance on reactive power flow can be analysed. Thereto a MATLAB© script has been programmed in order to visualise power flows in dependence of the parameters voltage difference and size of decoupling inductor.
In Figure 49 and Figure 50 results of a load flow calculations for a load of 3.5 kVA with a power factor of 0.85 (ind.) are given exemplary. The calculation results show that for very small values of the decoupling inductor high reactive power flows have to be provided in order to control the voltage in sub-network to claimed set point. For values of 10 mH for the decoupling inductor variations become less.

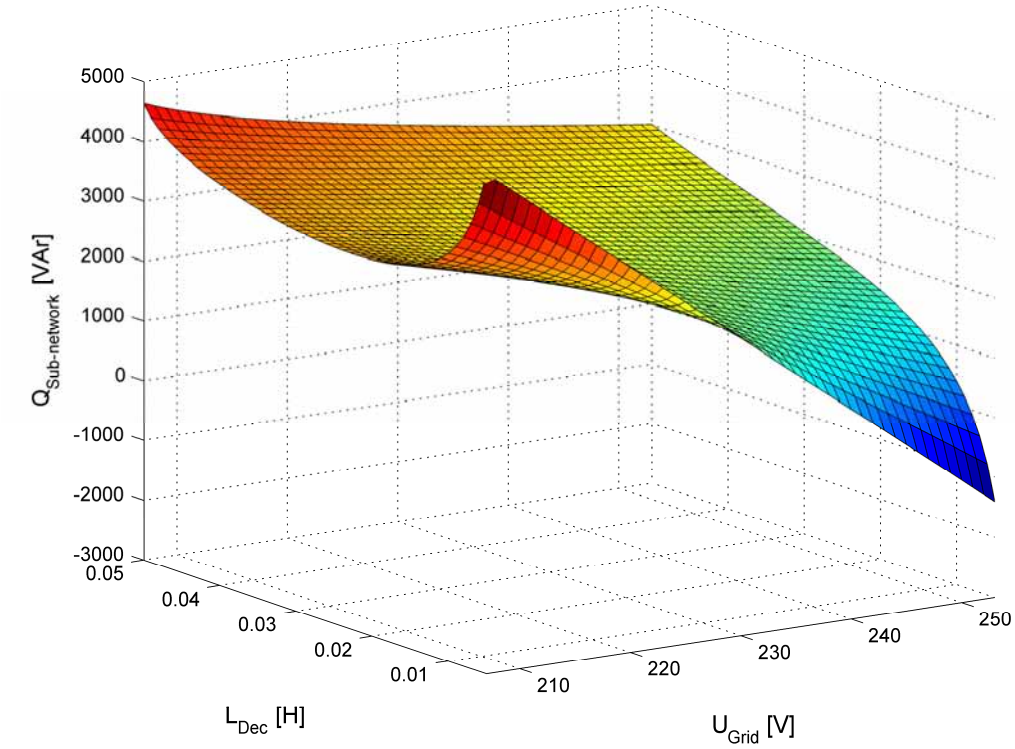

Figure 49: Reactive power contribution of sub-network voltage source for a load of 3.5 kVA, power factor cos φ = 0.85 (ind) and $V_{sub\text{-}network}$ = 230 V; MATLAB© calculation result.

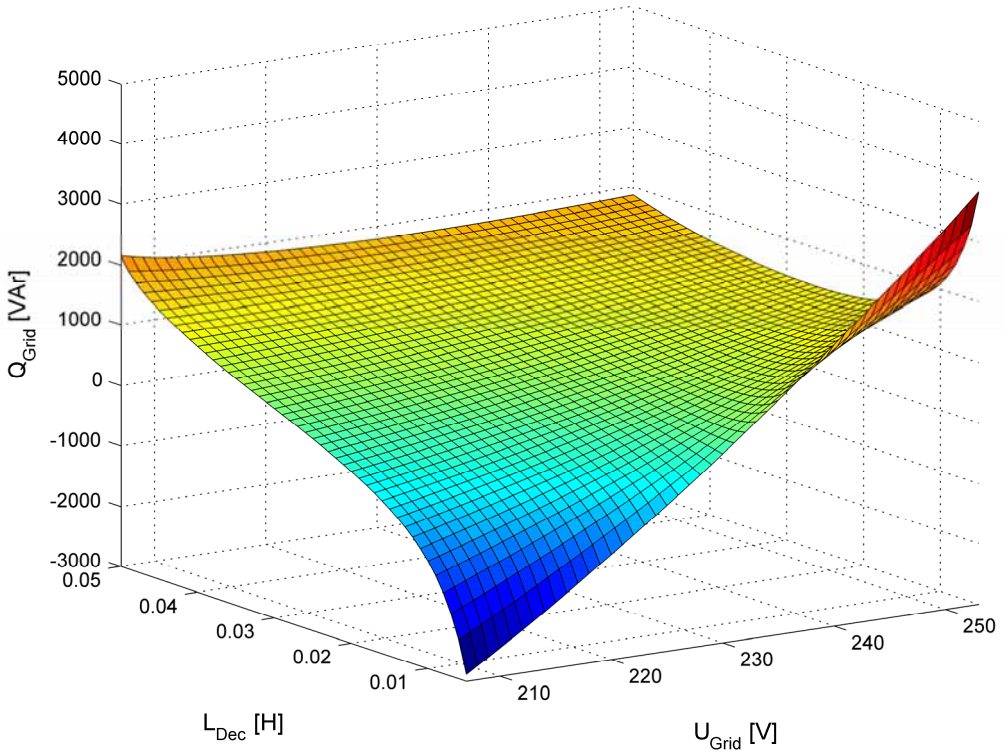

Figure 50: Reactive power contribution of superior grid voltage source for load conditions of Figure 49, MATLAB© calculation result.

For variations of the superior grid voltage a linear relation is obtained as assumed by equation (2.5). The gradient of line for each decoupling inductor is getting smaller for higher values of the inductor as described in the section before.
Therefore it would be advantageous if the decoupling inductor have a certain minimum size in order that the reactive power must made available by the voltage sources would not become unnecessarily high. Otherwise the decoupling inductor could not be made arbitrary high because the transferred active power would become to low rather the voltage drop at the decoupling inductor would become unnecessarily high.

In order to point out the relations for a decoupling inductor with a high inductance, a true to scale pointer diagram of voltages and currents calculated by a self-provided MATLAB application is shown in Figure 51. Although only 3 kW are transferred, the phase angle difference between the voltage sources already is 65°. The voltage drop at the decoupling inductor is 245 V.

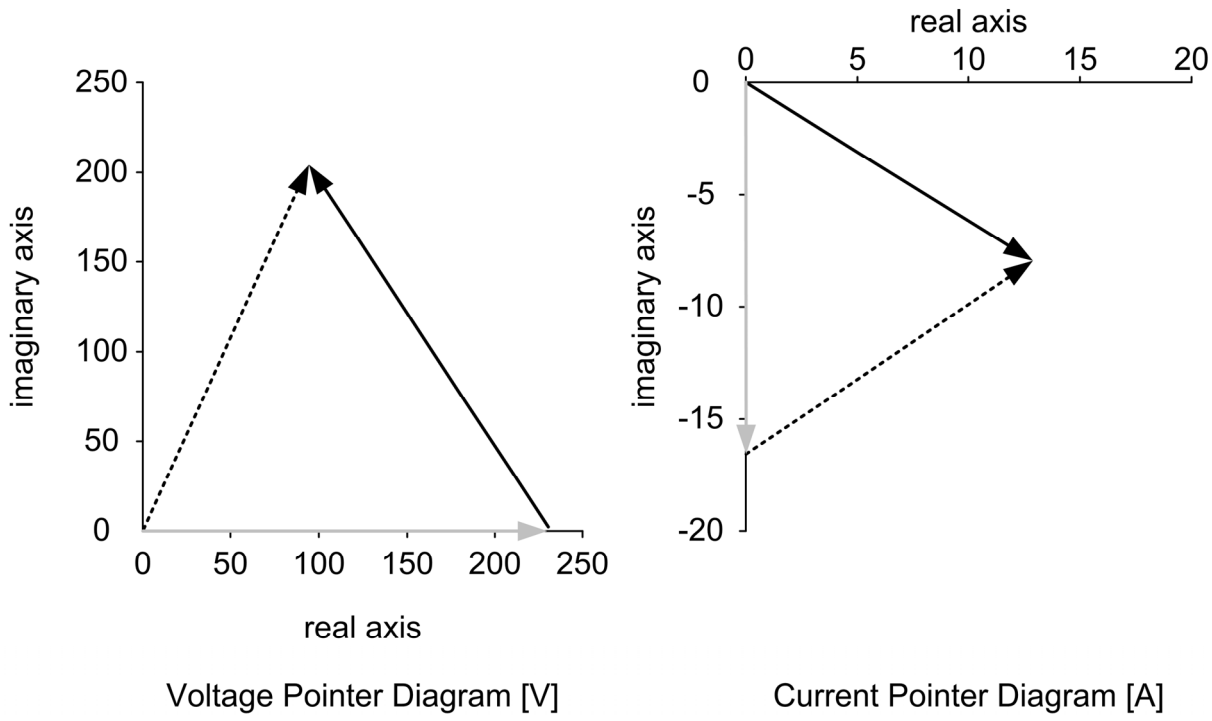

Figure 51: True to scale pointer diagram of voltages and current for a sub-network load of 3.5 kVA at a superior grid voltage of 225 V and a decoupling inductance of 50 mH. Left chart: $V_{sub\text{-}network}$ (grey), V_{grid} (black, dashed), $V_{L,Dec}$ (black). Right chart: $I_{sub\text{-}network}$ (grey), I_{Load} (black), I_{Grid} (black, dashed). MATLAB© calculation result.

5.1.3. Behaviour at non-sinusoidal network voltages

The up to now as ideal assumed network voltage profile $\underline{V}_{Network}$ is distorted due to non-sinusoidal currents flowing through the network impedance. The network voltage $\underline{V}'_{Network}$

being available for the consumer can differ from the ideal sinussodial curve (cp. Figure 45). For following simulations due to simplification it is assumed that the network voltage source $\underline{V}_{Network}$ already is distorted.

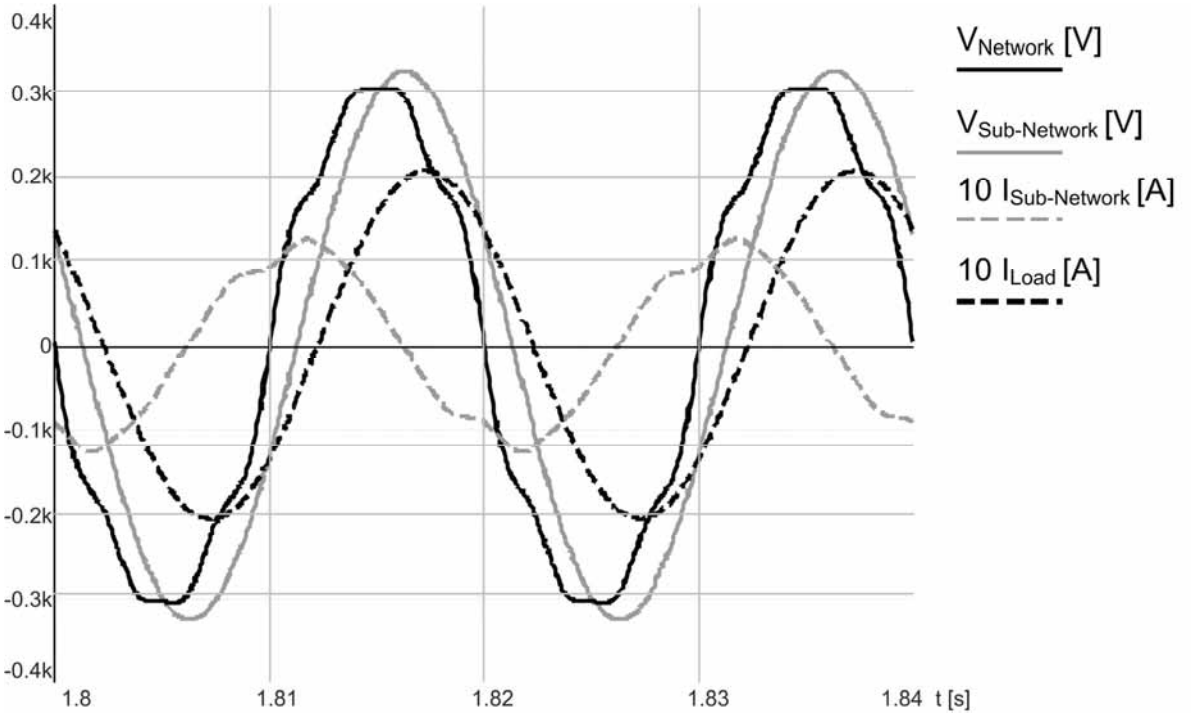

Figure 52: Simulation result for inductive decoupling of sub-networks according to Figure 47. Active power set value 0, resistive-inductive load in the sub-network. SIMPLORER simulation result.

Figure 52 shows the results of a simulation according to the circuit arrangement of Figure 47. The load ratios (S_{Load} = 3.52 kVA, cos φ_{Load} = 0.85) are selected due to made agreements in section 5.1.2. The network voltage source $\underline{V}_{Network}$ is distorted with regard to the 3rd, 5th and 7th harmonic order up to the allowable limit of DIN EN 61000-3-2. The improved voltage profile provided for a sinusoidal current consumption at the sub-network load can be seen clearly. The active power part is obtained across the decoupling inductor from the superior network.

For compensating the different voltage curve profiles, at both sites of the decoupling inductor non-sinusoidal equalising currents flow. These kinds of currents are normally avoided in order not to increase the impact of harmonics at the superior network. Therefore the effect of these non-sinusoidal currents is studied for the total system afterwards.

Considering only harmonics the system according to Figure 45 can be simplified by using the principle of superposition. In Figure 53 the simplified equivalent circuit diagram for harmonic

orders higher than one is shown with the assumption that the sub-network voltage source provides an ideal sinusoidal fundamental waveform.

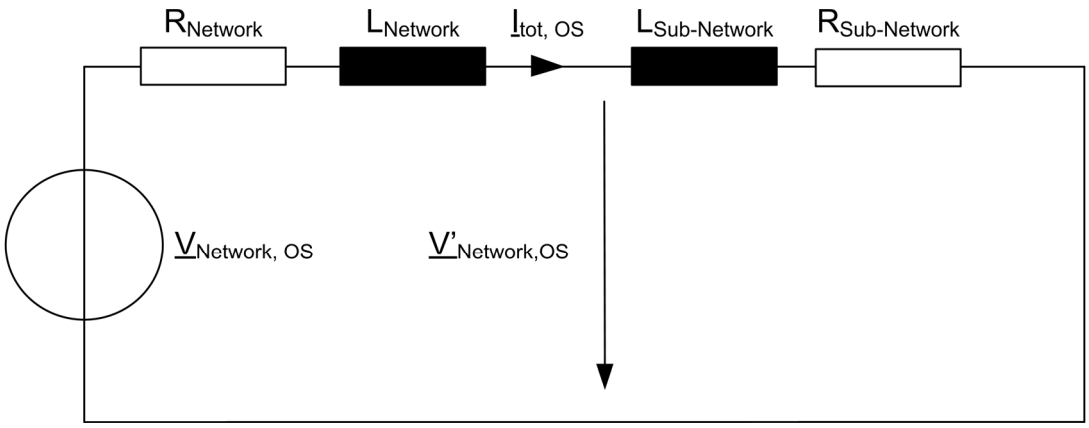

Figure 53: Simplified equivalent circuit diagram of an inductive decoupled sub-network for harmonic orders > 1.

The elements $R_{Network}$ and $L_{Network}$ of the network are substituted by $Z_{Network}$ for further simplification. The elements of the sub-network, the decoupling inductor L_{Dec} and the components of the sub-network voltage source L_{Inv} and R_{Inv} are substituted by $Z_{Sub\text{-}Network}$.
This equivalent circuit diagram can be interpreted in two ways. Regarding Figure 53 as complex voltage divider following equation is achieved:

$$\frac{\underline{V}_{Network,OS}}{\underline{V}'_{Network,OS}} = \frac{\underline{Z}_{Sub-Network} + \underline{Z}_{Network}}{\underline{Z}_{Sub-Network}} \tag{5.4}$$

Solving to $V'_{Network,OS}$ reults in:

$$\underline{V}'_{Network,OS} = \underline{V}_{Network,OS} \cdot \frac{\underline{Z}_{Sub-Network}}{\underline{Z}_{Sub-Network} + \underline{Z}_{Network}} \tag{5.5}$$

The inductive sub-network reduces harmonic voltages also beyond the decoupling inductance by trend. Hence no parasitic effects through the sub-network for the superior network are awaited.
Exact the same conclusion results in observing the total harmonic current $I_{tot,OS}$.

$$\underline{I}_{tot,OS} = \frac{\underline{V}_{Network,OS}}{\underline{Z}_{Network} + \underline{Z}_{Sub-Netzwork}} \tag{5.6}$$

The harmonic currents tend to decrease if the network impedance is increased by the sub-network. This is confirmed with simulation results shown in Figure 54.

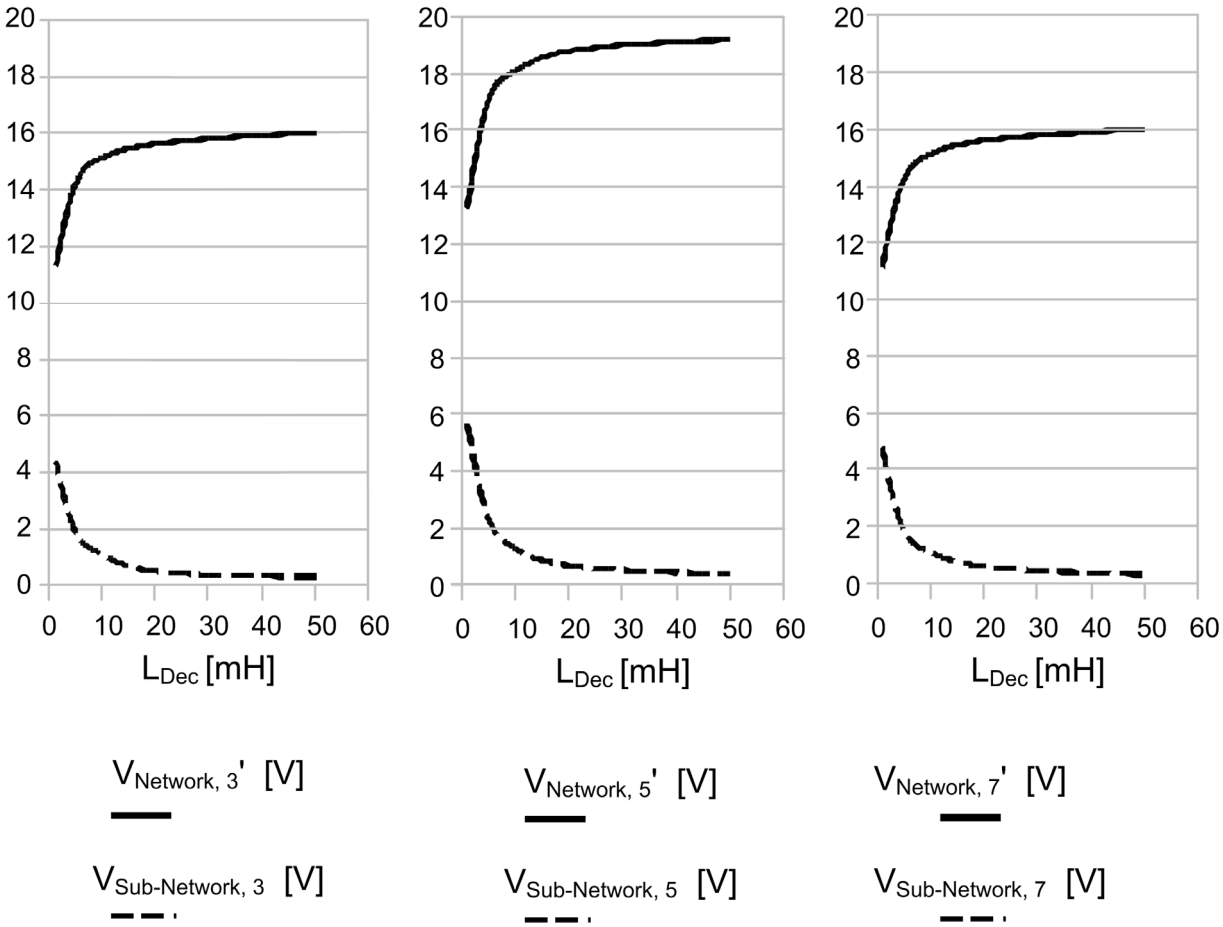

Figure 54: Share of voltage harmonics [V] before and behind the decoupling inductor dependent of the size of the decoupling inductor.

The harmonic content of the voltages $\underline{V}'_{Network}$ and $\underline{V}_{Sub\text{-}Network}$ depending from the size of the decoupling inductor is shown for the orders three, five and seven. It is obvious that for small inductances the harmonic content of the voltage $\underline{V}'_{Network}$ decreases and the voltage within the decoupled sub-network is relatively heavy distorted. For higher values of the decoupling inductor the harmonic content of the decoupled sub-network decreases very fast and the distortions of $\underline{V}'_{Network}$ aspire towards their initial value.

5.1.4. Dynamic Behaviour on network faults

For decoupling inductors with high values of the inductance the delivered active power from the superior network cause a high voltage drop at the decoupling inductor. This voltage drop has to be compensated again by a high amount of reactive power. In between an area with a minimal reactive power exchange exists.

Regarding networks operated in parallel mode as well as in islanding mode network failure detection and failure control is immense important. This includes the transition between both

operating modes similar to an Uninterruptible Power Supply (UPS). The mainly network faults are line faults (cp. Figure 55) or short circuit faults (cp. Figure 56).

The developed control algorithms seems to be suitable to detect both kinds of network failures, because in case of a failure the sub-network voltage source has to provide an active power varying from the set-value. This can be explained with an indirect effect of the voltage control provided by the sub-network voltage. As long as the voltage control provides through the provision of reactive power a voltage difference at the output terminals of the voltage source, the current is determined by the load even if the set-value for the active power would be permanently unmatched.

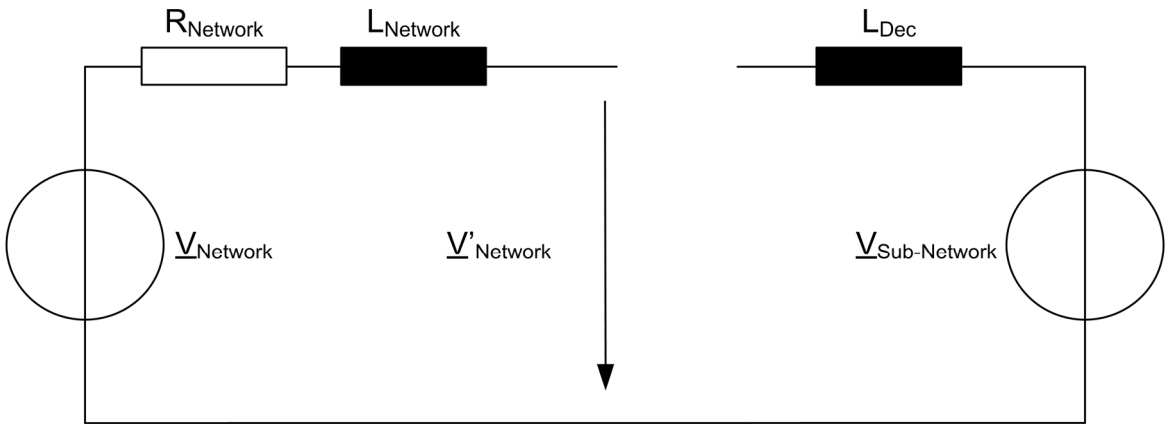

Figure 55: Schematically equivalent circuit diagram for line open circuit condition

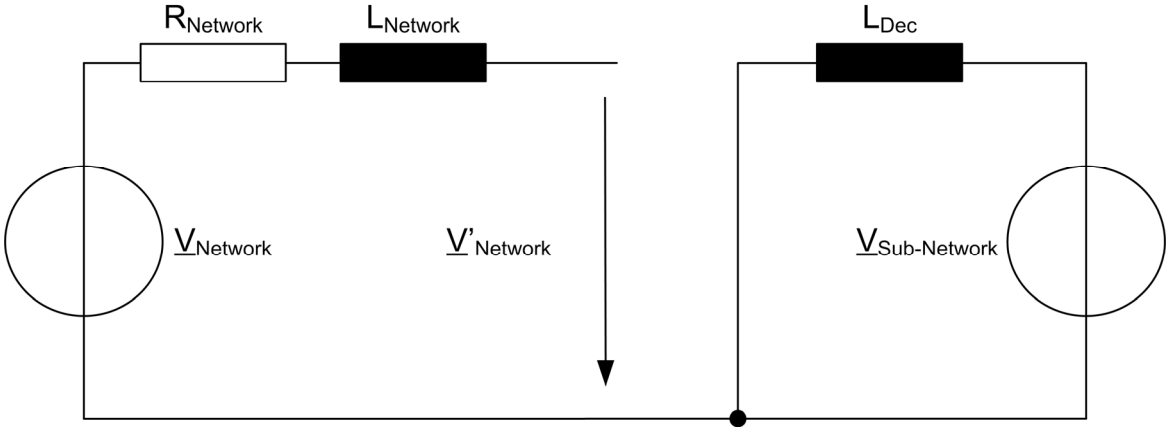

Figure 56: Schematically equivalent circuit diagram for line short circuit condition

5.1.4.1. High impedance faults – Line faults

An interruption of the active power supply through the superior network, as shown in Figure 57 at the time of t = 5 s, is recognised in the simulation that fast that the load can be supplied with electrical energy without interruption and without significant changes of the voltage amplitude. It is obvious that the complete active and reactive power is spontaneously

delivered by the sub-network voltage source. Reactive power provision is reduced due to the fact that no additional reactive power is needed for compensating the voltage drop at the decoupling inductance. The amount of reactive power is reduced to the demand of the reactive power demand of the sub-network load.

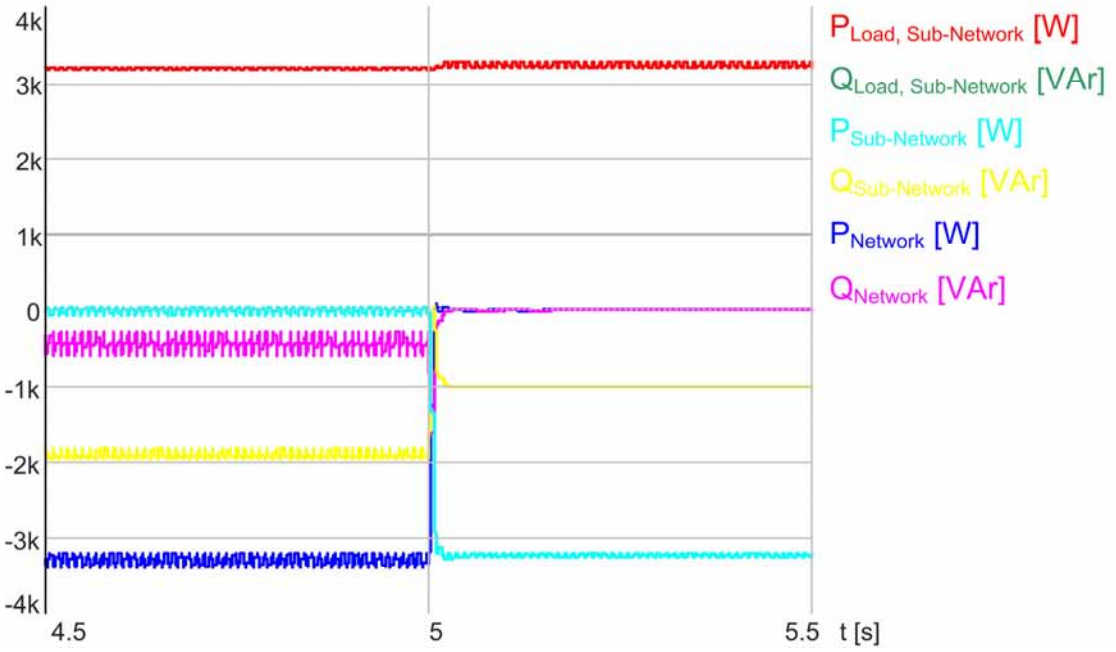

Figure 57: Active and reactive power flows for an open line circuit. SIMPLORER simulation result.

The voltage and current curves during a line interruption are presented in Figure 58. The sub-network load is continuously and without additional distortions supplied with voltage.

5.1.4.2. Low Impedance Faults – Short Circuits

Short circuits as shown in Figure 56 can also be handled with a sub-network voltage source with relatively small power ratings due to the fact that in case of a short circuit the decoupling inductor merely represents an additional, parallel inductive load. However the sub-network voltage source has to provide enough power for supplying the loads in the sub-network, independently from the superior network.

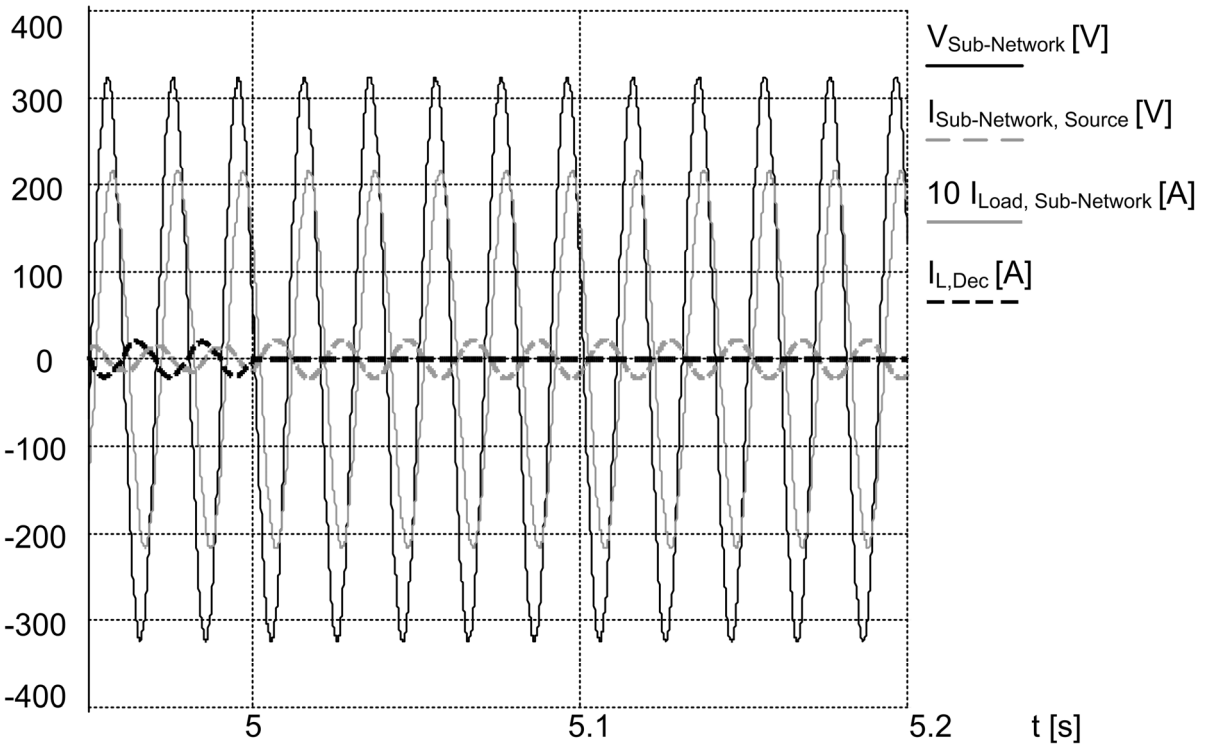

Figure 58: Voltage and current curves during open line circuit. SIMPLORER simulation result.

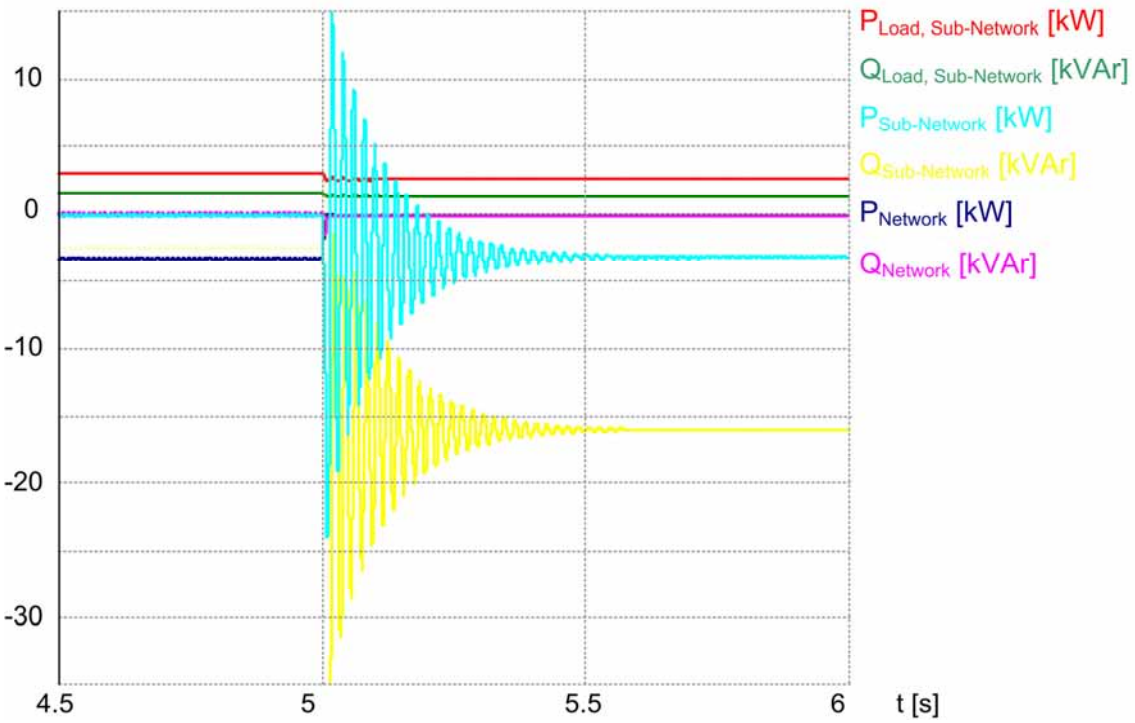

Figure 59: Active and reactive power flows during a short circuit. SIMPLORER simulation result.

In Figure 59 the power flows during a short circuit is simulated. Through the voltage dip at the decoupling inductor due to the short circuit, strong transients occur in form of power oscillations. These oscillations are damped by the impedance of the line, by the sources and by the decoupling inductor itself. Since using an ideal inductance for simulation the damping is quite low.

Within the simulation the sub-network load is supplied with energy constantly even if the power consumption is lightly lowered. This refers to the sub-network voltage which could not be held constant und therefore slightly decreases. With the decoupling inductor as additional load the reactive power flow within in the sub-network is strongly increased. For this reason a disconnection of the decoupling inductor with suitable breaker elements should be foreseen. Transients of the short circuit can be seen in the current curves in Figure 60. The extreme power values of Figure 59 could be explained with these transient recordings.

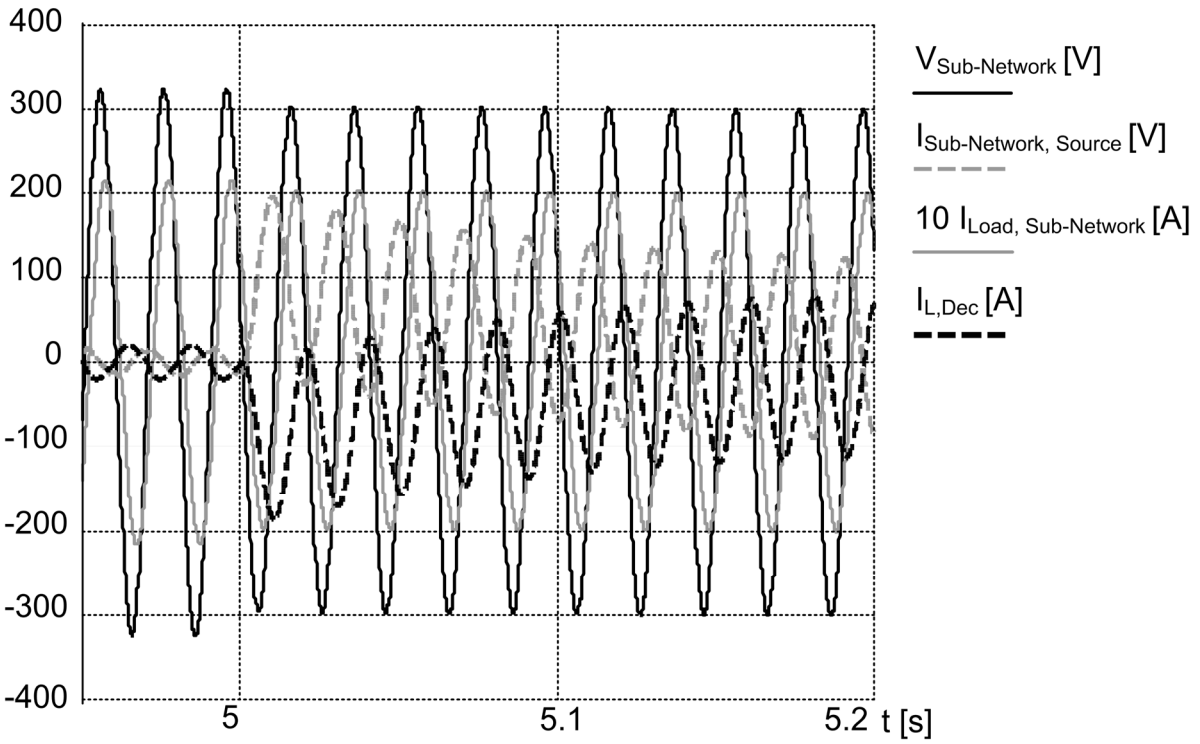

Figure 60: Voltage and current curves during a short circuit. SIMPLORER simulation result.

In Figure 60 the voltage and current curves according to the simulation of Figure 59 are shown. Here also a light decrease of the sub-network voltage and of the load current can be seen clearly. If the sub-network voltage would be stated as constant and a decoupling inductor of 10 mH would be used, significant transient currents will flow through the decoupling inductor in case of a short circuit.

$$I_{L,Dec} = \frac{V_{Sub-Network}}{X_{L,Dec}} = \frac{230\,V}{3.1\,\Omega} = 74.2\,A \tag{5.7}$$

This short circuit current has to be considered for the dimensioning of the inverter if it should be able to ride through this operating mode. In real systems the swinging of the power will be damped by the resistance of the inductor which was neglected within the simulation.

Recapitulate can be asserted that the developed method offers a possibility to enhance voltage quality within a network segment selectively. With traditional FACTS this would only be possible using serial device.

5.2. The prototype unit ISET-*Per*FACT[1]

The described method of inductive decoupling of sub-networks should be varyfied with laboratory measurements. For this practical realisation a hardware was built and the software algorithms were implemented.

5.2.1. The single-phase Dynamic Voltage Restorer ISET-*PER*FACT

The single phase Dynamic Voltage Restorer ISET-*Per*FACT bases on an inverter of the commercial available Sunny Island battery inverters of the SMA Solar Technology AG. Due to high investment and maintenance costs of battery storage systems only short time storage in form of a strongly oversized DC-Link is used (cp. Figure 61).

In order not to overload the backward diodes of the H-Bridge when switching on the network voltage, a charging resistor is used. During normal operation this resistor is by-passed.

For the oversizing of the DC-Link two printed circuit board with two different capacities were built. Technically feasible would also be a solution with SuperCaps. Since SuperCabs have much lower rated voltages in comparison with conventional condensers, a series connection with corresponding capacity losses or a DC/DC converter have to be introduced. Because setting up a prototype unit the main focus was on the effectiveness of the algorithms and not on the maximum DC-Link capacity.

[1] The ISET-PerFACT hardware was built during the European project *Improvement of Quality of Supply in Distributed Generation Networks through the Integrated Application of Power Electronic Techniques – DGFACTS*, contract number ENK5-CT-2002-00658, the control development and the implementation of the principle of inductive decoupled low voltage networks was carried out in the MoreMicroGrid project. Therefore chapter 5.2 is intended only for information for the reader.

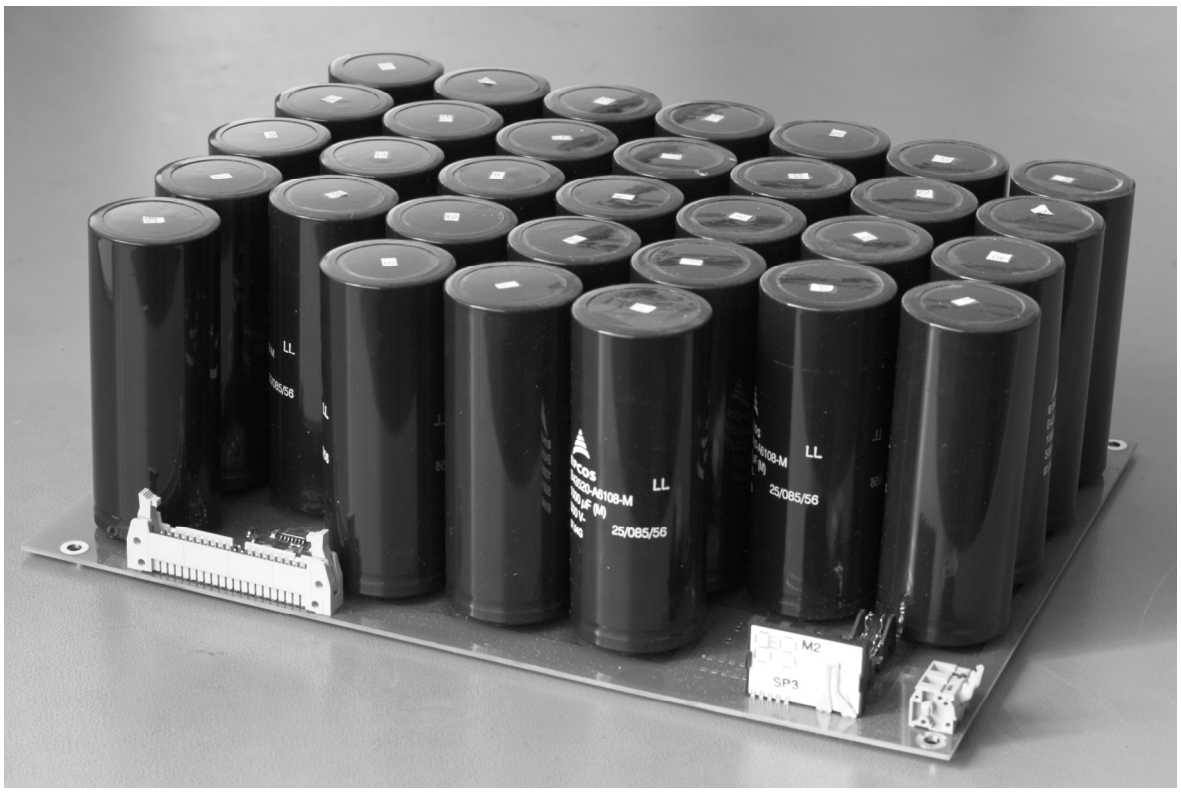

Figure 61: DC-Link of the prototype unit

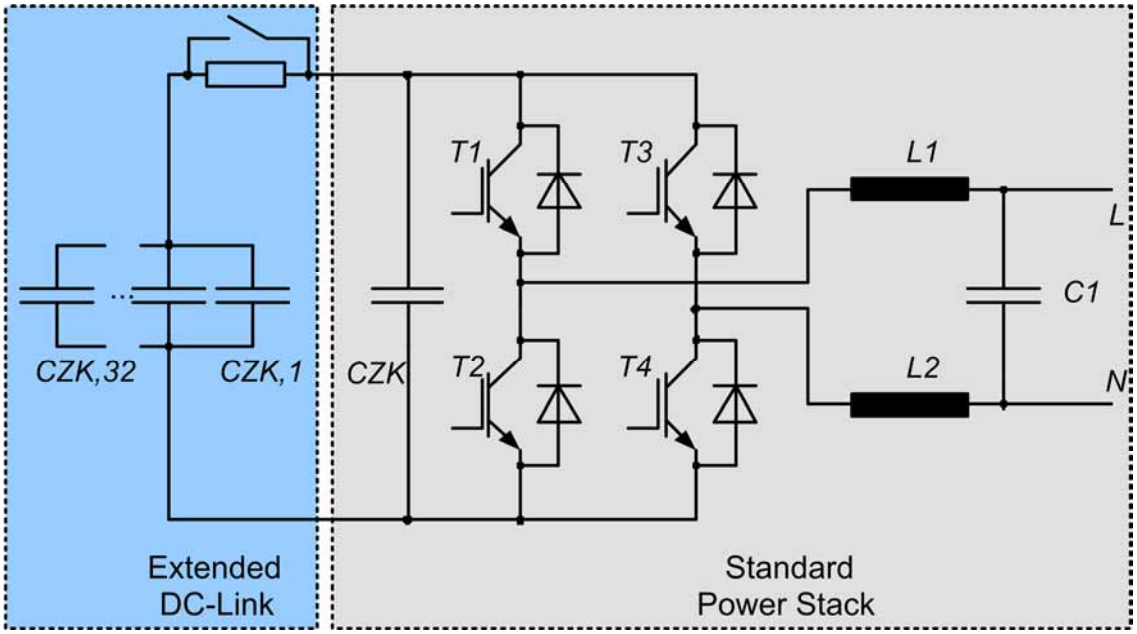

Figure 62: Equivalent circuit diagram of the ISET-*perFact*

5.2.2. The Rapid-Control-Prototyping System

Nowadays wide possibilities are open to speed up the development process of a device through the enormous progress and reduction of costs in the area of electronic processing systems.

Fundamental factors of these data processing systems are Hardware-in-the-Loop (HiL) and Rapid-Control-Prototyping-Systems (RCPS) which follow oppositional appendage. These appendages are presented in Figure 63.

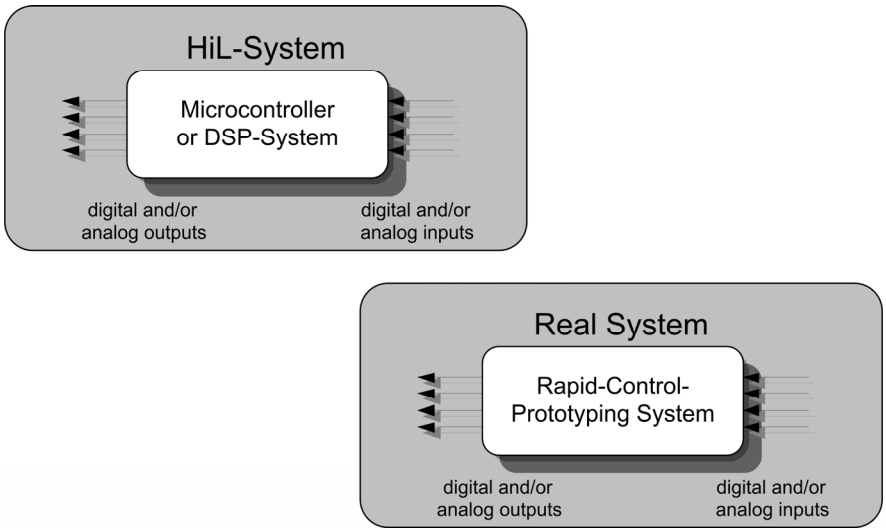

Figure 63: Comparison of Hardware-in-the-loop (HiL) and Rapid-Control-Prototyping

Using the HiL the real development unit – in most cases a microprocessor or a DSP-system – is developed and evaluated within a simulated environment. In contrary using RCPS the real development unit (in that case a real inverter prototype) is controlled by controller hardware with high computing power for calculation of models of the control algorithms in real time. The functionality and control functions of the prototype unit is mostly developed using graphical environment and afterwards code for the RCPS is generated automatically. Therefore a fast realisation of even extensive and complex functionality is possible. Many parameters could be changed online and a visualisation in real time is applicable.

In the present case it is about a realisation oriented prototyping that is described in [Spi01] as a work with highly specified prototypes only used for specific applications or where from existing components the functionality through use of a new component is extended or changed.

In order to use the Rapid-Control-Prototyping also for serial products of technical developments the method of simulation model based control development is used [Gei07]. The basics are simulation models of the control algorithms which can be used either with the

RCPS for the prototype unit or for a complete simulation of the environment with the control algorithms.

Within this work a RCPS of the company dSPACE has been used. The control algorithm development has been done with the simulation tool MATLAB/SIMULINK/STATEFLOW. By using special blocks it is possible to get access to the RCPS and to configure the interfaces. Additionally it is possible to integrate user-defined C-Code with Matlab and therefore more individual and more efficient possibilities can be achieved.

5.2.3. The dSPACE Rapid-Control-Prototyping-System DS1103

The platform DS1103 uses the PowerPC 604e with a speed of 400 MHz which is responsible for the execution of the main part of the compiled program. The principle design is shown in Figure 64.

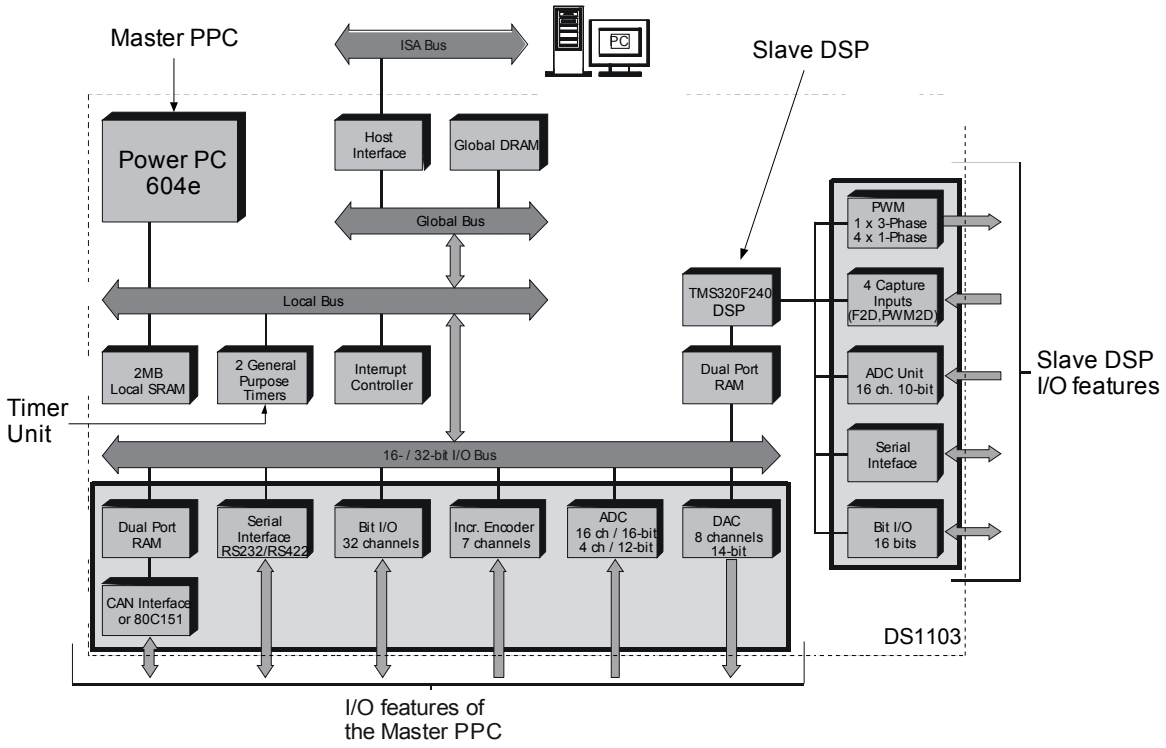

Figure 64: Schematically overview of the dSPACE DS1103 Rapid Control Prototyping System [Dsp04]

The connection to the Host-PC is done via ISA-Bus. For implementing an inverter control mainly following interface are needed:

- **A/D-Converter Unit**

  The Master PPC provides 4 parallel A/D-converter with each 4 channels and 16-bit resolution.

- **Bit I/O Interface**

  With the Bit I/O Interface digital signals can be received or be sent to the inverter.

- The **Host-Interface** is used for data communication and measurement visualisation.

The DS1103 is not able to work without the Host-PC. Therefore especially for field measurements the disadvantage of supplying the Host-PC with energy exists. Furthermore only a volatile memory is available so that in case of a supply voltage interruption the software has to be reloaded and restarted manually.

5.2.4. The User Interface Control-Desk

The software ControlDesk is used as User Interface. It is possible to load program code in the processor and to start or to stop the execution of the control software of the inverter. Beyond all measurement values which are available for the RCPS can be displayed in several ways, variables can be changed during runtime and settings for example of the desired operating mode can be provided to the RCPS. Error messages can be converted to plain text for the GUI (cp. Figure 65). Hence the complete operating procedure can be realised and visualised with this user interface.

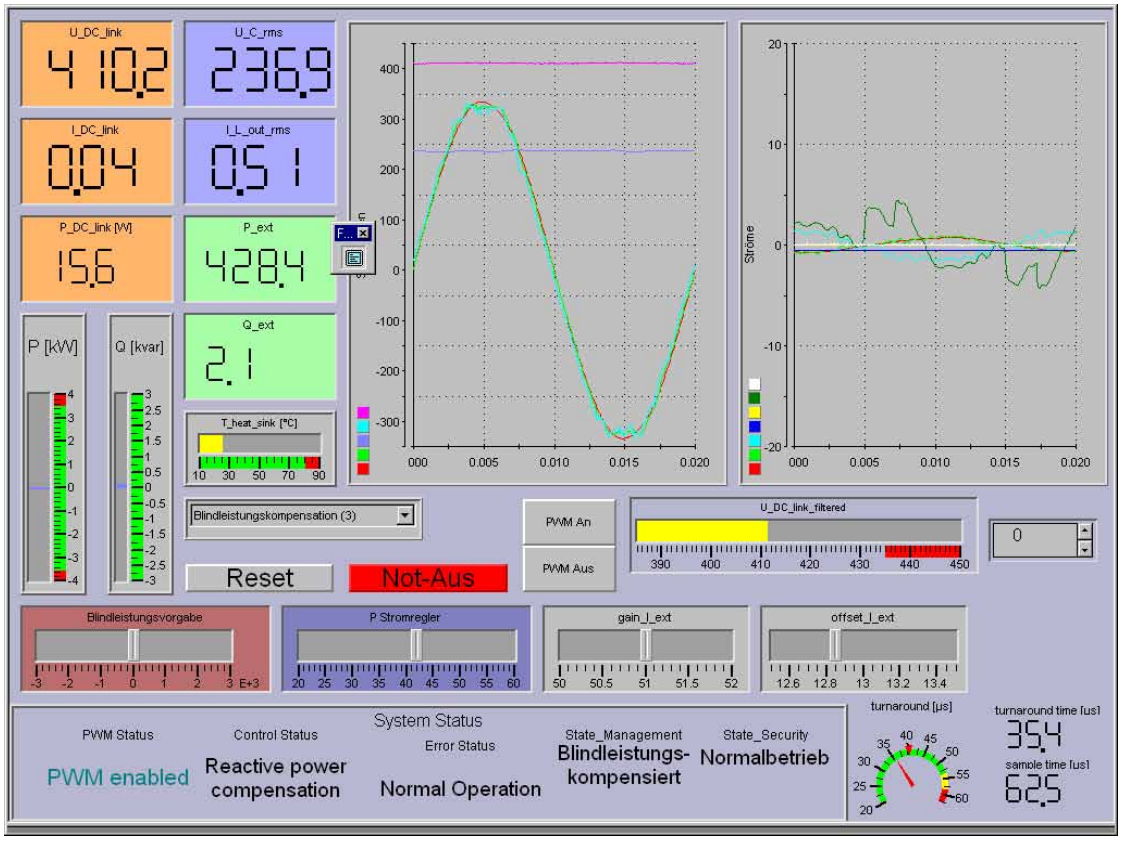

Figure 65: Control-Desk user interace for control of the prototype unit

5.3. Measurement Results of the Prototype unit

Within this section before described control algorithms are tested with the prototype unit in order to proof the effectiveness of the control algorithms. The complete experimental set-up is shown in Figure 66.

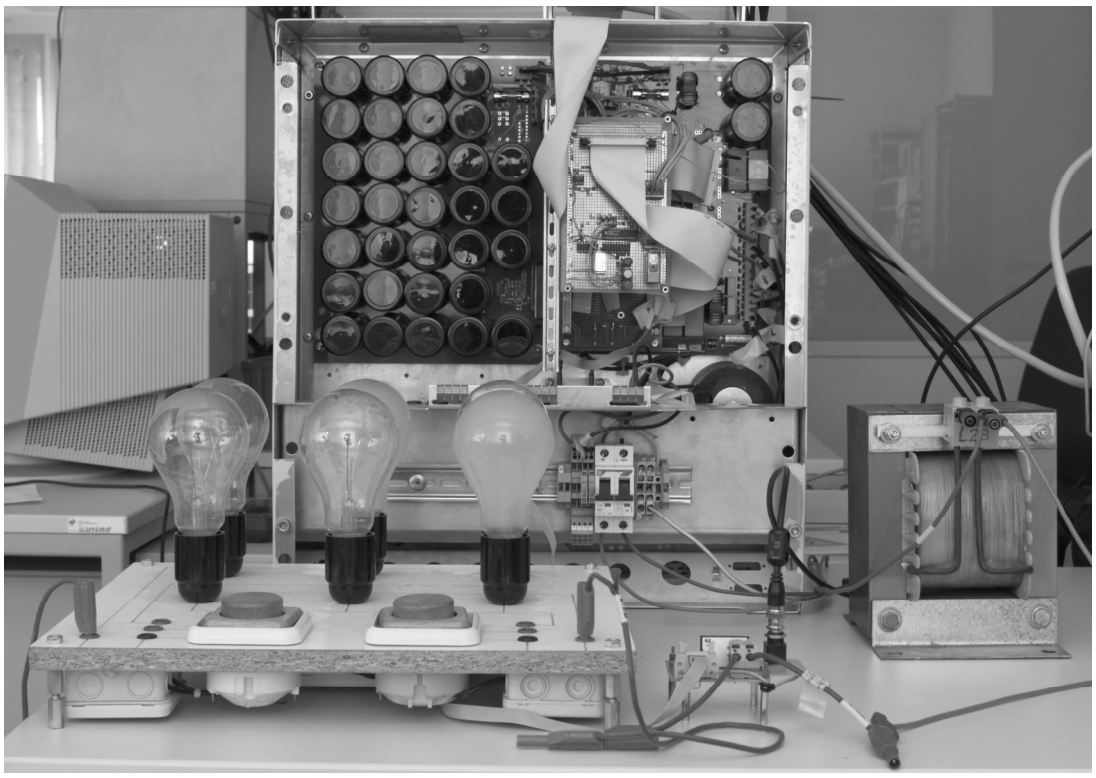

Figure 66: Experiment setup of the prototype unit. Left in the front light bulbs with dimmer switch, middle in the front external current measurement, decoupling inductance on the right.

5.3.1. Measurement at inductive decoupled sub-networks

For measurement of inductive decoupled sub-network a programmable voltage source is used for simulation of disturbed network behaviour $V_{network}$. The experiment setup is shown in Figure 67 schematically. The set value of the sub-network voltage should be constant at 230 V for all experiments. As load a pure resistive one is used with a consumption of about 600 W. The decoupling inductor had an inductance of 10 mH. Measurement values are recorded with an average time of 1 s for permanent records.

5.3.2. Quasi-stationary behaviour

For analysis of the reactive power flow a voltage ramp of the network voltage according to the limits of DIN EN 50160 (230 V ± 10 %) is simulated with the programmable voltage source. In order to achieve steady state conditions the slope of the ramp was chosen to

$$\frac{23V_{RMS}}{60\,s} \tag{5.8}$$

Figure 68 shows the voltage curve of the network voltage as well as the voltage curve of the sub-network voltage.

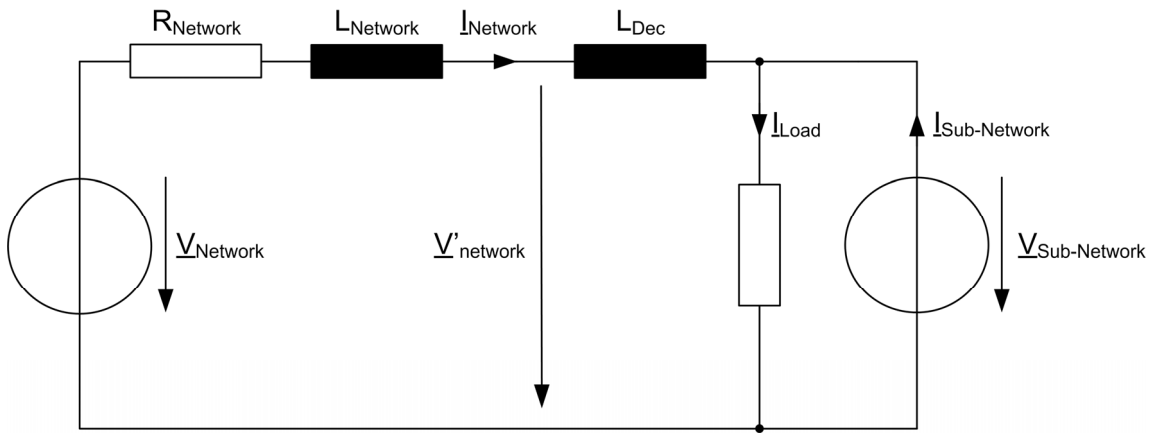

Figure 67: Measurement setup for test of inductive decoupling of sub-networks.

Even for the extreme values of the voltage ramp, at the minimum 207 V and maximum value of 253 V of the network voltage, the sub-network voltage is hold nearly constant at 230 V.

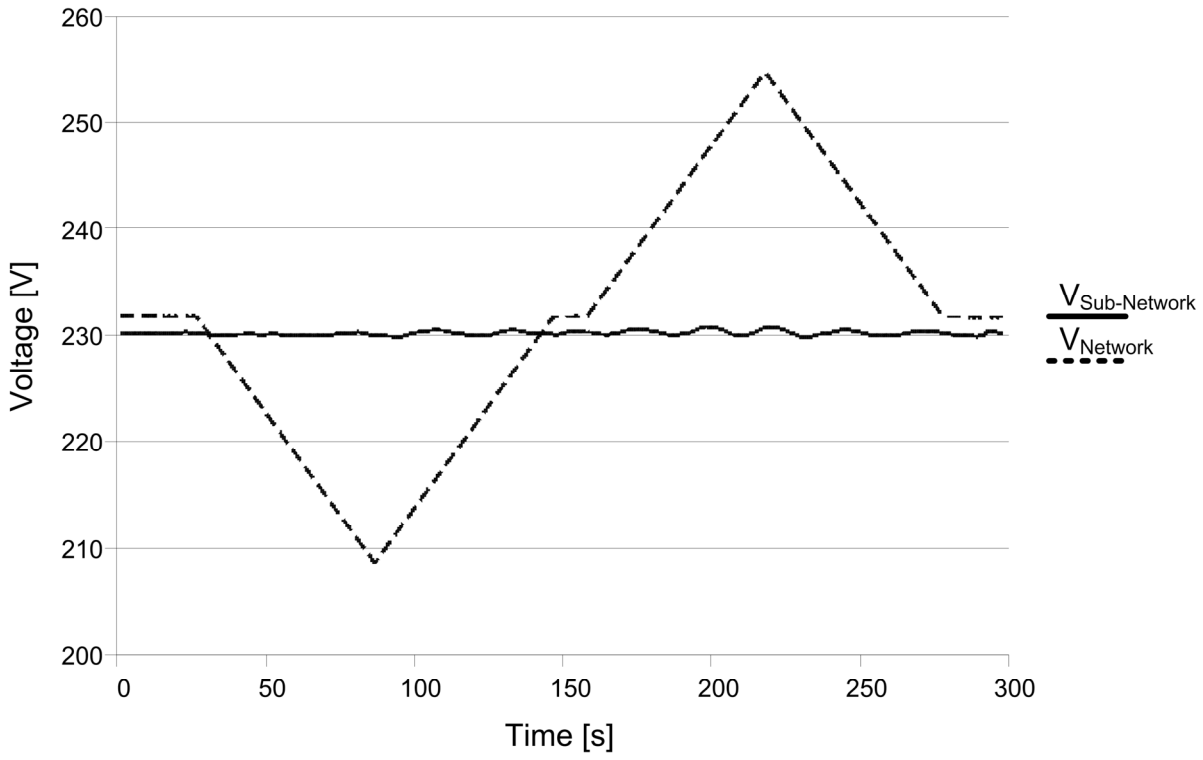

Figure 68: Voltage curve of the sub-network voltage (solid) during a network voltage ramp (dashed).

Figure 69 shows the reactive power flows during the voltage ramp of Figure 68. As one might expected due to the calculation results of section 5.1.2, reactive power flow increases with the voltage difference between network and sub-network voltage.

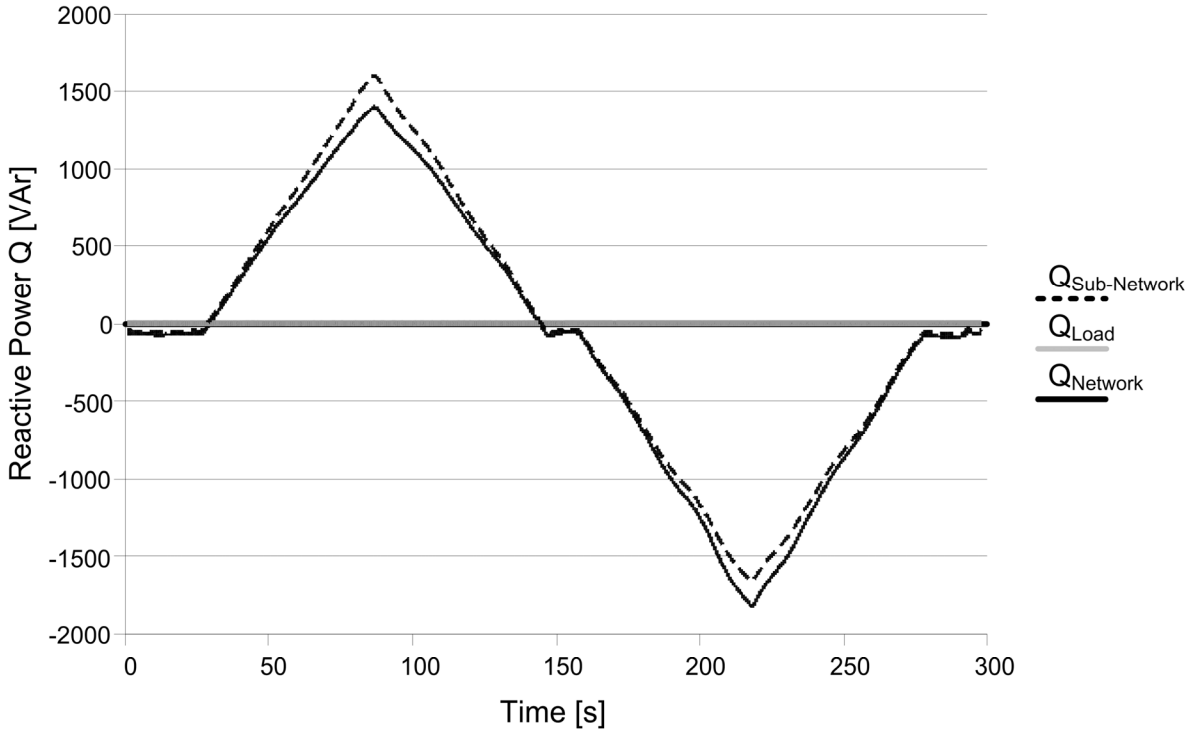

Figure 69: Reactive power flows of the load (solid grey), the sub-network source (dashed) as well as the network source (solid black) during a network voltage ramp.

A comparison between calculated and measured reactive power flow for a network voltage of 253 V and a sub-network voltage of 230 V for actual given load conditions is shown in Table 6. The deviation of about 90 VAr and 125 VAr respectively can be explained by the output filter as well as the internal losses of the prototype unit.

Table 6: Comparison between calculated and measured reactive power flow for a network voltage of 253 V and a sub-network voltage of 230 V

	$Q_{Sub\text{-}network}$ [VAr]	$Q_{Network}$ [VAr]
Calculated	-1674	-1862
Measured	-1582	-1735

In Figure 70 the active power flow during a network voltage ramp is presented. Through the varied reactive power flow the internal losses of the prototype unit are also changing. Therefore the active power consumption of the load is constant due to the constant sub-network voltage, but the loading of the network voltage source changes with the course of the power dissipation.

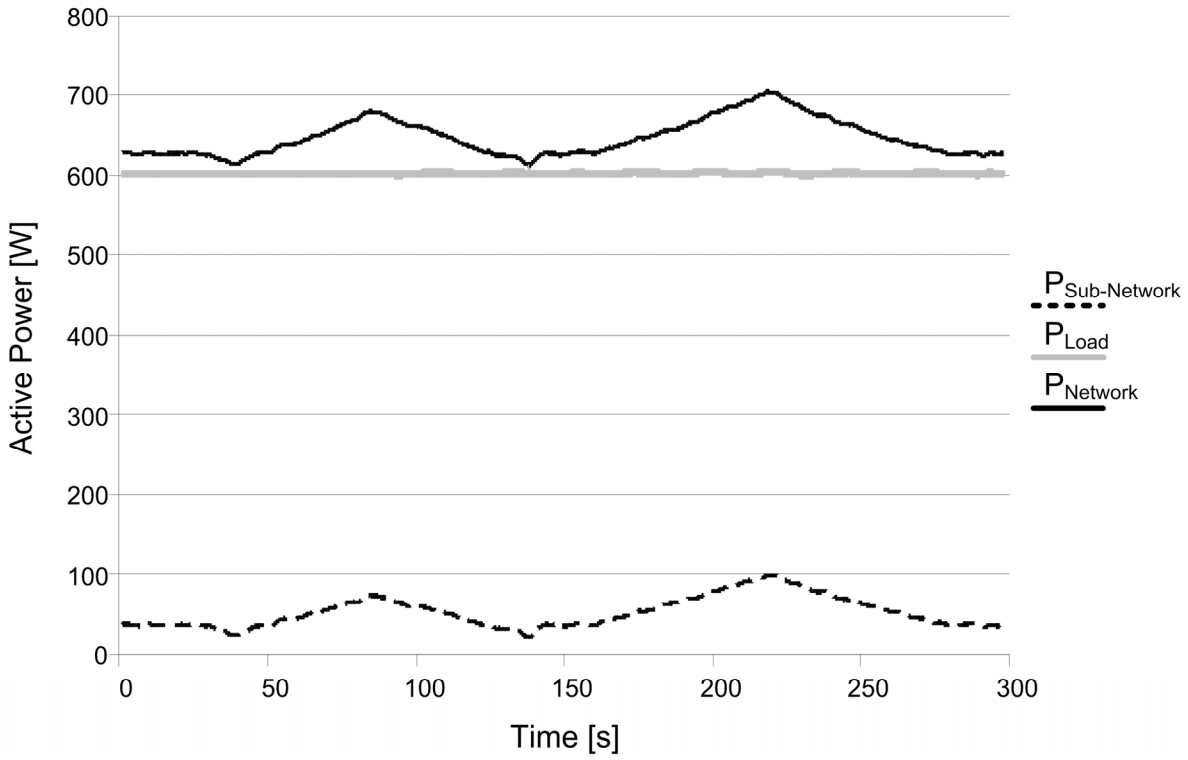

Figure 70: Active power flows of the load (solid grey), the sub-network source (dashed black) and the network source (solid black).

5.3.2.1. Dynamic behaviour

The voltage source simulating the network voltage source was programmed in the way to provide short time voltage dips for the sub-network. In Figure 71 the curves of the sub-network voltage and the network voltage are shown. The network voltage breaks in at a phase angle of 90° with remaining amplitude of 85 % of nominal voltage for 70 ms and return to its nominal value afterwards. It can be seen that the prototype unit is not able to hold the set-value of 230 V, but the voltage reduction within the sub-network during the voltage dip is reduced considerably.

Figure 72 shows the corresponding current curves. Although the changes of the load current amplitude are hardly noticeable, the deviation of the sub-network voltage from its set-value generates observable flicker.

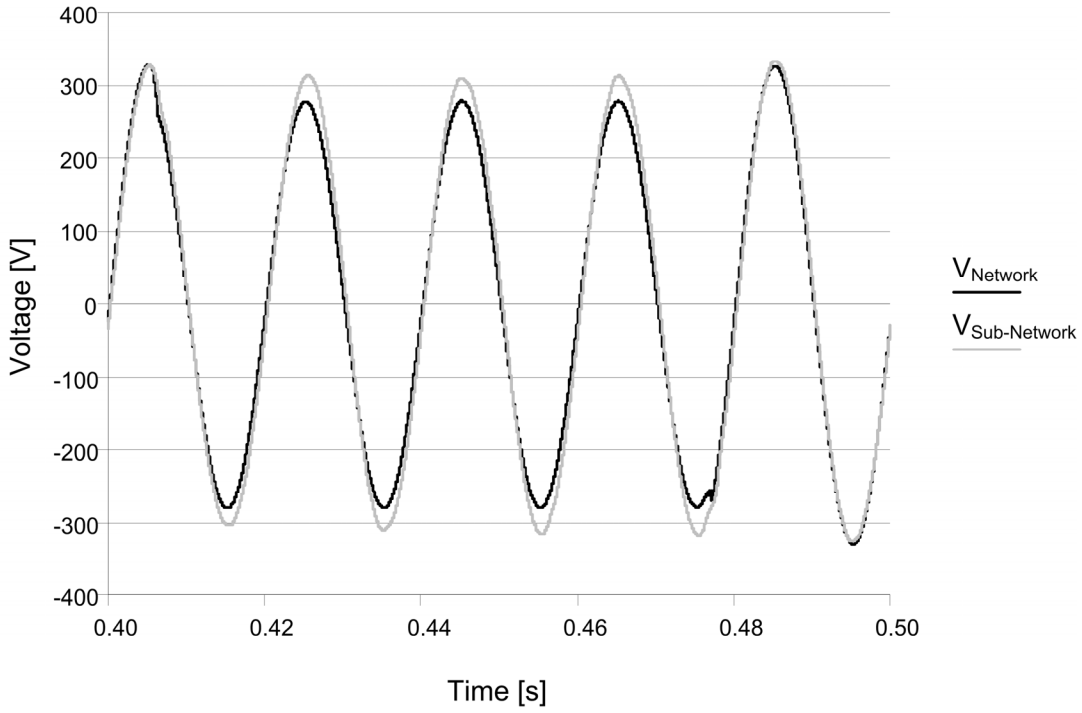

Figure 71: Transient recordings of a voltage dip with 85 % of nominal voltage as remaining network voltage. Curve of network voltage (black) and curve of sub-network voltage (grey).

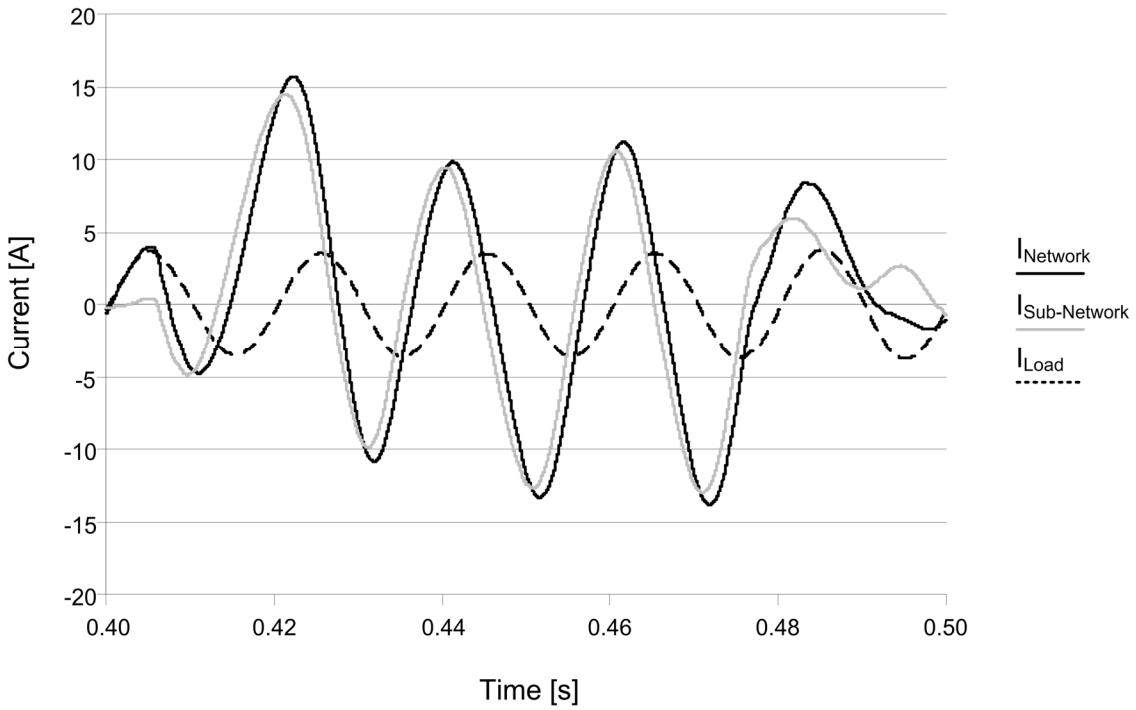

Figure 72: Transient recordings of the currents during a network voltage dip according to Figure 71. Sub-network current (grey), load current (dashed black) and network current (solid black).

The used parameters for the control are not chosen ideal in terms of dynamic behaviour. Since the voltage drop at the decoupling inductor increases due to the immediately increase of the network current, the angle between network voltage and sub-network voltage changes and generates a coupling between both control branches. Therefore not only the controller of the amplitude but also the controller of the phase angle has to be improved in its dynamic.

5.3.2.2. Improvement of voltage waveform

For demonstrating the improvement of the voltage waveform, the network voltage source was programmed with the set-values of Table 7.

Table 7: Specification of testing voltage

Harmonic Order	$V_{Network,RMS}$ [V]	Phase Angle
1	230	0
3	11.5	0
5	13.8	0
7	11.5	0

The values correspond to the limits of the DIN EN 50160 for the specified harmonic orders. The phase angles of the harmonic order were chosen randomly and consistently at 0 °. The set-value of the sub-network voltage was set to 230 V.

Table 8: Damping of selected harmonic orders within the sub-network area

Harmonic order	$V_{Network,RMS}$ [V]	$V_{Sub\text{-}Network,RMS}$ [V]	$V_{Sub\text{-}Network,RMS}$ / $V_{Network,RMS}$
1	230.7	230.3	1.00
3	11.5	5.1	0.45
5	13.8	6.2	0.45
7	11.5	6.0	0.52

The results of Table 8 show that the voltage harmonics within the sub-network area can significantly be reduced. The improvement expected due to simulation results could not be reached. This can be lead back to the non ideal voltage profile provided by the inverter, because for simulation was used an ideal one.

In order to validate the improvement of the voltage profile under real terms the prototype unit is connected to the public network. The results are shown in Figure 73. In right diagram the peak of the voltage curve in the sub-network is distinctive, although the peak is flattened at the network voltage (left diagram). Because of the improved voltage profile the current consumption of the resistive load in the sub-network is also only little disturbed.

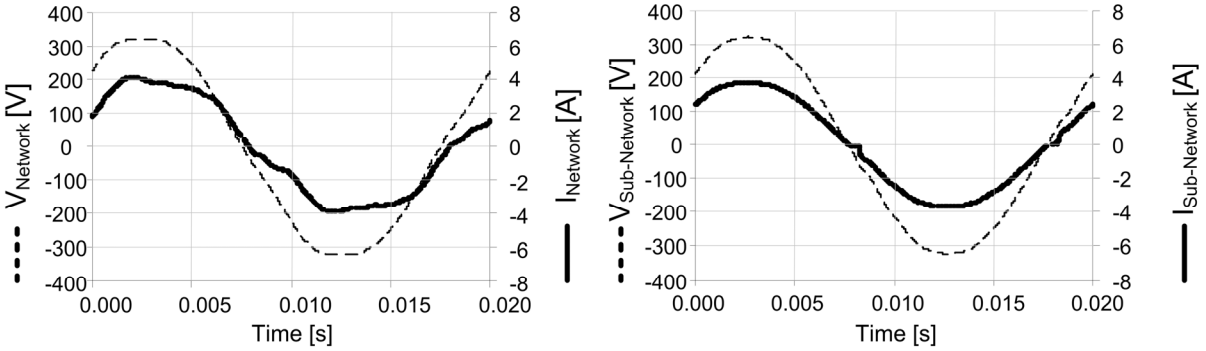

Figure 73: Voltage and current curves of the network voltage source (left part) and of the sub-network voltage source (right part).

This little grade of disturbance can also be proved by the THD of the voltages. While the network voltage has a THD of 3.1 % the THD of the sub-network voltage is with 1.9 % clearly lower (cp. Figure 74).

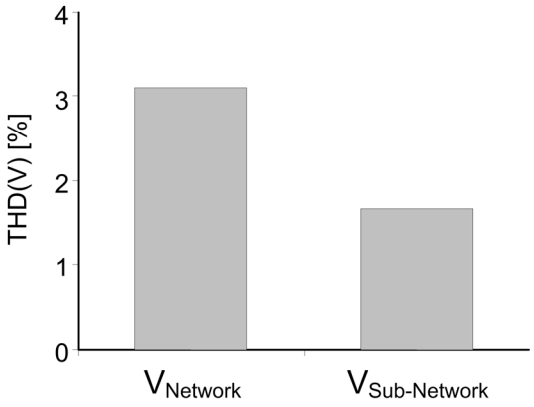

Figure 74: THD of the network voltage $V_{Network}$ and the sub-network voltage $V_{Sub-Network}$ for the measurement of Figure 73.

Totally it can be noticed that the principle of the inductive decoupling is working. The deviation to the simulation results for dynamic behaviour has to be reduced by improving choice of controller parameters. The improvement of the voltage profile could be proved, too.

6. References

[Han05] Handschin, E.: *Elektrische Energietechnik, Kapitel III, Elektrische Betriebsmittel*, Lecture Material, University Dortmund

[Sch05] Schlabbach, J., Metz , D.: *Netzsystemtechnik*, ISBN 978-3-8007-2821-3, VDE Verlag

[Eng01] Engler, A.: *Regelung von Batteriestromrichtern in modularen und erweiterbaren Inselnetzen*, PhD thesis, University Kassel, 2001

[Jah07] Jahn, J.: *Energiekonditionierung in Niederspannungsnetzen unter besonderer Berücksichtigung der Integration verteilter Energieerzeuger in schwachen Netzausläufern*, PhD thesis, University Kassel, 2007, kassel university press, ISBN 978-3-89958-377-9

[Heu05] Heuck, K., Dettmann, K.-D., Reuter, E., *Elektrische Energieversorgung*, 6. completely revised and extended edition, Vieweg-Verlag, Wiesbaden, 2005

[Org02] Orglmeister, G., *Symmetrierkompensator für Hochspannungsleitungen*, PhD thesis, ETH Zürich, 2002

[Klo97] Klosse, R., Santjer, F., Gerdes, G., *Flickererzeugung durch Windenergieanlagen*, DEWI Magazin Nr. 10, Deutsches Windenergie-Institut, 1997

[Wie01] Wiesner, Th., *Technische Aspekte einer großflächigen Integration dezentraler Energieversorgungsanlagen in elektrische Verteilnetze*, Activity report, VDI Reihe 21 Nr. 313, VDI-Verlag, Düsseldorf, 2001

[Hau02] Hauck M., *Bildung eines dreiphasigen Inselnetzes durch unabhängige Wechselrichter im Parallelbetrieb*, PhD thesis, University of Karlsruhe, 2002

[Val09] Valov B., *Auslegungskonzept des Netzanschlusses von PV-Kraftwerken zwecks Stabilisierung und voller Nutzung der Netzkapazität*, 24. Symposium – Photovoltaische Solarenergie, Bad Staffelstein, March 2009, Page 270-275, ISBN 978-3-934-681-93-4

[Eng05] Engler, A.: *Applicability of Droops in Low Voltage Grids*, International Journal of Distributed Energy Resources, Technology & Science Publishers, Kassel, Germany, 2005

[Tin08] Tinarwo D.: Design of Village Power and Micro-Grids for Rural Areas of Zimbabwe with Specific Attention to Voltage Regulation on Low Voltage Meshed Distribution Grids, PhD thesis, University Kassel, 2008, kassel university press, ISBN 978-3-89958-636-7

[Bra05] Braun M., *Models for Transient Simulations of Decentral Power Generation- Implementation and Verification* in *PowerFactory,* diploma thesis, March 2005, University of Stuttgart

[Dsp04] dSPACE, DS1103 PPC Controller Boeard Features, Release 4.1, dSPACE GmbH, 2004

[Spi01] Spitzer, B.: *Modellbasierter Hardware-in-the-Loop Test von eingebetteten elektronischen Systemen,* Dissertation, Karlsruhe, 2001

[Gei07] Geibel, D., Jahn, J., Juchem, R.: *Simulation based control development approach for a multifunctional PV-inverter*, 12th European Conference on Power Electronics and Applications, Aalborg, Denmark, September 2007

7. List of Abbreviations

THD	Total Harmonic Distortion
DER	Distributed Energy Resource
PCC	Point of Common Coupling
PoC	Point of Connection
UPS	Uninterruptable Power Supply
RCPS	Rapid Control Prototyping System

8. List of Figures

9. List of Tables